KTH ROYAL INSTITUTE
OF TECHNOLOGY

Degree project in Soil and Rock Mechanics
Second cycle 30 HP

Jet Grout Bottom Plug in Deep Excavations

Numerical Analysis of a Tunnel Project

IDA SCHJELDERUP

Stockholm, Sweden 2022

Preface

This master thesis marks the end of my studies at the Royal Institute of Technology in Stockholm and my master's degree in Soil- and Rock Mechanics. The thesis work was conducted in collaboration with the construction company NCC.

I would like to give special thanks to Jorge Yannie, my supervisor at NCC, for your support, guidance and all your time. It has been of invaluable help. A special thanks also to Stefan Larsson, my supervisor and Professor at the Royal Institute of Technology, for your support and encouragement.

This thesis work started in the spring semester of 2020 and the time of this thesis' genesis has been a very special one both personally and for the world. It will be a time I will never forget. Thank you to all my family and especially Klas, you are my rock.

Stockholm, June 30, 2022
Ida Schjelderup

Abstract

This master thesis has investigated the performance of a deep excavation with a jet grout bottom plug used to prevent bottom heave and hydraulic uplift failure. The concept of a jet grout plug as a structural and sealing component in a specific case was studied, namely one of the tunnel sections of The West Link tunnel project in Gothenburg. The section was to be built as a cut-and-cover tunnel with the excavation shaft consisting of secant pile walls, struts and a jet grout bottom plug. It is to be established where there are a lot of sensitive buildings and constructions close to the excavation site. This makes it important not to disturb the surroundings during construction with, for example, settlements.

The study was carried out by doing a literature study, analytical calculations and numerical simulations in the finite element software PLAXIS 2D. More specifically, the checks evaluated were uplift equilibrium of the jet grout plug and of the whole structure, structural performance of the jet grouted plug and hydraulic conductivity of the jet grouted mass.

The results show a design of a jet grout plug that together with the additional structures works sufficiently enough to make a secure construction for a deep excavation below the ground water table. The structural performance of the jet grouted plug to function as a strut level is fulfilled even if the jet grout is not perfectly performed. To work as a sealing component the jet grout column pattern and the centre-to-centre distance between the columns are important factors together with the alignment and diameter of the jet grout columns. To make a completely watertight construction is however almost impossible in this case since the jet grout plug is located at a large depth (around 20 m). To work properly against failure by uplift it does not need to be completely watertight. Instead, the use of relief wells makes sure that the pore water pressure is not larger than the vertical stress from the soil, otherwise failure by uplift is a real danger. Furthermore, to work properly against settlements it is not only the water tightness of the jet grout plug that decides whether it will work properly. Instead, it is also the pumping and infiltration system together with the, in this case, sensitivity of the lower aquifer that decides the risk of settlements.

Keywords: Jet grouting, jet grout bottom plug, cut-and-cover tunnel, tunnel design

Sammanfattning

I denna uppsats har en jetinjekterad bottenplugg i en tunnelkonstruktion undersökts. Bottenpluggen används som en del i den stabiliserande konstruktionen och ska även fungera som en tätande komponent för att förhindra hydrauliskt grundbrott och hydraulisk bottenupptryckning. Den jetinjekterade bottenpluggen som har studerats är en del av en av tunnelsektionerna i Västlänken i Göteborg. Sektionen ska byggas som en ”cut-and-cover”-tunnel bestående av sekantpåleväggar, stämp och en jetinjekterad bottenplugg. Platsen den ska byggas på är i centrala Göteborg vilket gör att det finns många omgivande byggnader som inte får påverkas med till exempel allt för stora sättningar.

Studien har genomförts med hjälp av en litteraturstudie, analytiska beräkningar och numeriska simuleringar i finita elementprogrammet PLAXIS 2D. Mer specifikt är det som har undersökts; statisk jämvikt för jetinjektionspluggen och hela konstruktionen, hållfasthetskrav för jetinjektionspluggen och hydraulisk konduktivitet för pluggen.

Resultaten visar en design av en jetinjektionsplugg som fungerar tillräckligt bra för att utgöra en säker konstruktion i en djup schaktning under grundvattenytan. Hållfastheten hos den jetinjekterade pluggen för att fungera som en stämp i schaktet är uppfylld även om jetinjekteringen inte är perfekt utförd. För att fungera som tätande komponent är mönstret av jetinjektionspelarna och centrum-till-centrum-avståndet mellan pelarna viktiga faktorer samt dessutom lutningen och diametern på pelarna. Det är dock nästintill omöjligt att kunna göra en helt vattentät konstruktion i det här fallet eftersom jetinjektionspluggen är placerad så pass djupt (ca 20 m). För att fungera mot hydraulisk bottenupptryckning behöver pluggen dock inte vara helt vattentät. Det är i stället blödarrör som ser till att porvattentrycket inte blir högre än det vertikala jordtrycket ovanför pluggen. Det som avgör risken för sättningar i omgivningen är inte enbart vattentätheten i pluggen utan även hur mycket vatten ett pump- och infiltrationssystemet kan klara av samt i det här fallet känsligheten i den nedre akvifären.

List of Symbols

Roman letters

B = width of jet grout plug [m]
c = cohesion [Pa]
D = diameter [m]
E = Young's modulus [Pa]
f_{t} = tensile strength [kPa]
G = shear modulus [Pa]
$G/s_{\mathrm{u}}^{\mathrm{A}}$ = ratio unloading/reloading shear modulus over active shear strength [-]
h_{jet} = thickness/height of jet grout plug [m]
h_{w} = height ground water pressure [m]
K_0 = coefficient of earth pressure at-rest [-]
k = hydraulic conductivity [m/s]
k_{JG} = hydraulic conductivity, jet grout [m/s]
l_{w} = length of secant pile walls [m]
M = critical state line [Pa]
M_0 = constant constrained modulus below the effective vertical preconsolidation pressure, Swedish method. [Pa]
M_{L} = constant constrained modulus between stresses σ'_{c} and σ'_{L}, Swedish method.
M_{p}= moment capacity [Nm/m]
OCR = over consolidation ratio [-]
$q_{\mathrm{sk,jet}}$ = characteristic bond strength, micropile/jet grout [Pa]
q_{u} = uniaxial compressive strength [Pa]
R_{d} = bond strength [Pa]
R_{inter} = interface bond [-]
R_{sw} = bond resistance between secant pile wall and soil [N]
S_{t} = sensitivity [-]
s_{u} = shear strength [Pa]
$s_{\mathrm{u,ref}}^{\mathrm{A}}$ = reference active shear strength [Pa]
$s_{\mathrm{u,inc}}^{\mathrm{A}}$ = increase of shear strength with depth [N/m^2/m]
$s_u^{\mathrm{P}}/s_{\mathrm{u}}^{\mathrm{A}}$ = ratio of passive shear strength over active shear strength [-]
$s_u^{\mathrm{DSS}}/s_{\mathrm{u}}^{\mathrm{A}}$ = ratio of direct simple shear strength over active shear strength [-]
T_{mp} = tension force, micropiles [N]
t_{p}= thickness of the steel strut pipes [m]
t_{w} = thickness of secant pile wall [m]
U = water pressure [N]
UCS = uniaxial compressive strength [Pa]
w = unit weight [N/m/m]
W_{jet} = jet grout plug self-weight [N]
W_{w} = secant pile walls self-weight [N]
w_{L} = liquid limit [-]
z = meter above sea level [m a.s.l.]

Greek letters

α = azimuth [°]
β = inclination [°]
β_E = coefficient [-]
γ = shear strain [%]
γ_a = partial factor, shaft resistance, tension [-]
γ_C = partial factor concrete [-]
γ_C = unit weight concrete [N/m^3]
γ_f^C = shear strain at failure in triaxial compression [%]
γ_f^{DSS} = shear strain at failure in triaxial direct simple shear [%]
γ_f^E = shear strain at failure in triaxial extension [%]
γ_S = partial factor steel [-]
γ_{JG} = unit weight, jet grout material [N/m^3]
γ_{sat} = unit weight, saturated soil [N/m^3]
γ_{unsat} = unit weight, unsaturated soil [N/m^3]
γ_w = unit weight, water [N/m^3]
ε = strain [%]
κ^* = modified swelling index (SSC swelling index)
λ^* = modified compression index (SSC compression index)
ρ = density [N/ m^3]
σ' = effective stress [Pa]
σ'_{vc} = vertical preconsolidation stress [Pa]
τ = shear stress [Pa]
τ_0/s_u^A = initial degree of mobilization over active shear strength [-]
υ = Poisson's ratio [-]
ϕ = friction angle [°]
ψ = dilatancy angle [°]

Abbreviations

ALS = accidental limit state
CRS = constant rate of strain
FEA = finite element analysis
MC = Mohr-Coulomb
MUR = (Swe = markteknisk undersökningsrapport) = Geotechnical investigation report
NGI-ADP = Norwegian Geotechnical Institute-Active Direct Passive
SF = safety factor
SLS = serviceability limit state
SS = Soft Soil
UCS = uniaxial compressive strength
ULS = ultimate limit state

Table of Contents

1 Introduction

The concept of jet grout bottom plugs in deep excavations has been studied in this thesis, more specifically a design idea for one of the tunnel sections in a large infrastructure project, the West Link, in Gothenburg. The jet grout bottom plug was considered in the design to function as a watertight barrier and as an extra horizontal support level. The study has foremost been performed with numerical simulations in the finite element software PLAXIS 2D but also a literature study and analytical calculations have been used. Things that were investigated were the jet grout bottom plug's ability to prevent bottom heave and hydraulic uplift failure and both short-term and long-term behaviour have been studied.

1.1 Jet Grouting

Jet grouting is a ground improvement method that generate changes in the mechanical and hydraulic properties of soils. The process of jet grouting consists of disaggregating the soil matrix, mixing it and partially replacing it with a cementing agent. The disaggregation is done with a high-energy jet of a fluid, which can be the cementing agent itself (EN12716:2018).

Jet grouting is widely used all over the world and a common ground improvement method today (Croce et al. 2014, Modoni et al. 2016, Akin 2019) and at the same time the most complicated grouting technology available (Burke 2012). The areas of usage are to improve the mechanical properties of the soil and/or to reduce the permeability of soil, or even to make a watertight barrier in the ground. These barriers can be both vertical and horizontal (Cheng et al. 2019).

In many deep excavations where the foundation level is below the ground water table there is a need for a watertight barrier, especially in high permeable soils. Several reasons demand for this type of solution, for example, not cause settlements on the surrounding structures due to lowering of the ground water table, avoid failure by uplift and workability on the excavation site. Some countries, there among Sweden, have strict regulations, which does not allow any alteration of the ground water table (Brinck & Stigenius 2019).

1.2 Aim and Purpose

There is a lot to considerate in a geotechnical design of the size of the West Link tunnel. To make the design studied here within the scope of this master thesis, focus was the jet grout bottom plug and its functions and properties. The purpose of the thesis was to study the concept of the jet grout plug as a structural and sealing component in a deep excavation. The research questions for this jet grout bottom plug were the following:

- How should a jet grout plug be designed to make a sufficiently secure construction in a deep excavation under the ground water table?
- How should a jet grout plug be designed for it to work properly against failure by uplift?
- What properties does a jet grout plug need to function as a sealing component?
- How watertight does the jet grout plug need to be for it to work properly?
- What properties does a jet grout plug need to function as a support level at the excavation bottom?

1.3 Method and Methodology

The methods used in this thesis to study the concept of jet grout plug are recently developed analytical and numerical calculations together with a literature study.

The literature study was focused on the analytical models for the design of jet grout plugs. In addition, it looked for previous experiences in numerical simulations and execution of excavation works. Another important aspect of the literature study was to know the material properties of the grouted material and which parameters to take into consideration to be able to perform a good jet grout design.

The analytical method used was to calculate the ultimate limit state (ULS) for different situations using partial safety factors according to Eurocode 7 (EN 1997-1:2005). The checks that were done were chosen according to Modoni et al. (2016) that presents a design method for jet grout plugs in their article: "Design of Jet Grouted Excavation Bottom Plugs". The checks were:

1. Uplift equilibrium, of the jet grout plug and/or of the whole structure
2. Structural performance of the jet grouted plug
3. Water inflow through possible imperfections of the jet grouted mass

For this thesis the first two checks were made with calculations using partial factors and state-of-the-art analytical calculations. However, for the third check a probabilistic method was used to estimate the possible waterflow due to imperfections in the jet grout plug. This method is based on Monte-Carlo simulations and was developed in a previous master thesis by Brinck and Stigenius (2019). More about this method and the other analytical calculations can be found in section 4 - Analytical Calculations.

The finite element software PLAXIS 2D was used for the numerical calculations where two different constitutive soil models were used for the clay, namely the NGI-ADP and Soft Soil (SS). The NGI-ADP model is an anisotropic undrained strength model using the input parameters for shear strength for the different states; active (A), direct simple shear (D) and passive (P). The calculation using NGI-ADP focused on the overall capacity of the structure and the deformations of the secant pile walls and jet grout plug. The SS-model could instead take the long-term behaviour into consideration such as consolidation of the excess pore water pressure in the clay layers. For both simulations, results such as deformations, forces, bending moments and safety factors are presented and compared. PLAXIS simulations have also been made by the West Link project's consultants prior to this master thesis work. The results reached in this thesis are compared with those as well. The PLAXIS simulations are explained more thoroughly in section 5 - Finite Element Analysis – PLAXIS 2D.

2 Jet Grouting

Jet grouting is a ground improvement method that improves the soil's mechanical and hydraulic properties. It is a highly versatile method when it comes to the tooling, procedures, fluids and energy in the jetting (Burke 2012). All kinds of different shapes and configurations can be made with the jet grouting technique and a wide range of applications exists making it a popular ground improvement method. It is also an attractive method due to its ability to be used in confined spaces or other places difficult to reach, because of its relatively light equipment and the ability to create large underground structures making just a small borehole to start with (Croce et al. 2014).

The earliest application of a high-pressure grouting technique dates back to the 1950s in the United Kingdom (Essler & Yoshida 2004). However, the real development of what we today call jet grouting took place in Japan in the 70s. In the first application it was intended to improve the soil water tightness using chemical grouting and creating vertical cut-off walls (Essler & Yoshida 2004). Due to environmental concerns the chemicals were soon replaced by cement grouts and since then the technique has gained popularity around the world (Njock et al. 2018).

The areas of usage for jet grouting are very versatile, for example, foundation reinforcement for the prevention of short- and long-term ground movements, watertight barrier used as protection against dewatering effects, solidification of contaminated soil and as ground stabilizing method for tunnelling (Croce et al. 2014). In this thesis the application of jet grouting is to function as a waterproof barrier and as an extra strut level between a secant pile retaining wall in a deep excavation.

2.1 The Process of Jet Grouting

The process of jet grouting is illustrated in Figure 1. It begins with drilling down to the required depth using a drill rod equipped with a jet nozzle holder and drill bit. After reaching the maximum depth, the jetting and grouting processes begin. The high energy jet fluid partially or completely replaces the existing soil as the drill rod is pulled upwards at the same time it rotates to create columns. The excess mixture of water-cement-soil (called spoil) is removed through the space between the drill rod and borehole wall to the surface.

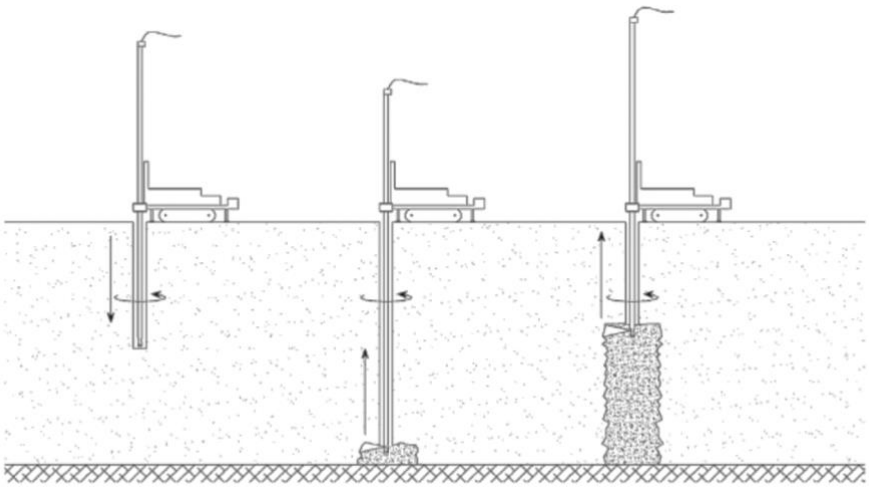

Figure 1. The stages of jet grouting; drilling, jetting and grouting of columns (Croce et al. 2014).

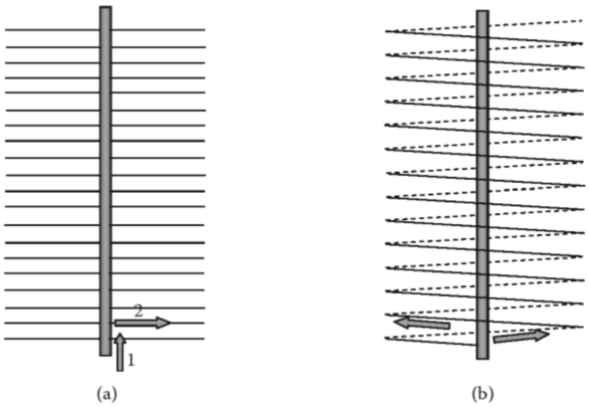

Figure 2. Different ways of lifting the rod while jetting, (a) stepwise and (b) continuously (Croce et al 2014).

The lifting and rotating of the rod can be done in steps of 40 to 100 mm or continuously in one spiral motion, see Figure 2. A stepwise movement of the rod has the advantage of the jetting passing the same area several times and, in that way, making the treatment more effective. This is also the most common way to execute the jetting (Croce et al. 2014).

At the same time as the drilling to desired depth is done the jet grout mixture can be used as drill flushing to stabilize the borehole, i.e. create a temporary "casing". To stabilize the drill hole is an important aspect when it comes to the removal of the spoil. This spoil, or return flow, needs to be removed sufficiently safe and fast as to not cause a build-up of too high pressure in the ground and cause movements in surrounding structures (Burke 2012). Trying to minimize the spoil is both environmentally friendly as well as cost-effective as it must be removed and disposed somewhere. Possibilities also exist to recycle the spoil, but it is not a general practice (Croce et al. 2014).

Other methods to perform the drilling and jetting exists, two of them being "pre-jetting" and "downward jet grouting". Pre-jetting is done by using water already at the drilling stage to start disaggregating material and in that way increase the overall efficiency of the jet grouting. The pre-jetting can also be done on the way up in one or more lifting phases before the last grouting phase. The method of pre-jetting is suitable for increasing the diameter in for example stiff clay and dense sands, soils that are hard to erode (Croce et al. 2014). The downward jet grouting is a method where the grouting is done simultaneously as the drilling. The method can be used together with pre-jetting and this can be a cost-effective solution producing a limited amount of spoil (Croce et al. 2014).

2.2 Single, Double and Triple Fluid Systems

The available jet grouting technique today can be divided into three groups, namely single, double and triple fluid systems. This is based on the number of fluids that are injected into the soil. The single system is based only on grout that is usually a water-cement mixture, double is with air and grout, and the triple system is grout together with air and water (Figure 3).

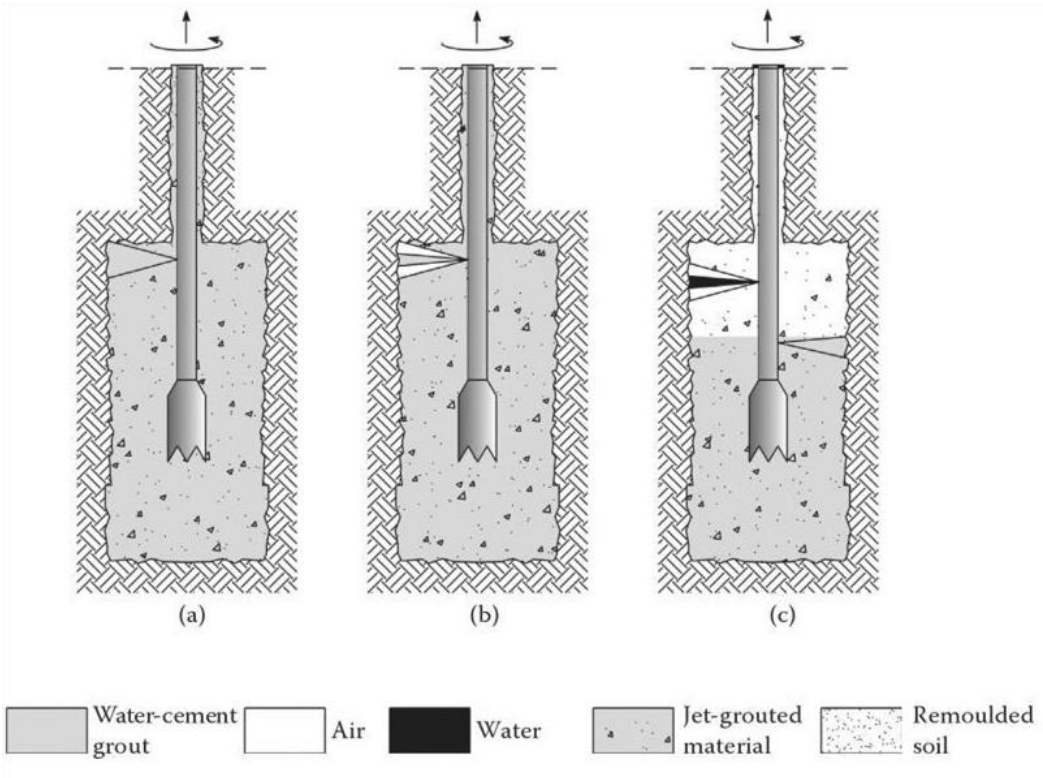

Figure 3. Schematic figures of the single (a), double (b) and triple (c) system (Croce et al. 2014).

A single system is relatively simple as it is only dependent on the grout for both eroding and mixing the soil. A large part of the jet energy is consumed by friction and viscosity effects in the soil that is exposed to the grout (Njock et al. 2018). Therefore, the columns created by a single system are smaller in diameter compared to columns created with double or triple systems. The single system is mainly used for horizontal jet grouting (Nikbakhtan et al. 2009).

A double system can make approximately twice as large columns as the single system. This is because of the compressed air significantly increases the eroding effect of the jet together with the grout (Njock et al. 2018).

In the triple system the soil is eroded by a water jet shrouded by compressed air from a nozzle situated above a second nozzle where the grout is ejected. Transport of existing soil is also done by the water and air which makes it possible for the in-situ soil to be completely replaced by grouting material. The triple system can make even larger diameters compared to the other two systems in the same soil type (Wen 2015). Since the double and triple system can make larger diameters, they are more suitable for slabs and bottom plugs (Wanik et al. 2017).

2.3 Material Properties

The material properties of a jet-grout soilcrete (mixture of soil and grout) are affected by many factors. For example, some factors are the soil type and its heterogeneity, the operating parameters during jet injection such as jet-pressure, rotation and withdrawal rate, the jet injection system (single, double or triple), properties of the grout such as cement-water ratio, cement type, amount of cement (Wanik et al. 2017; Tinoco et al.

2011) and environmental factors, like pore water chemistry and temperature (Toraldo et al. 2017). Furthermore, the column depth influences the strength due to changes in stresses (Arroyo et al. 2007 as cited in Croce et al. 2014).

2.3.1 Material Textures

Different soil types create different textures within the jet-grout columns mainly due to the mechanism of remoulding (erosion and clod cutting). In coarse-grained soils, the soil particles create a homogeneous matrix together with the cement, whereas in fine-grained soil the particles are not as easily separated. The texture is instead largely inhomogeneous containing clods of uncemented material (Figure 4) The size of these clods can be reduced with multiple passes of the jet (Croce et al. 2014).

2.3.2 Strength of the Jet Grouted Material (Soilcrete)

A significant factor affecting the material properties of the soilcrete is the soil type and its heterogeneity. Several studies have been performed (see Table 1 for references compiled by Toraldo et al. (2017)) investigating the material properties and foremost the uniaxial compressive strength (UCS) of the jet grouted column. This is the most common value used to measure the strength of soilcrete.

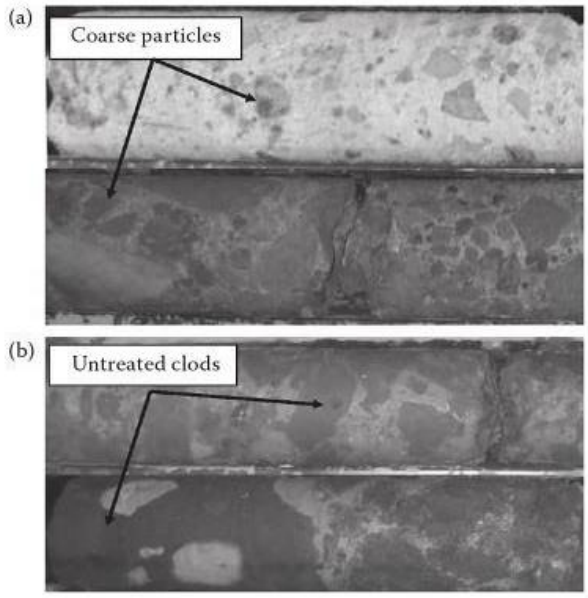

Figure 4. Different textures in different soil types. (a) coarse-grained soils and (b) fine-grained soils (Croce et al. 2014).

Table 1. Mohr-Coulomb failure parameters and uniaxial compressive strength for different jet-grouted materials (compiled by Toraldo et al. (2017), where a complete reference list can be found).

Reference	Soil type	ϕ [°]	c [MPa]	UCS [MPa]
Mitchell et al. (1981)	Clay	39.5	0.6	2.5
Yu (1994)	Clay - Silty sand	40.6	1.1	4.8
Fang et al. (1994.b)	Clay - Silty sand	42	4.2	18.9
Fang and Chung (1997)	Clay and silty sand	38.6	0.8	3.3
Nikbakhtan and Osanloo (2009)	Clay & sand	45	0.6	2.9
Nikbakhtan and Osanloo (2009)	Clay & sand	25	0.8	2.4
Yahiro et al. (1982)	Sand and Clay	28.5	0.7	2.4
Fang et al. (2004)	Silt and Sand	38.7	0.7	2.9
Fang et al. (1994.a)	Silty sand	35	4.2	16.1
Croce & Flora (1998)	Silty sand	26.1	3.2	10.3
Bzówka (2009)	Sandy	58.2	2.3	16.1
Mongiovì et al. (1991)	Gravel	52	2.1	12.2
Mongiovì et al. (1991)	Gravel	42	0.3	1.3
Miki (1982)	Various	25	0.8	2.5

The tensile resistance strength of the jet grouted material is experimentally observed to be in the range of 1/10 of the UCS, but this is usually neglected since it is reduced considerably when the material cracks (Modoni et al. 2016). Reinforcement, such as metal or fiberglass bars or tubes, can be used in jet grouted elements to improve the tensile resistance if needed (Croce et al. 2014).

The factors affecting the material properties of the jet grout are doing that on a local scale, i.e. the strength test results above are from tests made on a core sample of a column, representing the best part. It must be considered that the bottom plug that is going to be constructed in the project section studied consists of many overlapping columns. The intended idea is that these columns will form a uniform structure. However, as soil is heterogeneous and due to varying alignment and diameter of the grouted columns these will not perfectly overlap. Therefore, there will be a fluctuating structure with weaker and stronger zones, so the values obtained from core sample tests cannot be directly used as characteristic values of the entire jet grouted structure (Toraldo et al. 2017). Modoni et al. (2016) means that one conservatively can assume that the plug strength parameter is 1/5 of the one obtained from the core samples.

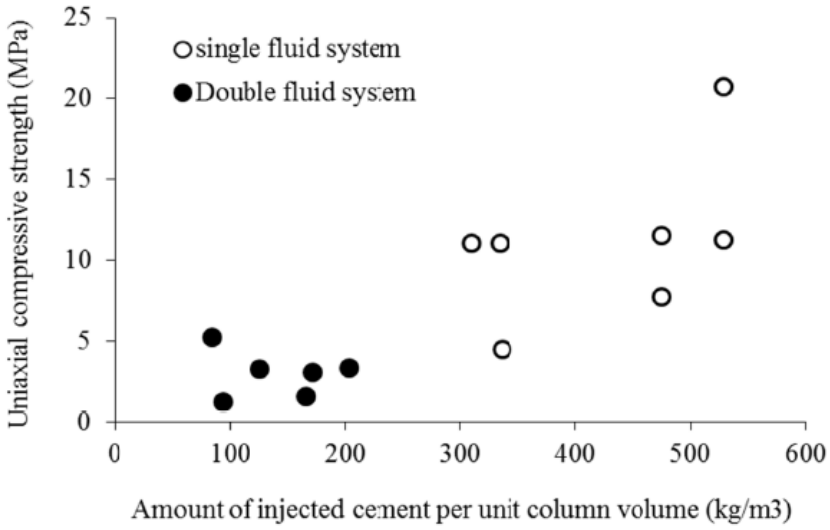

Figure 5. UCS as a function of the cement injected in the unit volume of column (Wanik et al. 2017).

As mentioned above it is not only the type of soil that affects the material properties of the jet grouted material, but another factor is the type and the amount of cement per unit volume used. The type of cement used is typically Portland cement but other types such as finely pulverized Portland, blast furnace and pozzolanic can be used as well. Furthermore, additives such as bentonite, calcium chloride and sodium silicate can be added to achieve different properties of the jet grout (Croce et al. 2014). The amount of cement per unit volume is partly connected to the selected jet-grouting system. For example, a double fluid system that can make larger diameters compared to a single fluid system spreads the cement over a larger area, resulting in a lower cement ratio and therefore weaker as illustrated in Figure 5 (Wanik et al. 2017).

Nikbakhtan and Osanloo (2009) observed the effect of the grout pressure and grout flow on the soilcrete properties and concluded that a higher grout flow gives a higher UCS and the same relationship is true for the grout pressure. They do however point out that their results are valid for tests at a depth of 5-10 m below ground surface. At larger depth these results may need to be adjusted as the confining pressure is increased with increasing depth.

2.3.3 Stiffness – Young's Modulus, E

The mechanical behaviour of soilcrete is for the most applications sufficiently represented by a linear elastic – perfectly plastic model. As the strength is represented by the UCS, the value of Youngs modulus, E, can be described with the following empirical linear relation:

$$\boldsymbol{E = \beta_E \cdot q_u} \qquad \textbf{(1)}$$

where q_u is the characteristic uniaxial compressive strength (=UCS) and β_E is a coefficient varying between $100 - 1200$. The lower values of β_E are for finer soils (clay and silty sand) and the highest values are found in coarse soils (gravel and sandy gravel) (Croce et al. 2014) but it is typically in the range of $300 - 500$ for all soil (Flora et al. 2017). Note that due to the large variations in the jet grout plug structure, this value could conservatively be reduced with $1/5$.

2.3.4 Permeability

To reach the wanted sealing effect and the hydraulic conductivity of the soilcrete one choses a suitable grout suspension. Bentonite can also be added to the mix, if necessary, for a higher sealing effect. Nevertheless, it is important to know the chemical and mineralogical composition of the bentonite to be able to use it properly (EN12716:2018).

There is not much information in the literature about specific values of the permeability of soilcrete. It is, however, reported to be very low and some values of the hydraulic conductivity (k) range between 10^{-5} and 10^{-8} m/s in studies compiled by Akin (2016). In practice, k is found varying in between 10^{-7} to 10^{-9} m/s on samples of homogenous, completely treated soil or at a laboratory scale.

The major problem about permeability and sealing properties of a jet grouted structure is its macro scale. Even if the grout suspension and the grouted material have a low permeability, the material that is not treated by the jet grout can have a high permeability and be passages for seepage. Burke (2012) means that creating a bottom seal for groundwater control requires perfection, particularly under a high head (> 70 kPa). Even a small imperfection can yield a significant flow, that can be enough to create a piping condition. In friction soil this can cause erosion of the ground material in untreated zones and hence exacerbate the problem.

For the success of a waterproof jet grouted bottom plug a good overlapping of the jet grout columns is the critical factor. The overlapping layout pattern creating a slab can vary in execution. There can be a square pattern resulting in a more conservative design (i.e. more overlapping) or a triangular pattern, which is more efficient for waterproofing (Figure 6). However, the overlapping of the columns is affected by the diameter, the column spacing and the alignment (Cheng et al. 2019, Modoni et al. 2016). More information about these factors is found in section 2.4.

For the construction of a jet grout plug to be completely watertight a perfect execution needs to be done and the pattern in which the columns are installed needs to be very precise. Modoni et al. (2016) means though that to have zero leakage in a construction is an over conservative and uneconomic solution.

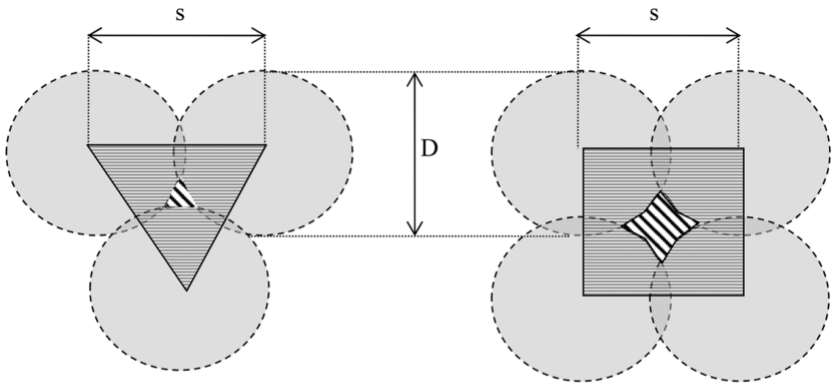

Figure 6. Triangular (left) and square (right) pattern for column arrangement. (Modoni et al. 2016)

2.3.5 Unit Weight

In the application of jet grouting as a sealing plug in deep excavations the unit weight of the material is of great importance as part of the supporting function is provided by this. The unit weight, w, must be experimentally determined as it depends on the specific weight of the soil, the specific weight of the hardened grout, the relative amount of soil and grout and the porosity. With double fluid systems a slightly lower w is obtained compared to single and triple systems due to bubbles of air that gets captured in the fresh mixture during grouting. In the triple systems the air used in the water-air jet can be expelled by the following remoulding by the grout jet (Croce et al. 2014).

2.3.6 Verification of Soilcrete Properties

Some of these factors effecting the material properties mentioned in the beginning of this section are to a large extent connected to the condition on-site where the jet grouting is being executed such as soil structure, temperature and depth. Furthermore, other factors such as cement ratio and parameters of installation are also highly connected with the in-situ situation and how they work together can be very different. Therefore, is it of great importance to check how the material behaves on a certain site, for example make a core-drilling test of the jet grouted material before construction starts. This way one can see how the different jet grouting parameters can be adjusted in the current situation to get the desired ground improvement. The European standard (EN 12716:2018) stresses the role of preliminary field tests and quality controls due to the variability of the jet grouted material properties. In general, controls help to verify that the material fulfils the design requirements and with the selection of the most effective system and jet grouting parameters.

2.4 Geometry of Grouting

One simplification to be made about the geometry is that the higher energy of the jetting will create larger geometry of the element (Burke 2012). Different shapes are possible for jet grout elements depending on the movements of the nozzle (Figure 7). Pulling the drill rod without rotation will create panels, swivelling will create segments of columns and pulling while rotating will create complete columns. Overlapping columns is the method used for creating slabs used for sealing and hence columns will be the only shape discussed within the scope of this thesis.

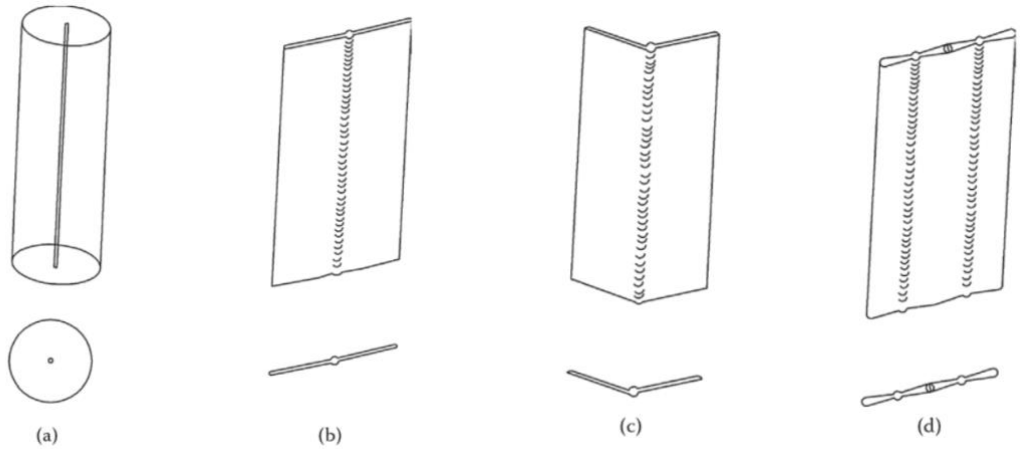

Figure 7. Different possible shapes of jet grout bodies: (a) column, (b) panel, (c) V-shape element and (d) candy shape element (Croce et al. 2014).

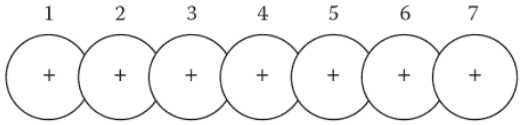

Figure 8. Schematic figure of the fresh-in-fresh sequence (Croce et al. 2014).

The drilling and grouting of overlapping columns to create a plug used for sealing can be done in different sequences. Either fresh-in-fresh or fresh-in-hard. The fresh-in-fresh sequence is a contiguous sequence where the columns are created next to each other without waiting for the previously grouted column to harden, as shown in Figure 8. A risk with this method is to wash out the previously created still fresh column by the drilling water. This must be handled with care but also to use water-cement grout as drilling fluid can reduce this problem (Croce et al. 2014).

The fresh-in-hard sequence is instead a sequence where columns are created with some distance and then closing the gaps with secondary columns after hardening of the first – primary – columns. This method requires a detailed treatment plan and can also include a third – tertiary – column set (see Figure 9 for example). The fresh-in-hard sequence can have a problem with a shadow effect as the first columns hinder the jet from reaching the sides if the columns, but it is even so the most popular method (Croce et al. 2014).

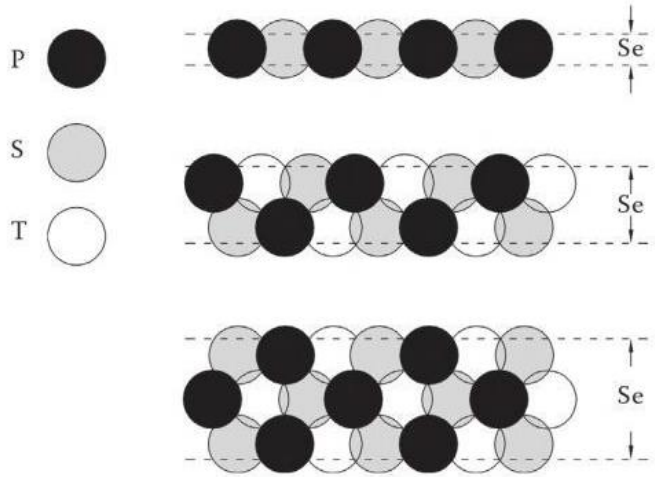

Figure 9. Different patterns of the fresh-in-hard sequence. P=primary, S=secondary and T=third column set (Croce et al. 2014).

2.4.1 Diameter of Columns

A way to guarantee the function of a watertight structure is to be sure that the grouted columns have the diameter used in the design. There is, however, a lot of factors affecting the diameter, and the main variables according to different authors have been compiled by Tinoco et al. (2016) and are shown in Table 2 below. These factors are then correlating in different ways according to different authors.

There can be large variations of the soil in all three space dimensions and the soil decides to a large extent the properties of the jet grout and the geometry. The erosive action between the soil and the jet energy decides the diameter of the jet grout column. Generally, the coarse-grained soil is more easily eroded than fine-grained soil and hence larger diameters can be obtained in coarser soil when using the same energy. In heterogeneous soil there is a large scatter of the diameter (Croce et al. 2014).

Table 2. Main variables affecting the diameter of jet grouted columns according to different authors. (For full references, see Ticono et al. (2018)).

Variable	Reference
Diameter of grout nozzles	Modoni et al. 2006, Carletto 2009, Kanematsu 1980
Withdrawal speed of the rod	Modoni et al. 2006, Carletto 2009, Nikbakhtan & Ahangari 2010, Shibazki & Yoshida 1997
Rotation frequency, rpm	Modoni et al. 2006, Carletto 2009, Nikbakhtan & Ahangari 2010
Velocity of injected fluid at nozzle	Modoni et al. 2006
Soil type	Modoni et al. 2006, Langbehn 1986
Soil properties	Wang et al. 2012, Croce & Flora 1998
Number of nozzles	Modoni et al. 2006, Wang et al. 2012
Jet properties	Modoni et al. 2006
Grout pressure	Nikbakhtan & Ahangari 2010, Shibazki & Yoshida 1997, Langbehn 1986
Water-cement ratio	Nikbakhtan & Ahangari 2010
Flow rate of grout slurry	Wang et al. 2012, Shibazki & Yoshida 1997
UCS, Uniaxial compressive strength	Wang et al. 2012
Atmospheric pressure	Wang et al. 2012
Diameter of the rod	Wang et al. 2012
Type of injected fluid	Shibazki & Yoshida 1997
Volume of injected grout	Croce & Flora 1998
Amount of cement in the soil	Croce & Flora 1998

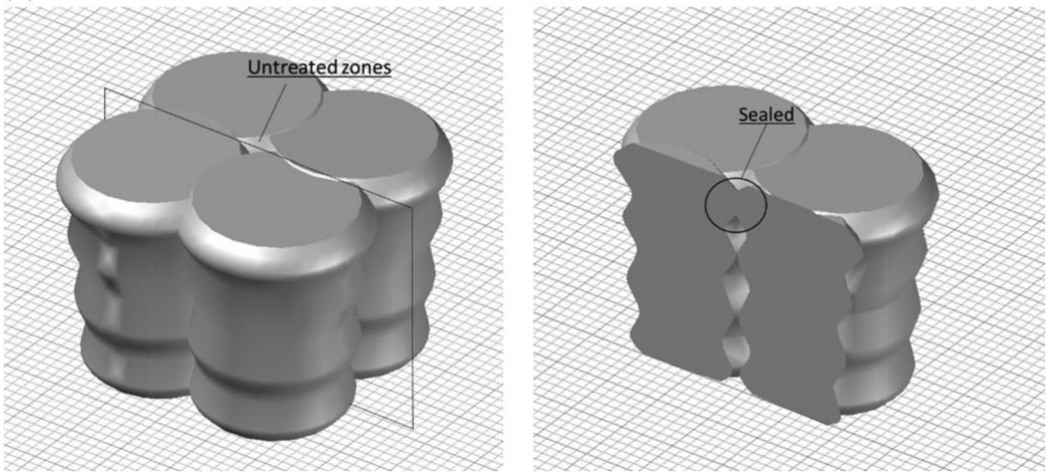

Figure 10. The "calabash-shape" of jet grouted columns (Pan et al. 2017).

Modoni et al. (2016) states that the further down in the ground one is jetting the higher shear strength in the soil, which causes a smaller diameter of the columns. Pan et al. (2017) however do not agree that the column diameter only gets smaller the further down it gets but also that the jet grouted column has a fluctuating shape. They mean that a grouted column in practice is "calabash-shaped". As can be seen in Figure 10 this creates untreated zones between the columns, but not necessarily along the whole length of the column. One untreated zone may be sealed further down in the construction and the other way around.

It must be considered that not all soils are erodible and that obstructions such as boulders can cause a shadow effect (Burke 2012), for example in glacial till. In this case the large boulders create obstacles in the ground where the jet grout treatment cannot reach behind making areas of untreated soil. These areas are a risk as these can be potential leakage paths through the jet grout plug, not making it a watertight construction.

However, for the structural functionality of the jet grout plug the material does not need to be perfect. Hsieh et al. (2003) describes partial ground improvement using jet grouted piles installed with a ratio of 7 % of treated ground. The 6 m thick treated zone worked as an extra strut level in a deep excavation with diaphragm walls. The ground treatment increased the pressure in the existing soil as the return flow was less than the material put into the soil, which was enough to limit the displacements of the diaphragm wall and keep the movements of adjacent structures within limit values.

Modoni et al. (2016) also say that imperfections that may appear in a jet grout plug are shown to be less important when it comes to the structural behaviour of the plug. It is however more important when it comes to the analysis of seepage as described in Section 2.3.4.

2.4.2 Alignment of the Columns

One more aspect that affects the quality of the jet grout plug is the alignment of the columns. The columns both need to be positioned correctly on the ground surface in the designated pattern and not deviate from verticality (if the columns are supposed to be vertical). This is crucial to make a continuous and watertight jet grouted mass. Even if the

positioning of the start of the columns are made with highest possible accuracy the axis often deviates (Modoni et al. 2016) and hence causes imperfections and zones where water can leak. The deviation can be described with two angles, one being the azimuth, α, and the other the inclination, β, see Figure 11. The area of the holes of non-grouted material through the plug is mainly governed by the deviation of verticality of the columns and can be assumed to vary almost linearly with depth (Modoni et al. 2016).

Drilling alignment is highly dependent on the drilling method used, drilling tool selection, equipment quality, the ground conditions and the experience of the operator (Cheng et al. 2019, Croce et al. 2014). The magnitude of deviation is of course also dependent on the length of the grouting columns (Croce et al. 2014). There is almost always some deviation of the designated alignment, usually between $0.2° - 0.6°$ and a deviation of 0.6° can exceed the maximum tolerance of 1/100 that is permitted by the Eurocode EN-12716:2018 (Cheng et al. 2019).

Croce et al. (2014) show with a Monte-Carlo simulation the deviation in geometries that are likely to be obtained in jet grouting. In Figure 12 a cross-section 10 m from the head of the borehole is shown and compares the differences between the Monte-Carlo simulation and the ideal condition. β has been given a standard deviation (SD) of 1° and the diameter (D) a coefficient of variation (CV) of 0.2. It is obvious that the massive element lay-out (used in a grouted plug) does not consist of 100 % treated ground and hence it is not 100 % impermeable.

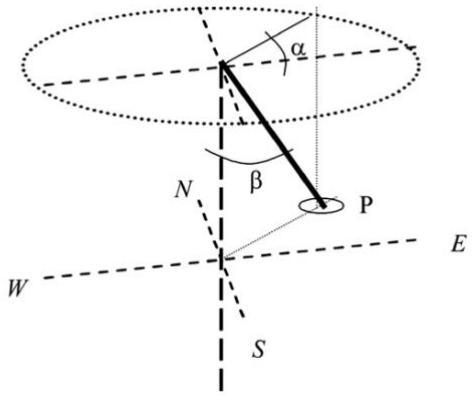

Figure 11. Possible angles of deviation of jet grouted columns (Modoni et al. 2016).

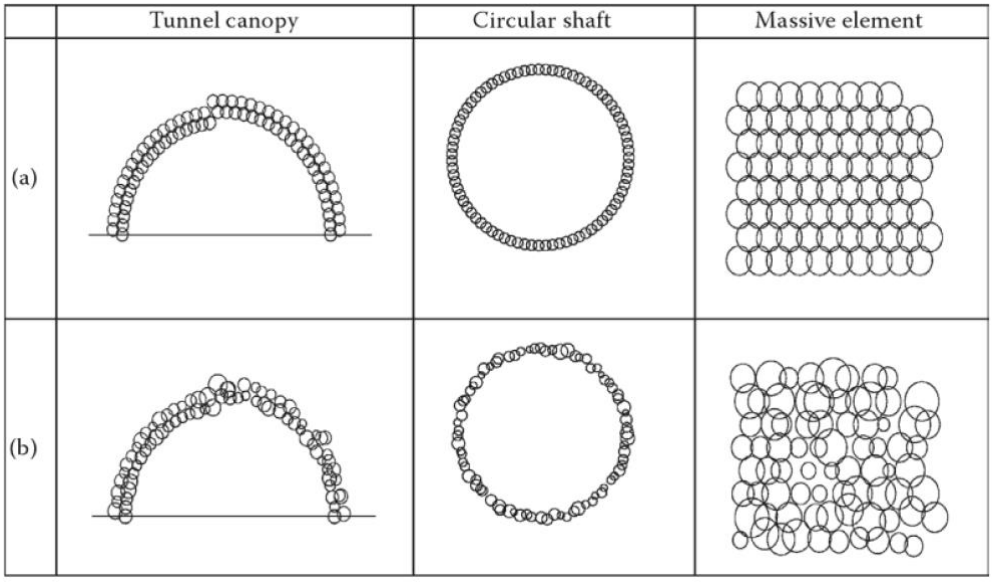

Figure 12. Some typical layouts of jet grouted elements, (a) shown under ideal conditions and (b) with variability (SD(β)=1° and CV(D)=0.2) (Croce et al. 2014).

2.5 Quality Control Systems of Jet Grouting

The different qualities wanted from a jet grouted structure gives certain demands that needs to be fulfilled for the structure to work as planned. The different properties of the grout and grouted columns have been described in Section 2.3 and 2.4 and especially the quality of a watertight jet grout structure demands high accuracy of the diameter and alignment of the jet grout columns. How these properties are fulfilled and controlled are described in Section 2.5.2 and 2.5.3. The quality of the material strength, the movements of surroundings and the permeability of the grouted structure are also descried below.

In general, it is the soil and its properties, such as strength and permeability, that to a large extent dictates the outcome of the jet grouting and the quality of it. These variations of quality that the ground can cause is something that needs to be design for and what makes it important with pre-production in-situ tests on site in the soil layers that are to be treated (Burke 2012). EN12716:2018 also stresses the importance of pre-production tests for all kind of properties, both geometry of the structure as mechanical properties of the grout.

2.5.1 Position of the Column

To have a watertight structure also means to have a good overlap of the jet grout columns. For this, the positioning of each column is also an important factor to monitor during execution of the grouting. The position of the column shall not deviate more than 0.10 m from its original placement, not horizontally nor vertically (EN12716:2018). The positioning of the drill rod can be done with a total station or surveying instrument and must be done for every column.

2.5.2 Diameter of the Columns

The diameter is to be controlled if specified in the project. For a watertight construction it is a must as the columns need to overlap. The methods given in EN12716:2018 to control the geometry are by visual inspection, core drilling, destructive drilling, radius

bars, heat of hydration method, CPT (=cone penetration test), SPT (=standard penetration test), borehole camera and geophysical measurements.

Visual inspection can include excavating of the entire column to see the geometry or excavating down to the top of the column to see the top diameter of the columns. That does not give the entire picture as the column can fluctuate along its length as explained above (Section 2.4).

Core drilling is to take a sample from the jet grouted structure and test properties in a laboratory such as UCS, *E*, density and permeability, to see if the ground has been treated as wanted in each location. It is possible to take inclined cores that pass through several columns to study the resulting diameter and overlapping gaps.

A non-invasive quality control is to do geophysical measurements, for example seismic methods. Niederleithinger and Guerreros (2015) developed a quality assurance method for jet grouted columns applying seismic crosshole and downhole measurements. The transmitter sends P- and/or S-waves through the underground construction and different materials gives different velocities of the waves and hence the material and the size of the columns in different locations underground can be decided (the seismic crosshole and downhole methods are both standardized in civil engineering) (Figure 13).

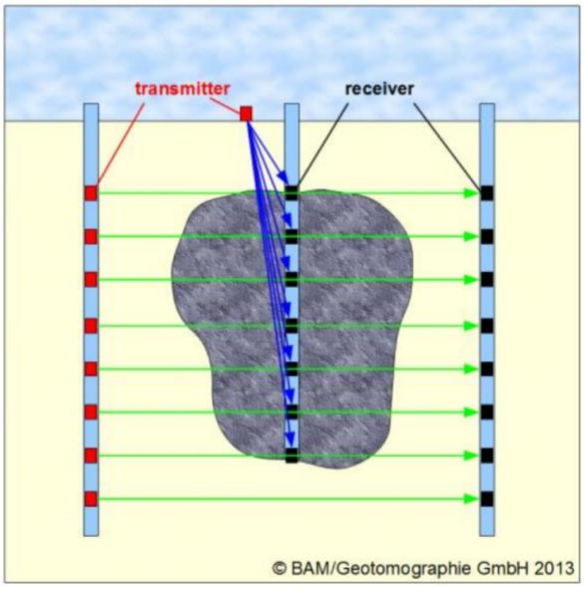

Figure 13. Crosshole (green lines) and downhole (blue lines) seismic measurements (Niederleithinger & Guerreros 2015).

2.5.3 Alignment of the Columns

To control the alignment of the columns different inclinometers can be used during drilling. This is an economic alternative compared to methods using satellite or magnetic induction positioning, which also exists. It is also beneficial to use the kind of inclinometers that can be inserted inside the drill rod. Inclinometers that demand a removal of the drill rod takes extra time, something that is uneconomic but also threatens the stability of the drill hole (Cheng et al. 2019).

The deviation of the inclination for vertical jet grouting elements shall be less than 2 % of the maximum drilling length according to EN12716:2018. A different value can be specified in the design because the tolerances and their potential effects needs to be evaluated in each specific project and design.

2.5.4 Characteristic Strength – Uniaxial Compressive Strength (UCS)

To determine the characteristic material strength of the jet grouted material test samples can be taken from either core drilling, fresh sampling or from the spoil return. Core drilling is to take a sample from the jet grouted structure and test properties in a laboratory such as uniaxial compression, *E*, density and permeability. The size of the core samples is given in Eurocode as well as the number of samples, where they are to be taken and quality class (EN12716:2018 - Annex A & B). The spoil return can be used for strength determination only if it can be expected to be representative of the finished jet grouting structure. The characteristic strength that is determined as the UCS also needs to be statistically verified. The grout mixture is also tested in advance, for properties like density, viscosity and bleeding, ensuring the consistency and mix quality (EN12716:2018).

The execution of the grouting and the parameters used are also to be monitored and documented on site. These can be used to interpret the results from other tests.

2.5.5 Movements of Adjacent Structures

The acceptable limits of movements to surrounding structures must be set in advance in the design of the jet grouting (EN12716:2018). These movements, that can be settlements, heave and distortion, must then be monitored during construction to see that they are not exceeded. One way to monitor movements is to use a total station at the site and measure movements of adjacent buildings. In addition, tiltmeters can be used on the buildings as well. The secant piles walls can also be monitored for movements and inclination using inclinometers. Movements are especially relevant for those systems that inject big amount of grout and where movements need to be closely monitored during the construction (Eramo et al. 2011).

2.5.6 Permeability

Where permeability is of importance shall the design state the parameters that are to be measured. To test the permeability and water tightness of a jet grouted structure one can use pumping tests, piezometric readings, borehole water tests, borehole camera and laboratory tests on samples. Water levels must be monitored both on site and in the surroundings and the most unfavourable construction stage should be considered when evaluating the overall permeability of a jet grouted structure (EN12716:2018; more about geohydraulic testing in can be found in EN ISO 22282 – Geotechnical investigation and testing – Geohydraulic testing).

3 The West Link Tunnel Project, Section Korsvägen

The West Link (Västlänken) infrastructure project is currently being built in Gothenburg, Sweden. One of the tunnel sections, Korsvägen, is to be established in the central parts of Gothenburg where there are a lot of sensitive buildings and constructions close to the excavation site. Therefore, it is important that the excavation goes according to plan and not to disturb the surroundings during construction with, for example, settlements. One of the section's design proposals was to be built as a cut-and-cover tunnel with the excavation shaft consisting of secant pile walls and a jet grout bottom plug. This design idea and the jet grout bottom plug are the focus of this thesis.

The ground at the excavation site consists of the following soil layers: fill closest to the ground surface, then clay overlying friction soil that overlays the bedrock. There are two aquifers, a top one in the fill material and clay and a bottom one in the underlaying friction material. The groundwater in the bottom aquifer is flowing with a high pore pressure. At some depth during excavation, the pore water pressure in the frictional material will be higher than the total stress of the clay layer above. This will cause the clay layer to be pushed upwards by the water pressure, a so-called failure by uplift. To prevent this kind of failure in the excavation shaft some measure needs to be taken.

Furthermore, the ground water level must not be changed as to not cause settlements in the surroundings, as the clay is very sensitive to subsidence. The water must therefore not leak through the jet-grout plug as that would mean changing the water pressure as well as a risk of failure by uplift as described above. The suggested design is to make a jet grout plug in the bottom of the excavation shaft anchored to the bedrock using micro piles. This jet grout plug will then work as sealing layer for the excavation shaft and together with the micro piles prevent failure by uplift.

Another function of the jet grout plug is to work as a final strut level for the secant pile wall through improving the passive resistance of the soil. This means that the plug material has demands on its structural properties such as compressive strength and stiffness. It is important that the secant pile wall do not have too large movements as to not cause settlements in the surroundings and in that way cause damage to adjacent buildings.

The section *Korsvägen* covers several different sections; *Liseberg Öst I* and *II* and *Liseberg Väst I* and *II*. For this study *Liseberg Väst II* is the one chosen and focused on, because in this section the deep friction material creates some distance between the jet grout plug and the bedrock where the groundwater must flow without restrictions. For the project several geotechnical investigations have been done in the construction area. The results from these investigations were used in this master thesis and they are compiled in Section 3.1.

3.1 Geological Conditions

The ground level varies between +2 and +5 m above sea level (a.s.l.). The soil profile can be seen in Figure 14 where the uppermost soil layer consists of fill overlying an approximately 20 m thick clay layer. Between the fill and clay there is a thin layer of soil similar to a dry crust but assumed to have the same properties as the fill in the calculations. The top clay transitions into a silty clay layer overlying silty sand and

bottommost and closest to the bedrock is a moraine layer. Two aquifers exist in the profile divided by the clay layer, the upper in the fill layer and the lower aquifer in the friction soil underneath the clay deposit. The groundwater level in the lower aquifer varies approximately with the ground level, but the highest measured value of +3.5 m (RKFM 2019-04-30) was chosen in the design as that would be the worst design situation. The storability of the lower aquifer is low which makes it sensitive to extraction and its hydraulic conductivity, k, in the lower aquifer has been found to vary between $5 \cdot 10^{-6}$ m/s and $2 \cdot 10^{-4}$ m/s but somewhat lower in silt (Bygghandling 2019-11-05b). The soil profile used in the section *Korsvägen* (Figure 14) was based on different field and laboratory tests from the geotechnical investigation report of the area (MUR).

The jet grout plug (shaded area in Figure 14) is located to some extent in the silty clay and in the friction soil, which consists of sandy moraine with gravel and the silty sand. These types of soils cover almost the entire scale of UCS-values given in Table 1, however moraine is not homogenously gravel. Therefore, a value of the UCS can be expected to be in the range of approximately 2 to 16 MPa. According to construction documents (RKFM 2019-10-23) the value of the UCS of the jet grout plug is supposed to be between 2 MPa and 10 MPa, which agrees well with previous observations in the literature.

In the upper part of the moraine layer, the presence of large boulders is considered unlikely and smaller boulders in the range of decimetre size are limited in their probability of causing a shadow effect. They are also likely to sink through the already treated jet grouting columns during production and hence be fully embedded in the grout (SU 2019-08-26).

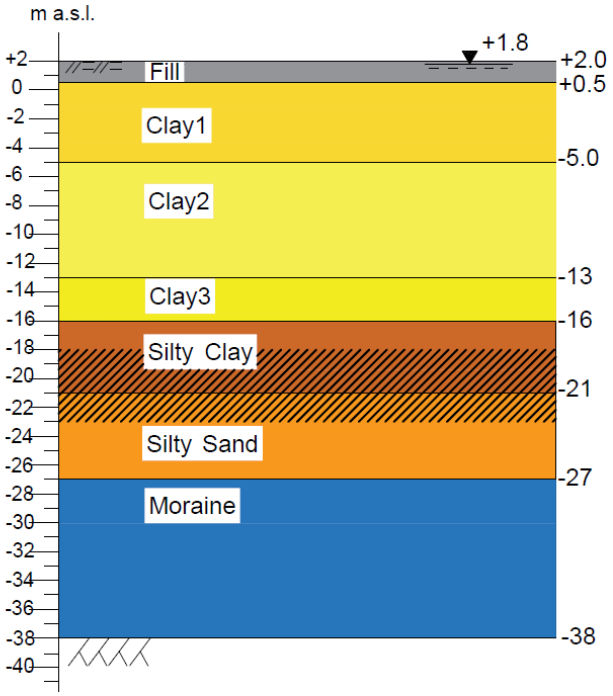

Figure 14. Soil profile used in the calculations of section Korsvägen. The shaded part is the zone for the jet grout plug.

3.1.1 Soil Properties of the Clay Layers

Clay can be classified according to its undrained shear strength, s_u , and the sensitivity, S_t. S_t gives the ratio between the s_u in undisturbed and remoulded state (Larsson 2008). The clay at *Liseberg Väst II* has a high $S_t > 30$ from level -11 to -13 m and below (Figure 15), and also approaches the definition of a quick clay ($S_t > 50$ and an s_u of 0.4 kPa in remoulded state). This can be due to the layer of friction soil that is underneath the clay, which has a significant water flow. This water is to some extent adsorbed into the clay layer, creating a "quick" state (Das & Sobhan 2017).

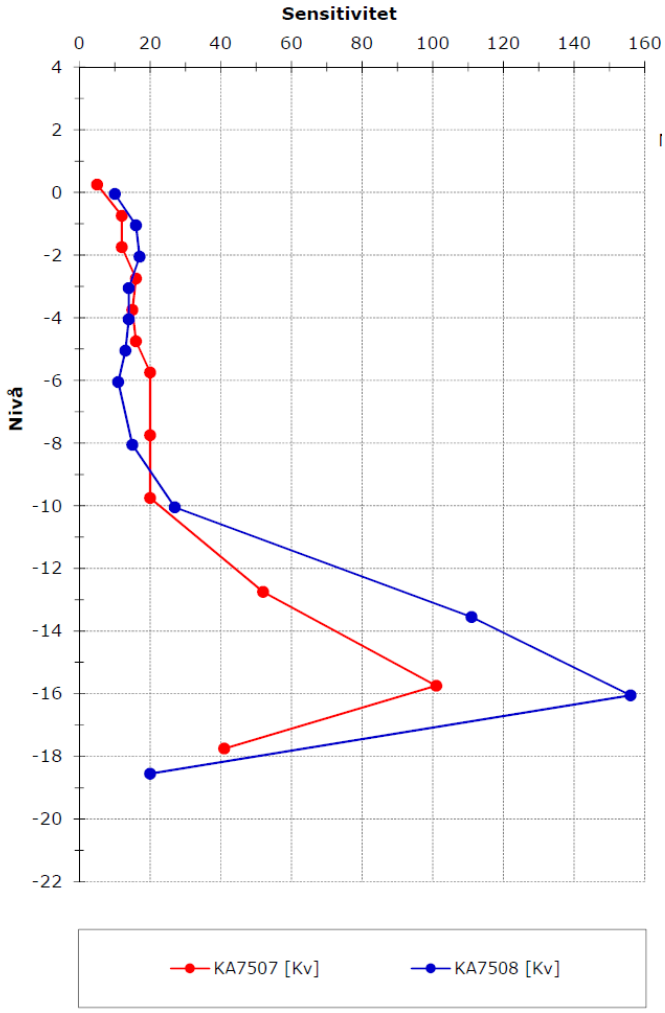

Figure 15. Sensitivity, S_t [-] of the clay layer on the x-axis and level [m] on the y-axis (MUR, Bilaga 8).

The specific weight, γ, of each clay layer is shown in Table 3, some other parameters are presented in the following sections and the model specific parameters needed for PLAXIS simulations are found in section 5 Finite Element Analysis – PLAXIS 2D.

Table 3. The specific weight, γ, of each clay layer.

Property	Clay 1	Clay 2	Clay 3	Silty clay
$\boldsymbol{\gamma}$ **[kN/m³]**	14.7	15	15	18.7

3.1.1.1 Coefficient of earth pressure K_0-value of the Clay

To get the K_0-value, empiricism is used with formulas taken from Larsson et al. (2007) and Trafikverket (2014) (§5.2.2.2.3).
For normal consolidated clay the K_0-value can be assumed to be:

$$\boldsymbol{K_{0NC} = 0.31 + 0.71(w_L - 0.2)} \quad \textbf{(2)}$$

where w_L = liquid limit, in formula expressed in decimal numbers. The over consolidation state if the clay is considered with the formula:

$$\boldsymbol{K_0 = K_{0NC} \cdot OCR^{0.55}} \quad \textbf{(3)}$$

The calculated K_0-values are presented in Table 4, where the values of w_L and *OCR* were gotten from construction documents (RKFM 2019-05-24).

Table 4. Calculated K_0-value. Values of w_L and OCR gotten from RKFM Väst II.

Elevation	Layer	w_L (%)	K_{0NC} min	K_{0NC} max	OCR	K_0 min OC	K_0 max OC	Assumed K_0 in RKFM 2019-05-24
0 to −5	Cl1	100 ± 10	0.807	0.949	2	1.18	1.39	0.95*
−5 to −13	Cl2	90 ± 20	0.665	0.949	1.3	0.77	1.10	0.81
−13 to −16	Cl3	68 ± 7	0.6011	0.7005	1.25	0.68	0.79	0.71
−16 to −21	SiCl	48 ± 22	0.3526	0.665	1.2	0.39	0.74	0.55

**the value cannot be above 1 in PLAXIS-calculations.*

The assumed values of K_0 from RKFM 2019-05-24 (the column at the far right in Table 4) are somewhat high and a higher value of K_0 gives a higher horizontal pressure back of the secant pile wall and hence will give a more conservative design load. The PLAXIS simulation in this thesis was however made with more realistic values of the coefficient K_0. These were calculated with the assumption of K_{0NC} being 0.52 in Equation (3) and presented in Table 5 (L'Heureux et al. 2017; Lindgård & Ofstad 2016; Olsson 2013).

Table 5. Calculated K_0-values with the assumption of K_{0NC} being 0.52.

Elevation	Layer	K_{0NC}	OCR	K_0
0 to −5	Cl1	0.52	2	0.76
−5 to −13	Cl2	0.52	1.3	0.60
−13 to −16	Cl3	0.52	1.25	0.59
−16 to −21	SiCl	0.52	1.2	0.57

3.1.1.2 Friction Angles for Clay

The friction angles, ϕ, seen in Table 6 were obtained from triaxial test on clay samples from the site (the procedure can be seen in Appendix A – Calculation of Friction Angles in Clay). A K_0-value of 0.6 was used in the triaxial tests, which is a typical value for Gothenburg-clay (Olsson 2013). The cohesion, *c*, was also obtained from these triaxial tests. These are considered reasonable ϕ as Larsson et al. (2007) argues that ϕ for clays in Sweden can be assumed to be approximately 30°.

Table 6. The different clay layers and approximate friction angles, ϕ, and cohesion, c.

Clay layer	ϕ [°]	c [kPa]
Clay 1	34	6.0
Clay 2	35	2.0
Clay 3	29	5.0
Silty clay	26	8.0

3.1.1.3 Hydraulic Conductivity of Clay layers

The hydraulic conductivity, *k*, for the different clay layers was taken as a mean value from different CRS-tests made in the geotechnical investigation (MUR, bilaga 2). The calculation of these can be found in Appendix C –Soft Soil (SS) Parameters.

Table 7. The hydraulic conductivity, k, for each clay layer.

Property	Clay 1	Clay 2	Clay 3	Silty clay
k [m/day]	$3.4 \cdot 10^{-5}$	$7.3 \cdot 10^{-5}$	$8.6 \cdot 10^{-5}$	$8.6 \cdot 10^{-5}$

3.1.2 Soil Properties for the Friction Soil Layers

The properties of the friction soil layers obtained from in-situ and laboratory tests can be found compiled in Table 8. These were to some extent also based on empirical data from the literature study. The typical grain size distribution of the moraine layer that is to be jet grouted can be seen in Figure 16.

Table 8. Properties of the friction soils.

Property	Fill	Silty Sand	Moraine
Specific weight, γ (γ sat) [kN/m³]	17 (18)	18 (19)	20 (21)
Cohesion, c' [kPa]	0	0	0
Friction angle, ϕ' [°]	35	31	35
Young's modulus, E' [kPa]	30 000	25 000	35 000
Poisson's ratio, υ' [-]	0.3	0.33	0.3
Coefficient of earth pressure, K_0 [-]*	0.4264	0.4850	0.4264

**Based on Jacky's empirical relation.*

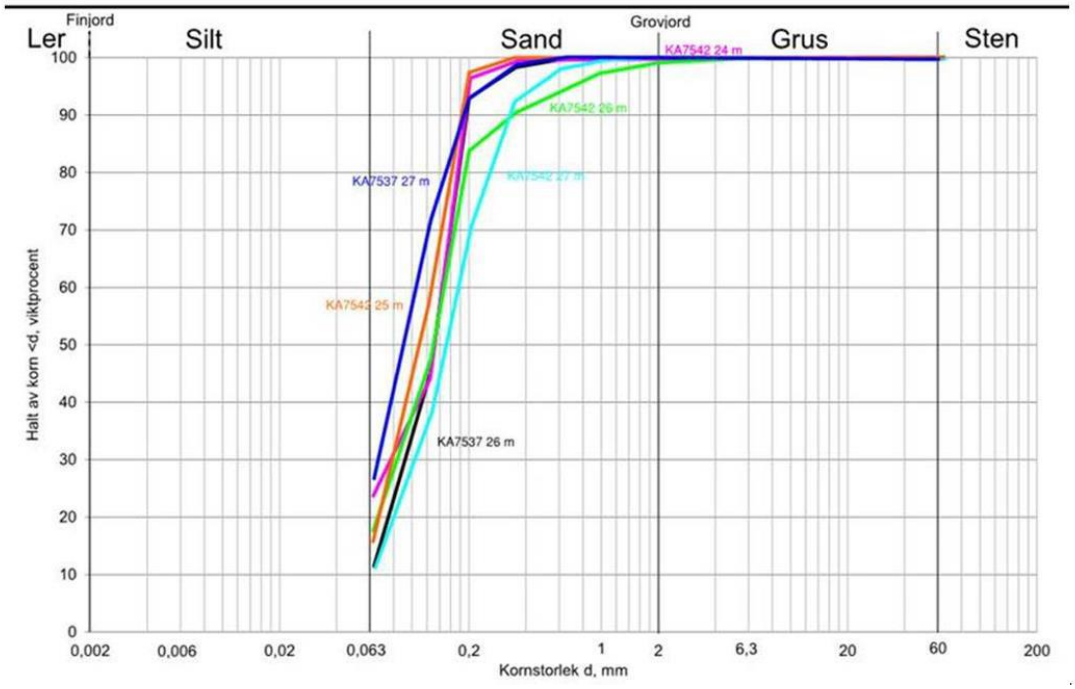

Figure 16. Typical grain size distribution of the upper moraine layer (SU 2019-08-26).

3.2 The Design of the Retaining Structure

The jet grout plug would be grouted approximately −20 to −25 m below the ground level in this design (SU 2019-08-26) i.e. it will be 5 m deep below the final excavation level. The jet grout plug would be anchored by micropiles that will connect the plug to the bedrock (RKFM 2019-05-24).

The secant pile wall would to be supported by two steel struts (level −1.50 and −13) and the pile toe level of the secant pile wall is designed to be located 3.5 m below the top of the jet grout layer. After construction of the tunnel, the top and bottom slab (level −9 and −17.3) would substitute the two struts. See Figure 17 and Figure 18 for a sketch of the design.

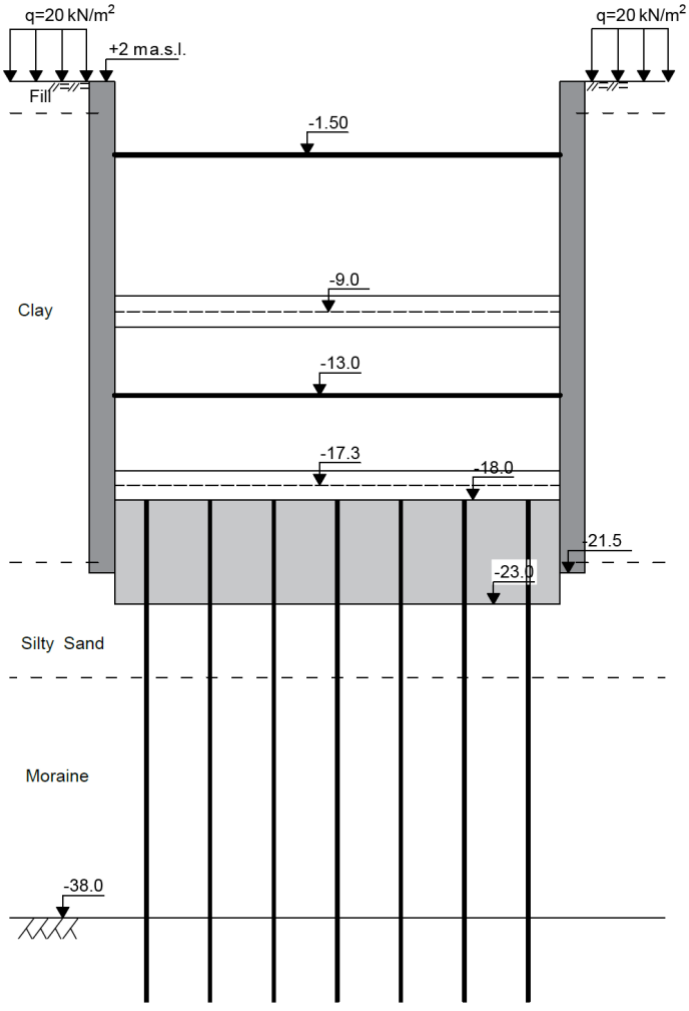

Figure 17. A sketch of the design section.

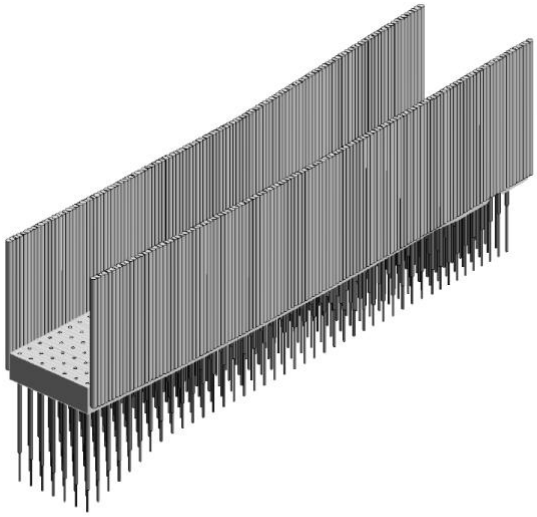

Figure 18. A 3D-sketch of the construction at Liseberg Väst II section (Bygghandling 2019-11-05a).

It is stated in the construction documents that it is the jet grout sub-contractor that to a large extent has the responsibility of the jet grout plug's properties. It is listed that they are to decide the jet grout methodology (single, double or triple fluid) and the parameters of the execution of the jet grout plug such as sequence and rate of execution, nozzle diameter, pressure, flow rate, rotation and withdrawal speed. They also are the ones to decide the design diameter of the grouted columns and the center-to-center spacing between the columns, but there is a recommendation in the construction documents of a diameter of 1.8 m and a spacing of 1.4 m (RKFM 2019-10-23). It is also explicitly stated that the jet grout columns need 100 % overlap and contact to the secant pile walls.

The execution sequence of the tunnel construction is going to be a combination of top down and bottom up and is shown in Stage 1 to 9 in Figure 19. The jet grouting stage is not visible in Figure 19 but that is bound to happen in Stage 1 after the installation of retaining walls.

3.3 Requirements of the Jet Grout Plug

The jet grout plug is a temporary structure and will therefore have a design life of 10 years and no durability criterion. The plug only needs to function during the construction of the permanent concrete tunnel. It must have enough water tightness to enable the casting of the permanent concrete structure and, also, to not significantly disturb the ground water level in the area. Except for working as a ground water cut off between the lower aquifer and the excavation shaft the plug will work as a structural improvement of the passive resistance of the secant pile wall as well, functioning as an extra strut level.

Some explicitly stated performance criteria exist concerning the required material strength, unit weight, permeability and the pull-out resistance of the micropiles to ensure the fulfilment of the uplift equilibrium (Bygghandling 2019-11-05b). These are compiled in Table 9 and are the section *Korsvägen* conclusions about what properties that are needed for the jet grout.

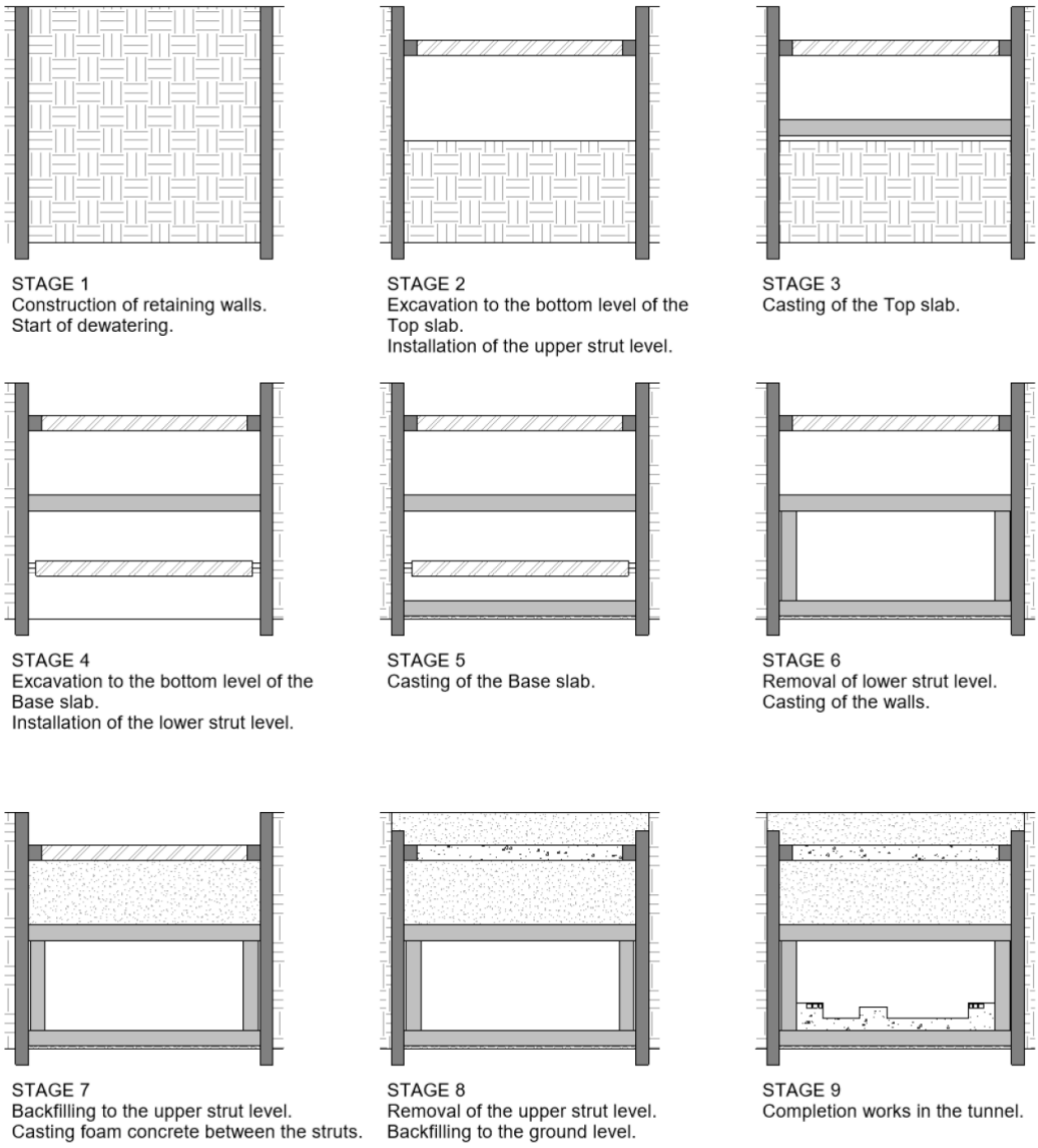

Figure 19. The execution sequence (RKFM 2019-04-30).

Table 9. Properties wanted of the jet grout material.

Jet grout material	**Unit weight.** γ_{JG} **[kN/m³]**	**UCS** $f_{m,k}$ **[MPa]**	**Young's modulus,** E **[MPa]**	**Bond strength micropile and jetgrout,** $q_{sk,jet}$ **[kPa]**	**Hydraulic conductivity,** k_{JG} **[m/s]**
Lower bound	16.5	2	400	400	$\leq 10^{-8}$
Upper bound	16.5	10	2000	400	$\leq 10^{-8}$

3.3.1 Hydraulic Conductivity

In the case of *Korsvägen* a value of maximum 10^{-8} m/s is desired for k according to the construction documents for the overall jet grout plug (SU 2019-08-26). The excavation can handle some leakage if the amount of water can be drained, pumped and infiltrated at the same rate. A value for this leakage and a tolerable flow rate is not easy to define as it depends on the drainage and pumping system, but a limit given in different codes of practice is 0.5 l/s over 1000 m^2 (Modoni et al. 2016). For this excavation that would mean a value for k of $5 \cdot 10^{-7}$ m/s.

3.3.2 Bond Resistance Between Micropiles and the Jet Grout Plug/Bedrock

The characteristic bond strength, $q_{\mathrm{sk,jet}}$, between the microplies and the jet grout is to be at least 400 kPa and between the micropiles and the bedrock it is to be at least 1000 kPa.

3.3.3 Stability Criteria

A stability criterion of vertical equilibrium is also central to the construction. This equilibrium must be between the uplift force from the water pressure and the downward forces from the jet grouting plug's self-weight, the secant piles' self-weight, the lateral adhesion interface between secant pile and soil and the micropiles in tension, which transfer load via skin friction/bond between the grouted pile body and the jet grouting plug (Bygghandling 2019-11-05b).

3.3.4 Movements of the Surroundings

An important aspect of the water tightness of the jet grout plug is to not cause settlements to the surroundings due to lowering of the groundwater table. Maximum values of horizontal and vertical movements of adjacent buildings are set to values between ± 5 mm to 20 mm and tilt to $0.1 - 0.2\%$ (RKFM 2019-05-24 and RKFM 2019-10-23).

3.3.5 Testing and Quality Control of the Requirements

The supervision, testing and monitoring of the jet grout plug and its performance requirements is to be in accordance with EN12716, chapter 9 (described more thoroughly in Section 2.5). The permeability of the excavation system (jet grout plug and secant piles) is important to be monitored. This is to be done through piezometric readings of levels just outside the site. The testing should focus on the water tightness of the jet grout plug as this is the part facing the lower aquifer, while the secant pile walls are facing clay, which is much less permeable. Verification of the water tightness will be done during the execution of the jet grout plug as a part of the quality assurance system by the jet grout subcontractor for verticality and diameter for each column. This enables additional columns where defects have been recorded. Monitoring wells are to be installed both inside the excavation pit and outside the retaining walls. They are to be installed in all aquifers and in the bedrock as there can be fractured zones. To keep the piezometric levels stable possible infiltration wells will be placed outside the retaining walls to be used if necessary (RKFM 2019-05-24).

Preliminary field tests are to be performed according to SS-EN12716 to cover the jet grout treatment in the relevant soil layers. These tests shall document if the performance requirements stated in Table 9 are fulfilled with the adopted methodology and parameters. The micropiles are also to be tested by preliminary field tests, according to EN14199 as static load tests, to assure the fulfilment of bond performance (SU 2019-08-26).

4 Analytical Calculations

Analytical calculations were performed for the ultimate limit state (ULS) using partial safety factors according to Eurocode. The calculations were performed for the jet grouted bottom plug and not for the secant pile walls or the struts. This was considered out of scope for this thesis work as it was the jet grout plug that was of interest here.

4.1 Possible Failure Modes for the Jet Grouted Bottom Plug

Modoni et al. (2016) presented a design method for jet grout plugs in their article "Design of Jet Grouted Excavation Bottom Plugs" where they take into consideration the defects and variation of the jet grouted columns. The three checks that needs to be performed on a jet grouted bottom plug according to the authors were:

1. Uplift equilibrium, of the jet grout plug and/or of the whole structure
2. Structural performance of the jet grouted plug
3. Water inflow through possible imperfections of the jet grouted mass

Checks 1 and 2 were divided into the failure situations seen in Figure 20. These were calculated and the complete calculations can be found in Appendix D – Analytical Calculations: Safety Factors. For check 3, the water inflow and the permeability of the plug were checked with MATLAB calculations described in section 4.2. The calculated safety factors for each studied situation, (a)−(c) below, are presented in the Results.

(a) *Overall uplift failure.* Water pressure lifts the whole structure upwards. The downward forces of the self-weight of the jet grout plug, the retaining walls and the friction force of the shear strength at the interface between the retaining walls and the soil as well as the micropiles' tension force are not enough.
(b) *Plug uplift failure.* Water pressure lifts the plug up because of insufficient self-weight and insufficient shear strength between the plug and the retaining walls and not enough micropiles or lack in the bond between micropiles and the other structures.
(c) *Structural failure of the plug*. Failure due to bending as the plug is too slender and jet grouted material has (almost) zero tensile strength (due to cracks in the material).

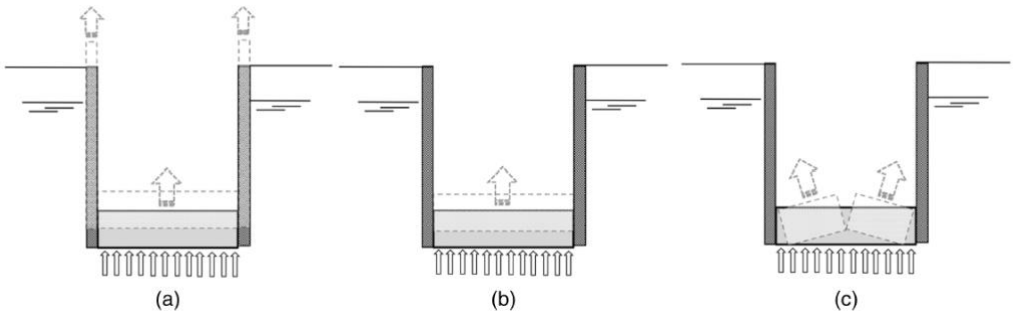

Figure 20. Failure situations for the jet grout bottom plug (Modoni et al. (2016).

The plug also resists horizontal forces and works as an extra strut level. However, when the primary function of the plug is to be a water barrier the function as a strut is considered secondary. As described in section 2.4.1, the plug should work as the whole ground is grouted and the compression resistance is high in soilcrete.

4.2 Permeability

It was of great interest to examine how large the water flow through the jet grout plug would be and that demanded knowledge of the amount of not treated material in the jet grout plug. Soilcrete, as well, has some permeability but since this is a temporary construction the soilcrete was regarded as an impermeable material. Seepage was assumed to occur only through the untreated portions of the plug since the permeability is much higher in untreated friction soil compared to the jet grouted material (Modoni et al. 2016). Eventually water will also flow through the grouted material but after the excavation is finished the sealing will be done by other means of waterproof linings.

It is not possible to calculate exactly how large portion of the treated plug that has or has not been treated and hence the exact waterflow through the plug. In this thesis, probabilistic methods were used to estimate the possible waterflow due to imperfections in the jet grout plug. The method used was developed in a previous master thesis by Brinck and Stigenius (2019). The method is based on Monte-Carlo simulations for estimating the area of untreated material using the parameters that mainly affects the geometry of jet grout columns. The resulting untreated area was then used to estimate possible waterflow with help of Darcy's law. Brink and Stigenius (2019) implemented the analytical calculation in a MATLAB code. They stressed that the model has not been validated with the three cases that they used to compare their MATLAB results with, but that the model can be used as an estimation tool.

The parameters needed for the MATLAB calculation were the mean value and standard deviation of the position, inclination and diameter of the columns. The values used in this thesis are presented in Table 10. The mean diameter of the columns was chosen to be the same as the recommended diameter from construction documents, 1.8 m and the standard deviation of the diameter is approximately 10 % = 0.18 m. The parameters of the position and the inclination of the columns were evaluated from Croce et al. (2014), the same way as Brinck and Stigenius (2019) did it.

Table 10. Input stochastic variables for the permeability analysis made with MATLAB.

	Position [m]	**Diameter [m]**	**Inclination [rad]**
Mean value, μ	$\mu_{\mathrm{p}} = 0.038$	$\mu_{\mathrm{d}} = 1.8$	$\mu_{\mathrm{i}} = 0.005$
Standard deviation, σ	$\sigma_{\mathrm{p}} = 0.02$	$\sigma_{\mathrm{d}} = 0.18$	$\sigma_{\mathrm{i}} = 0.0025$

To get the water flow, [m^3/s], through the jet grout plug Darcy's law was used:

$$\boldsymbol{Q = k \cdot A \cdot \frac{dh}{dL}} \quad \textbf{(4)}$$

where,
k = hydraulic conductivity [m/s] for the untreated soil. The jet grouted material was considered impermeable compared to the soil.
A = area [m^2] (in this case the untreated area calculated from the MATLAB code with 80 % certainty)
$\frac{dh}{dL}$ = hydraulic gradient [m/m] (in this case = 1 as the difference in pressure head through the jet grout plug is the same as the height of the jet grout plug)

The input data that were used in the MATLAB code apart from the parameters in Table 10 are presented in Table 11. The centre-to-centre distance of 1.4 m was recommended in one construction document (RKFM 2019-10-23) but that was also altered in the calculations to get a k that satisfied the code of practice $5 \cdot 10^{-7}$ m/s (Modoni et al. 2016) and the project's required value of 10^{-8}. The calculations and results can be seen in Appendix F – Analytical Calculations: Hydraulic Conductivity and Results respectively.

Table 11. Input data used in the MATLAB code.

Parameter	Value
Column depth (top)	20 m
Column depth (bottom)	20 + 5 m
Centre to centre distance	1.4 m
Number of columns in x-direction	15*
Number of columns in y-direction	72**

**21 m wide plug/1.4 m=15*
***100 m long plug/1.4 m=72*

5 Finite Element Analysis – PLAXIS 2D

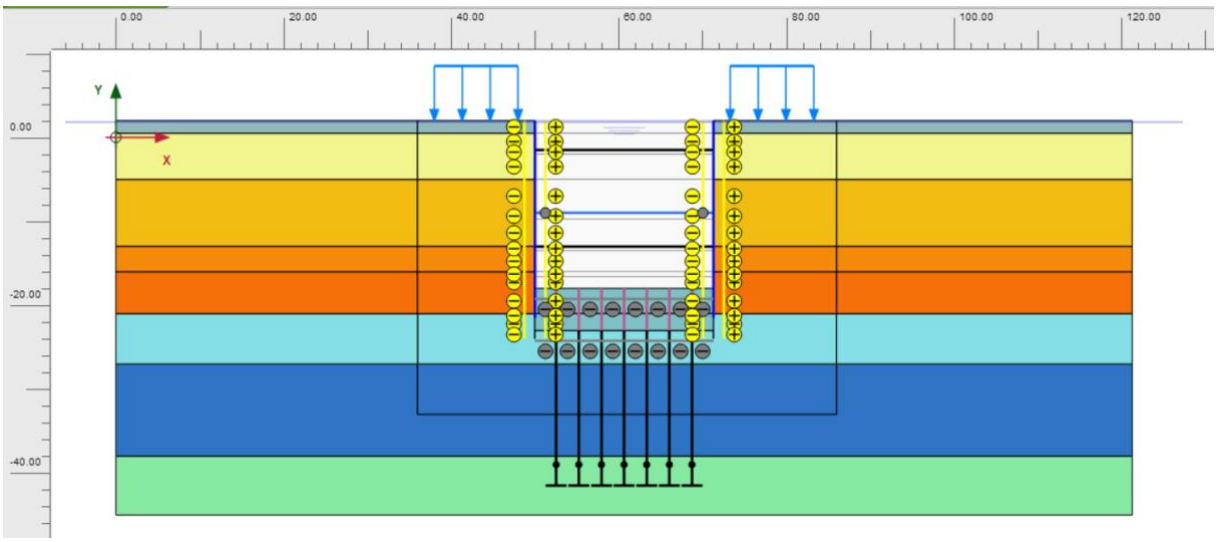

Figure 21. A picture of the PLAXIS model in the last phase of staged construction.

A finite element analysis, FEA, has been performed using the commercial software PLAXIS 2D to analyse and study the design of section *Korsvägen*. With a numerical analysis it is possible to capture the SLS as well as confirming the ULS of the construction system. The PLAXIS model (Figure 21) was built as a 2D, plain strain model as the excavation is much longer than the width of it.

The purpose of the analysis must be defined in order to choose appropriate soil models and this is described in the following chapters. Different soil models can also be used for the same soil to capture different phenomena such as deformations and time effects. The two soil models used for the clay in this thesis were the NGI-ADP model and the Soft Soil (SS) model.

The simulations were also performed with different values of some of the parameters, for example the hydraulic conductivity and the cohesion of the jet grout as well as the removal of some/all micropiles. This was performed to test the construction's sensibility for error as one cannot guarantee a perfectly grouted plug.

The results from the simulations herein were compared to the results from the PLAXIS simulations made in project section *Korsvägen* (only a NGI-ADP model was made in the project's simulations) where these exist and are relevant and everything is presented in chapter 6 Results –
PLAXIS 2D.

5.1 Water Conditions

The ground water table was set to level +1.8 m for the fill, which is the upper aquifer, and the four clay layers. In the lower aquifer there is a higher pore water pressure of +3.5 m which was set for the silty sand and the moraine layer.

For each excavation stage the water level was lowered to the surface in the excavation pit and the water conditions were interpolated from the surface level in the excavation pit and down 2 to 3 meters.

In the SS model's third excavation stage the ground water level in the excavation pit was instead set to the same level as the top of the jet grout plug to simulate that relief wells were installed all the way to the top of the jet grout plug. Also, in this stage the jet grout plug's water condition was interpolated between the top of the jet grout plug and the lower aquifer.

5.2 Clay Parameters

The clay layers were modelled as NGI-ADP materials and as SS materials in two different simulations. The NGI-ADP is a total stress model and that uses the anisotropic undrained shear strength as a direct input. This model was used for obtaining safety factors and checking the structural capacity in the ULS. The NGI-ADP model is however limited to short-term analysis as it cannot take time effects into consideration such as deformation with time. The SS model was instead used to be able to consider the time effects and to study the consolidating of the excess pore water pressure and long-term settlements. Parameters that were the same in both models are presented in Table 12.

Table 12. Clay parameters used in both the NGI-ADP and Soft Soil model.

Property	Clay 1	Clay 2	Clay 3	Silty clay
Specific weight, γ [kN/m³]	14.7	15.0	15.0	18.7
Coefficient of earth pressure, K_0 [-]	0.76	0.60	0.59	0.57
Hydraulic conductivity [m/day]	$3.4 \cdot 10^{-5}$	$7.3 \cdot 10^{-5}$	$8.6 \cdot 10^{-5}$	$8.6 \cdot 10^{-5}$

5.2.1 Clay Parameters in the NGI-ADP Model

The clay soil was thoroughly examined both in field and with laboratory tests. To make sure that the parameters used in the PLAXIS model coincide with the reality, simulated soil tests were performed in PLAXIS and compared to the results from different laboratory tests. For the NGI-ADP model the stiffness parameters $\frac{G}{s_u^A}$, $\gamma_f^C, \gamma_f^E, \gamma_f^{DSS}$ were the ones altered to make the PLAXIS soil test coincide with the laboratory results. Other parameters remained the same as the ones from the project section *Korsvägen*.

All the parameters of stiffness and strength are shown in Table 13 and Table 14, which were used in the PLAXIS model. The soil test settings and how these results were reached can be seen in Appendix B – Soil Tests for NGI-ADP . The stiffness parameters that were used in project section *Korsvägen* that differ from the selected ones in this thesis are also presented in Table 14 (inside parentheses).

Table 13. Parameters of strength for NGI-ADP model (Undrained C).

Layer	Level top	Level bottom	Ref level	s_u^A [kPa]	$s_{u,inc}^A$ [kPa]	s_u^P [kPa]	s_u^P/s_u^A [kPa]	s_u^{DSS} [kPa]	s_u^{DSS}/s_u^A [kPa]
Clay 1	0.5	−5	0	23	0	12.19	0.53	14.95	0.65
Clay 2	−5	−13	−5	23	1.5	12.19	0.53	15.87	0.69
Clay 3	−13	−16	−13	35	1.4	19.25	0.55	24.15	0.69
Silty clay	−16	−21	−16	39.2	1.4	21.56	0.55	27.05	0.69

Table 14. Parameters of stiffness and other soil parameters for NGI-ADP model (Undrained C). Values inside parentheses are values from project section Korsvägen.

Layer	OCR	$\frac{G}{s_u^A}$	γ_f^C [%]	γ_f^E [%]	γ_f^{DSS} [%]	τ_0/s_u^A (mid layer)
Clay 1	2	150 (600)	3 (1.5)	6 (3)	5 (2)	0.1427
Clay 2	1.3	150 (600)	3 (1.5)	6 (3)	5 (2)	0.398
Clay 3	1.25	150 (600)	3 (1.5)	6 (3)	5 (2)	0.4752
Silty clay	1.2	150 (600)	3 (1.5)	6 (3)	5 (2)	0.5713

A lower value of $\frac{G}{s_u^A}$ was selected in this thesis compared to the one used in the project section *Korsvägen*. This was because of the better fitting when comparing the laboratory values and the PLAXIS soil test simulations. Furthermore, this value (150) is better to use in the modelling of the deformations that will occur behind the secant pile walls as G is affecting mainly the elastic state of the soil. Whereas the higher value will work well for the modelling of the unloading at the excavation bottom as this has to do with heave and G is mainly affecting the elastic state of the soil. This also depends on whether there is clay under the jet grout plug or if the jet grouting goes down into the moraine layer. The pre-investigations show that the plug will in fact go down to friction soil and in that case the clay properties is of no interest in this case as there will be no clay there.

Furthermore, the selected stiffness parameters are also different from the one calibrated in the project section *Korsvägen*. These values seen in Table 14 are similar with results obtained from the project section *Centralen* (one other section of the *West Link project*) and are reasonable values of Gothenburg clay (Design-PM 2019-02-12).

The clay layers were all set as "Undrained C" in the model except for the initial phase of the staged construction where the clay materials need to be set to "Drained". This is because as "Undrained C" at that phase, the total stress is equal to the effective stress and the initial shear stress will be larger than the input undrained shear strength.

5.2.2 Clay Parameters in the Soft Soil Model

For the SS model some different parameters were needed, and these are compiled and presented in Table 15. The calibration of the parameters was done with soil tests in PLAXIS and the procedure and calculations are thoroughly explained in Appendix A – Calculation of Friction Angles in Clay and Appendix C –Soft Soil (SS) Parameters.

Table 15. Properties for the clay layers in the Soft Soil model.

Property	Clay 1	Clay 2	Clay 3	Silty clay
λ^*	0.15	0.16	0.30	0.30
κ^*	0.01	0.022	0.03	0.025
Cohesion, c' [kPa]	6.0	2.0	5.0	8.0
Friction angle, ϕ' [°]	34	35	29	26

5.3 Friction Soil Parameters

The fill material and the friction soil separating the clay layer and the bedrock were all modelled as Mohr-Coulomb materials. That is an isotropic linear-elastic perfectly plastic model. The drained type was selected as "*Drained*" as it was assumed that little excess pore pressure builds up during volume changes due to the high *k* of these materials.

The friction soil parameters, compared to the clay material, all rely more on empirical values and therefore no calibration of these were made in PLAXIS. In Table 16 the Mohr-Coulomb model parameters used in PLAXIS are presented for each friction soil layer, all with the drainage type "*Drained"*.

Table 16. Mohr-Coulomb parameters for the friction soils.

Layer	ρ (sat) [kN/m³]	c' [kPa]	ϕ' [°]	ψ' [°]	E' [kPa]	v' [-]	$k_x = k_y$* [m/d]	R [-]	K_0 [-]
Fill	17 (18)	0	35	0	30 000	0.3	0.6	0.7	0.4264
Silty sand	18 (19)	0	31	0	25 000	0.33	0.6	0.7	0.4850
Moraine	20 (21)	0	35	0	35 000	0.3	0.6	0.7	0.4264

**Default-values from PLAXIS.*

5.4 Jet Grout Parameters

The jet grout treated part of the soil was modelled using the Mohr-Coulomb model. Certain parameters need to be set for a Mohr-Coulomb model, and these are presented in Table 17. These parameters were gotten from the previously mentioned articles in section 2.3 about material properties and were therefore considered reasonable. In the PLAXIS models the lowest values of E and tensile strength, f_t, were used to be sure of not overrating the construction.

The jet grout material was set as non-porous when modelled in the NGI-ADP model. In the SS model it was modelled as porous. When the jet grout is modelled as porous the ground water parameters is of importance. *k* was set to 0.2886 m/day which was the value calculated with the probabilistic method for the proposed design from the project section *Korsvägen* with 1.4 m centre-to-centre distance. However, a simulation was also made with the recommended *k* from *Korsvägen* = $8.64 \cdot 10^{-4}$ m/day to compare how sensitive the jet grout plug construction is to change in permeability.

The sensitivity of the jet grout plug structure was also tested with the change of its *c*. Both the NGI-ADP and the SS model was also simulated with half c (=500). The SS model was furthermore run with ϕ of the jet grout set to 35° and the ψ set to 5°.

Table 17. Parameters for jet grout material used in PLAXIS.

Property	Value
γ_{JG}, unit weight [kN/m^3]	16.5
E, Young's modulus [MPa]	400 (to 2000)
υ, Poisson's ratio [-]	0.2 (same as for concrete)
c', cohesion [kPa]	1000 (also 500)
ϕ', friction angle [°]	0.1 (SS also 35)
ψ, dilatancy angle [°]	0 (SS also 5)
f_t, tensile strength [kPa]	100 (to 800) (1/10 of UCS/2)
$k_x = k_y$, hydraulic conductivity [m/day]	0.2886 (also $8.64 \cdot 10^{-4}$)*
K_0 [-]	0.8

**for the NGI-ADP model this does not matter as the material is set to non-porous.*

5.5 Interfaces Jet Grout Plug and Secant Pile Wall

A special interface was modelled between the jet grout plug and the secant pile wall and its properties are presented in Table 18 for the NGI-ADP model and Table 19 for the SS model. In the SS model, a special interface was also created for the secant pile walls facing the soil and its properties are presented in Table 20.

Table 18. Interface properties for the NGI-ADP model.

Property	Value
E, Young's modulus [MPa]	50*
c', cohesion [kPa]	500
ϕ', friction angle [°]	0
ψ, dilatancy angle [°]	0

**Assuming the jet grout close to the secant pile walls is a success.*

Table 19. Interface properties between jet grout plug and secant piles for the SS model.

Property	Value
E, Young's modulus [MPa]	50*
c', cohesion [kPa]	0
ϕ', friction angle [°]	25
ψ, dilatancy angle [°]	0
$k_x = k_y$, hydraulic conductivity [m/day]	$8.64 \cdot 10^{-4}$
K_0 [-]	0.6

**Assuming the jet grout close to the secant pile walls is a success.*

Table 20. Interface properties for the secant pile wall facing the soil in the SS model.

Property	Value
E, Young's modulus [MPa]	10
c', cohesion [kPa]	1
ϕ', friction angle [°]	25
ψ, dilatancy angle [°]	0
$k_x = k_y$, hydraulic conductivity [m/day]	$8 \cdot 10^{-4}$
K_0 [-]	0.6

5.6 Secant Pile Walls

The secant pile walls were set as an elastoplastic, isotropic material with properties presented in Table 21. Elastoplastic was set to most of the structures in the model, making it possible for them to reach failure.

A varying amount of reinforcement bars was used in different sections of the secant pile wall. The chosen capacity for PLAXIS calculations was 5400 kNm/secondary pile, and to get the value needed in PLAXIS, this was divided with 1.8 since this is the c/c-distance between the reinforced piles. This moment capacity is high and guarantees that the supporting wall does not fail. This was desired as the focus is set to the jet grout plug as the weak link.

Table 21. Properties of the secant pile walls.

Property	Value
c/c between reinforced/secondary piles [m]	1.8
E, Young's modulus [GPa]	35
A, area [m²]	1.2
w [kN/m/m]	20.4
EI [kNm²/m]	$5.04 \cdot 10^6$
v, Poissons ratio [-]	0.2
M_p, moment capacity [kNm/m]	3 000
N_p, axial force capacity [kN/m]	40 000

5.7 Top Slab

The top slab was set as an elastoplastic, isotropic material and its properties are presented in Table 22. Also, in this case the moment capacity is somewhat high, but again, the top slab is not the construction part of interest.

Table 22. Properties of the top slab.

Property	Value
E, Young's modulus [GPa]	35
A, area [m²]	1.5
w [kN/m/m]	37.5
EI [kNm²/m]	$9.844 \cdot 10^6$
v, Poissons ratio [-]	0.2
M_p, moment capacity [kNm/m]	4 000
N_p, axial force capacity [kN/m]	40 000

5.8 Steel Struts

The steel struts were also set to an elastoplastic material with properties presented in Table 23.

The maximum axial force, $F_{\max}$, the struts can take, also called the critical load, was calculated with Euler's formula:
$F_{\max} = \frac{\pi^2 EI}{(KL)^2}$ and Eurocode's buckling curves and reduction factors.
In this case:
I (area moment of inertia) $= \frac{\pi}{64}(D_{\text{outer}}^4 - D_{inner}^4) = 0.007395$ m⁴
Where ($D_{\text{outer}} = 1$ m, $D_{\text{inner}} = 0.96$ m)
K(column effective length factor) $= 1$
L (unsupported length of struts) $= 21$ m
$F_{\max} = 33\,100$ kN
With reduction factors according to Eurocode, $F_{\max} = 17\,000$ kN

Table 23. Properties of the steel struts.

Property	Value
E, Young's modulus [GPa]	200
t_p, pipe thickness [m]	0.02
A, area [m²]*	0.0616
D, diameter [m]	1
$L_{spacing}$, distance between struts [m]	5
$F_{max,tens/comp}$, max axial force [kN]	17 000

* $A_{outer} - A_{inner}$

5.9 Micropiles

The micropiles were represented as three different materials in the PLAXIS simulations. One material for the part inside the grout body in connection to the jet grout body, one for the part in soil and one for the part embedded in the bedrock. An assumption was made that there were no friction in the soil which was why the micropiles were modelled as separate parts. The part of the micropile embedded in the grout body was assumed to be the weak link and therefore the properties of the part in the bedrock were assumed to be much better.

5.9.1 Micropiles in Grout Body

The micropiles part inside the jet grout plug was modelled with embedded beams elements in PLAXIS. The material type was set to elastic and the predefined beam type to a massive circular beam. The maximum capacity was limited at the skin resistance between the grout body and jet grout plug. Its properties can be seen in Table 24.

Table 24. Properties of the micropiles in grout body.

Property	Value
E, Young's modulus [GPa]	20
D, diameter [m]	0.15
$L_{spacing}$, distance between micropiles [m]	2.6
T_{skin}, axial skin resistance [kN/m]	270

5.9.2 Micropiles in Soil

The micropiles part inside the deep soil layers was modelled as node-to-node anchors elements in PLAXIS. The material type was set to elastoplastic and the material properties (Table 25) are taken from a data sheet of GEWI PLUS BAR 670/800 57,5 (as suggested in construction documents).

Table 25. Properties of the micropiles in soil.

Property	Value
E, Young's modulus [GPa]	200
A, area [m²]	0.0026
$L_{spacing}$, distance between micropiles [m]	2.6
$F_{max,tens/comp}$, max axial force [kN]	2 080

5.9.3 Micropiles in Bedrock

The micropiles in the bedrock were modelled as fixed end anchors in PLAXIS with the material type elastoplastic. Its properties are presented in Table 26.

Table 26. Properties of the micropiles in bedrock.

Property	Value
E, Young's modulus [GPa]	20
A, area [m²]	0.01767
$L_{spacing}$, distance between micropiles [m]	2.6
$F_{max,tens/comp}$, max axial force [kN]	400

5.10 Mesh

The model in PLAXIS was built with 15-noded elements. The mesh was generated with expert settings with the relative element size = 0.5 and element dimensions = 3.903 m. The quality of the mesh was checked and can be seen in Figure 22 where 1 is the best and 0 is the worst, and for the most interesting parts of the construction the quality was good.

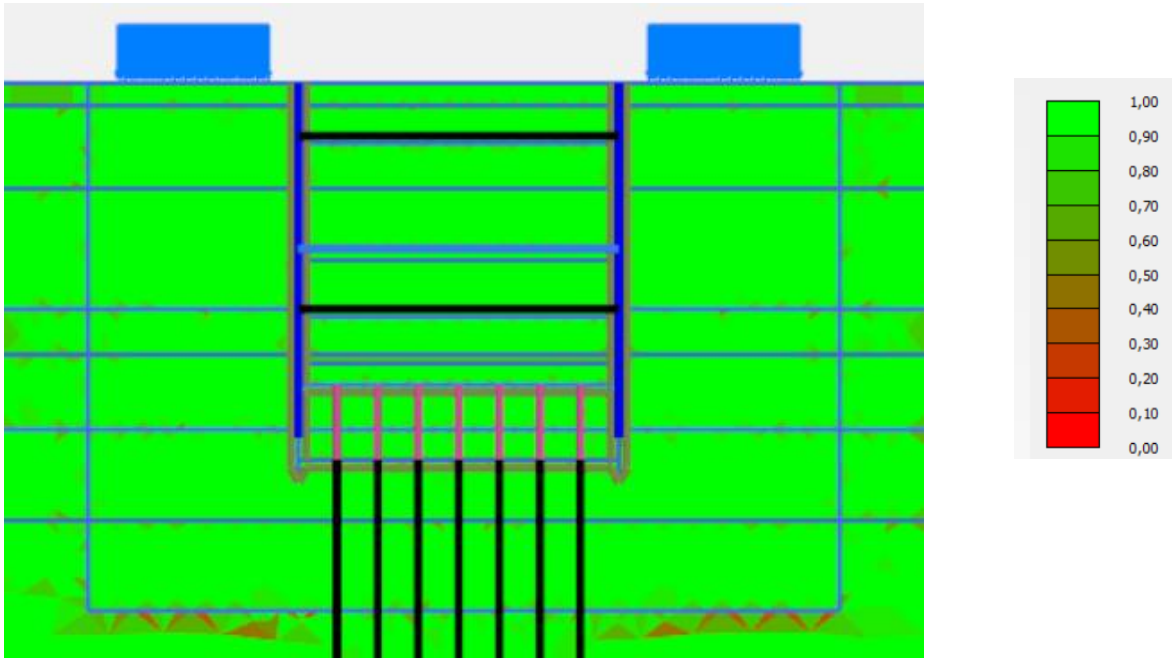

Figure 22. Quality of the mesh where 1 is the best.

5.11 Time Intervals in the Soft Soil Model

In Table 27 the estimated time intervals for each construction stage are presented. The time per phase was estimated with experience from the West Link project section *Centralen* (Yannie 2020).

Table 27. Time intervals in the SS model.

Construction phase	Time [days]
Initial phase	0
Surface load and wall installation	30
Installation of jet grout plug and anchors	60
Excavation to level −2	7
Installation of first strut	7
Excavation to level −10	14
Installation of top slab	45
Excavation to level −13	7
Installation of second strut and open flow to excavation bottom	7
Excavation to level −18	14
Open excavation one year	360

6 Results

This section presents the results from the analytical and numerical calculations for the jet grout plug capacity in ULS and performance in SLS.

6.1 Analytical Calculations

The safety factors calculated for different failure situations based on the method proposed by Modoni et al. (2016) are presented in Table 28 and the calculations in Appendix D – Analytical Calculations: Safety Factors.

Table 28. Safety factors for different failure situations.

Failure situation	Safety factor, SF
(a) Overall uplift failure	1.11
(b) Plug uplift failure	1.75
(c) Plug's structural failure*	0.78

**Calculated with no regard to the micropiles that also helps retaining the plug.*

6.1.1 Hydraulic Conductivity

The hydraulic conductivity, k, in the jet grout plug calculated for different centre-to-centre distances using the method proposed by Brinck and Stigenius (2019) are presented in Table 29. These can be compared with the code of practice value of $5 \cdot 10^{-7}$ m/s and from the project requested value of 10^{-8} m/s. The MATLAB code and the calculations are to be found in Appendix E – MATLAB Code and Appendix F – Analytical Calculations: Hydraulic Conductivity.

Table 29. Results from hydraulic conductivity calculations.

Centre-to-centre distance [m]	k [m/s]
1.4	$3.34 \cdot 10^{-6}$
1.3	$7.36 \cdot 10^{-7}$
1.2	$1.01 \cdot 10^{-7}$
1.1	$9.52 \cdot 10^{-9}$

6.2 PLAXIS 2D

In PLAXIS the two different soil models were used for the clay layers, one using NGI-ADP-parameters for the clay and one using SS-parameters with time effects taken into consideration. The results from these simulations are presented and compared in the following sections. Comparisons with results from previously made simulations in the project section *Korsvägen* before this thesis are also presented where these were found.

6.2.1 Safety Factor

To study the reliability and capacity of the whole system, a safety calculation was performed after each excavation stage. The safety factor, SF, obtained from the safety calculations was plotted against the ground surface displacement (Figure 23 and Figure 24) as well as the displacement at the bottom of the shaft (Figure 25 and Figure 26) for each excavation stage, as these displacements give an indication of the failure mechanism. A parametric study was also performed by changing some of the geometrical and material properties. In this case, the results are also presented for the case where, a) the removal of three micropiles (red curves), b) removal of all micropiles (green curves) and c) the jet grout having reduced its *c* to half = 500 kPa (purple curves).

The figures below show that the NGI-ADP model reached a sufficient SF for the displacement of the ground surface for all excavation stages and different changes in the model (Figure 23). This can be seen as the curves level out at a value over the limit of 1.65. The same is valid for the SS model except for the model run with no micropiles (green curve). In this simulation PLAXIS could not calculate a sufficient SF (Figure 24).

For the displacements of the excavation bottom there was also the model variation with no micropiles (green curve) that does not have sufficient SF in the third and fourth excavation stage (no levelling out of the curves). This is true both for the NGI-ADP model (Figure 25) as well as the SS model (Figure 26). Otherwise there was enough SF with the exception of the third excavation stage in the SS model where all model variations fail in reaching equilibrium, except for the model variation with the recommended *k* where equilibrium was almost reached at a sufficient SF (blue curve Figure 27).

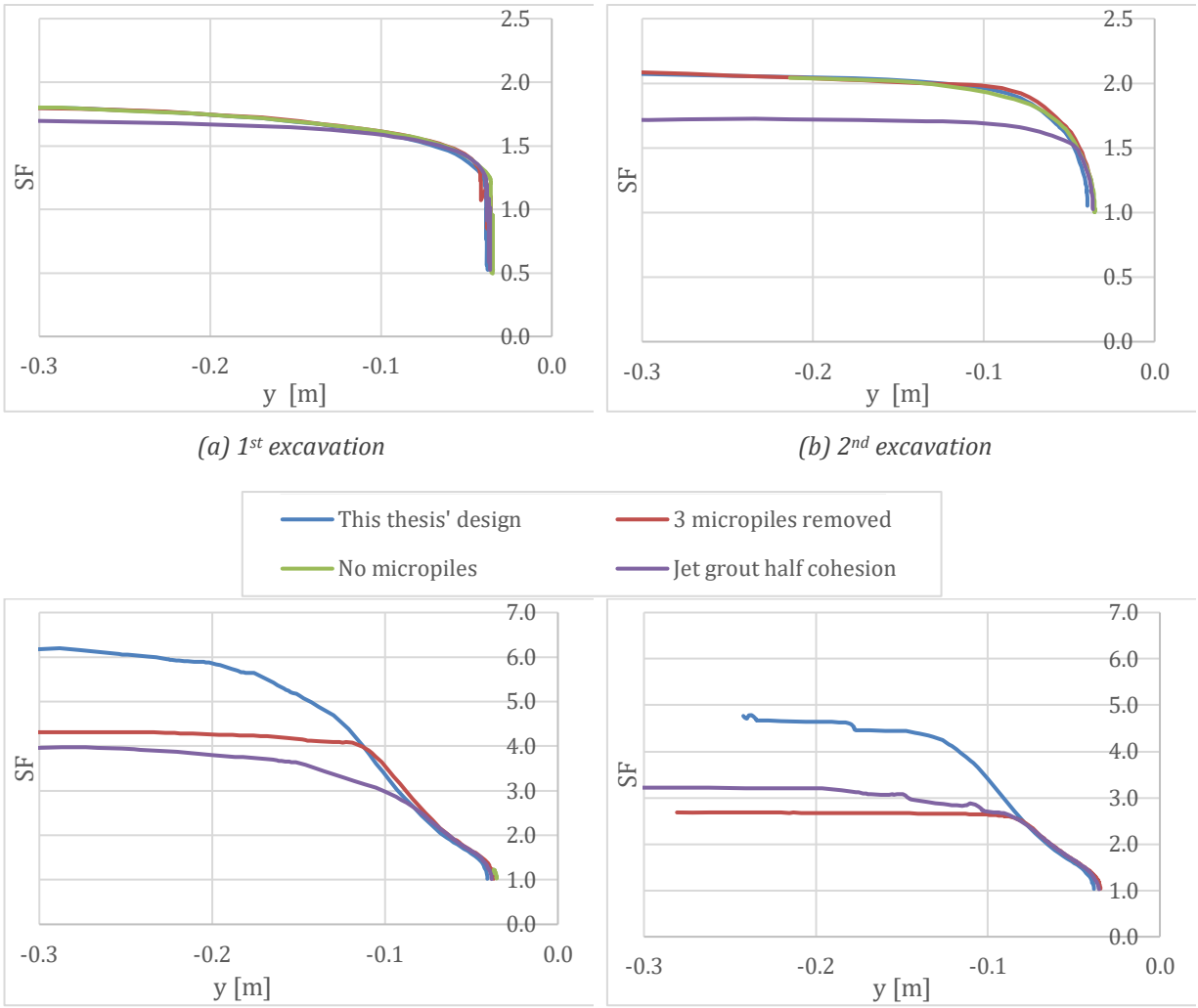

(a) 1st excavation

(b) 2nd excavation

(c) 3rd excavation

(d) 4th excavation

Figure 23. SF for the displacement of the ground surface, y, in the NGI-ADP model.

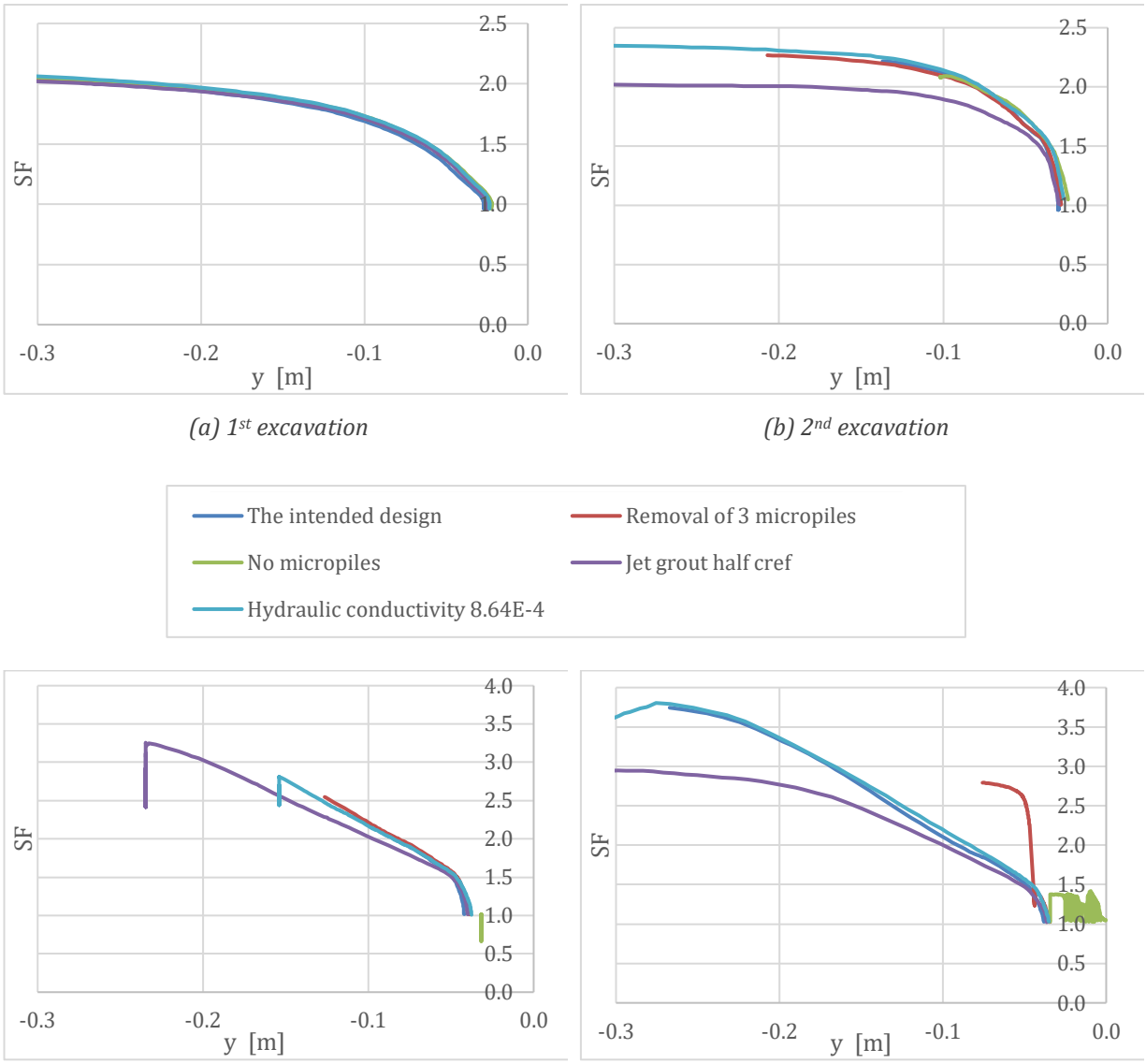

(a) 1st excavation

(b) 2nd excavation

(c) 3rd excavation

(d) 4th excavation

Figure 24. SF for the displacement of the ground surface, y, in the SS model.

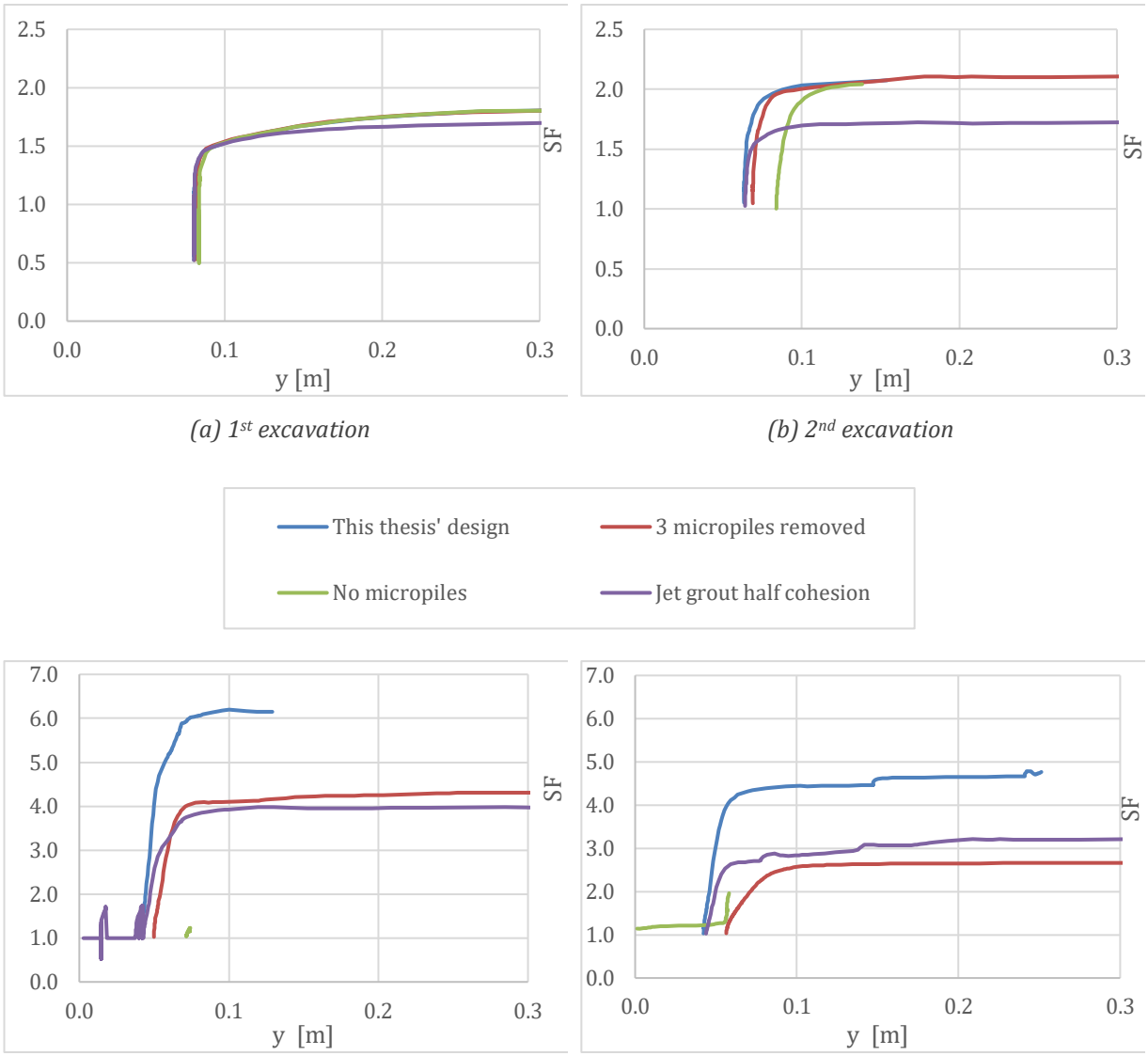

(a) 1st excavation

(b) 2nd excavation

(c) 3rd excavation

(d) 4th excavation

Figure 25. SF for the displacement of the bottom of the shaft, y, in the NGI-ADP model.

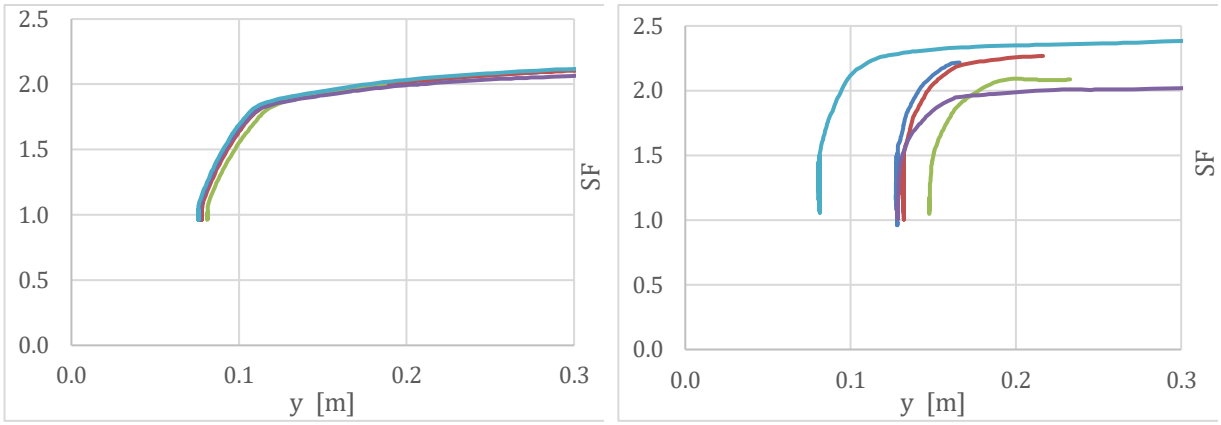

(a) 1st excavation

(b) 2nd excavation

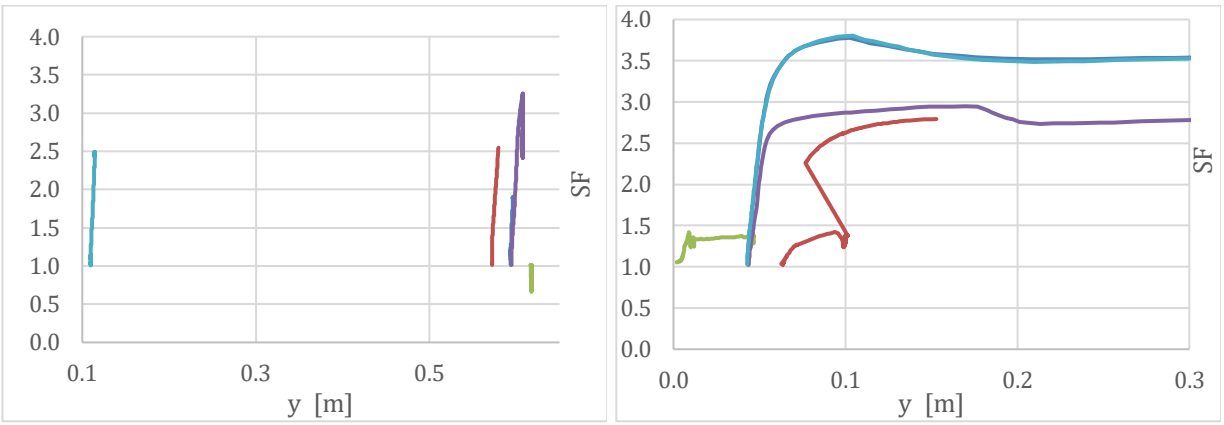

(c) 3rd excavation. NOTE! the scale on the x-axis.

(d) 4th excavation

Figure 26. SF for the displacement of the bottom of the shaft, y, in the SS model.

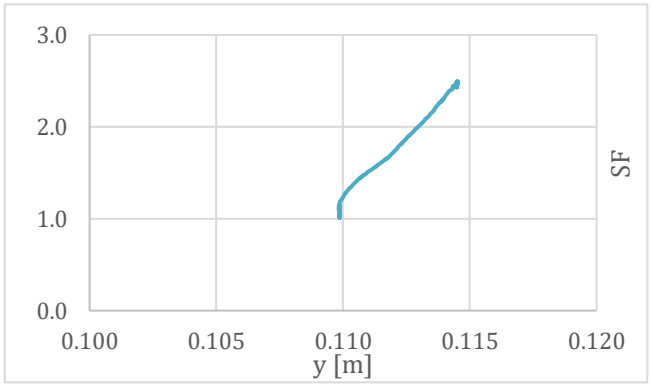

Figure 27. Enlargement of Figure 26 (c).

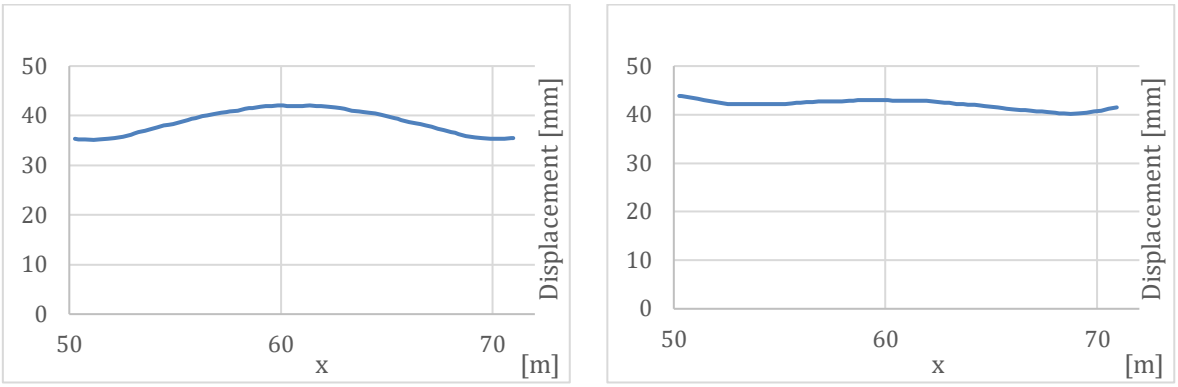

(a) NGI-ADP Model *(b) SS Model*

Figure 28. Displacement of the jet grout plug in the last excavation stage.

6.2.2 Jet Grout Plug

The displacement of the jet grout plug was checked in the models simulated in this thesis and presented in Figure 28. The largest movement was around 45 mm seen in the SS model and they were almost as large in the NGI-ADP model.

6.2.3 Micropiles

In Figure 29 and Figure 30 the displacements of the micropiles are shown. Figure 29 shows the NGI-ADP model at the last excavation step and Figure 30 shows the SS model after one year of open excavation. The different micropiles are represented by the different columns, a-d, in the figures and since it is a symmetrical construction only 4 columns are shown. One can see that it is the largest displacement in the middle column (d). The displacements are between 32 and 38 mm for the NGI-ADP model and around 39, almost 40 mm in the SS model.

Figure 31 to Figure 32 show the axial forces in the micropiles embedded in jet grout. The axial force in the micropiles embedded in the jet grout is calculated with the highest measured value of the axial force from PLAXIS, times the length 5 m of the micropiles, divided by 2. The micropile in the middle takes the largest axial force, around 1000 kN.

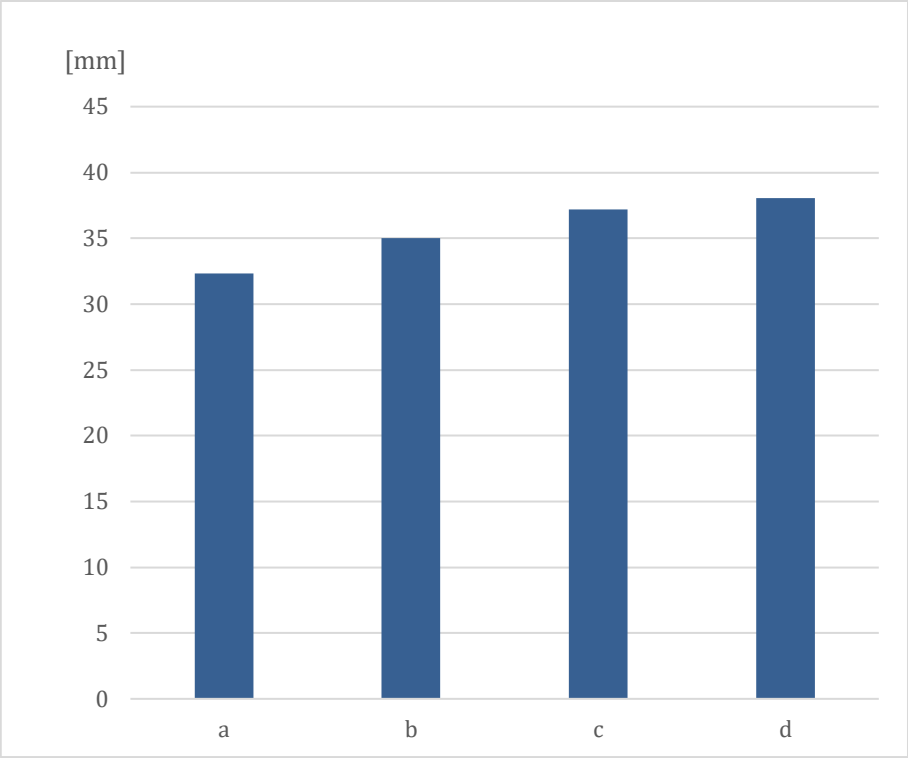

Figure 29. NGI-ADP model. Last excavation step. Displacement of the micropiles in the jet grout plug, where column a-d represents the micropiles.

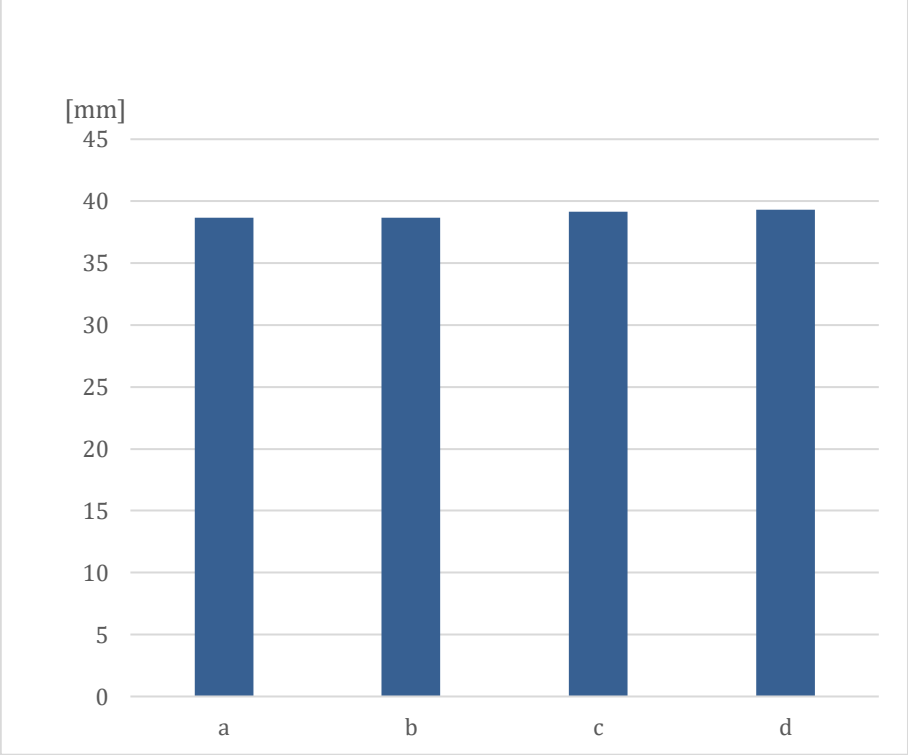

Figure 30. SS Model. Open excavation 1 year. Displacement of the micropiles in the jet grout plug, where column a-d represents the micropiles..

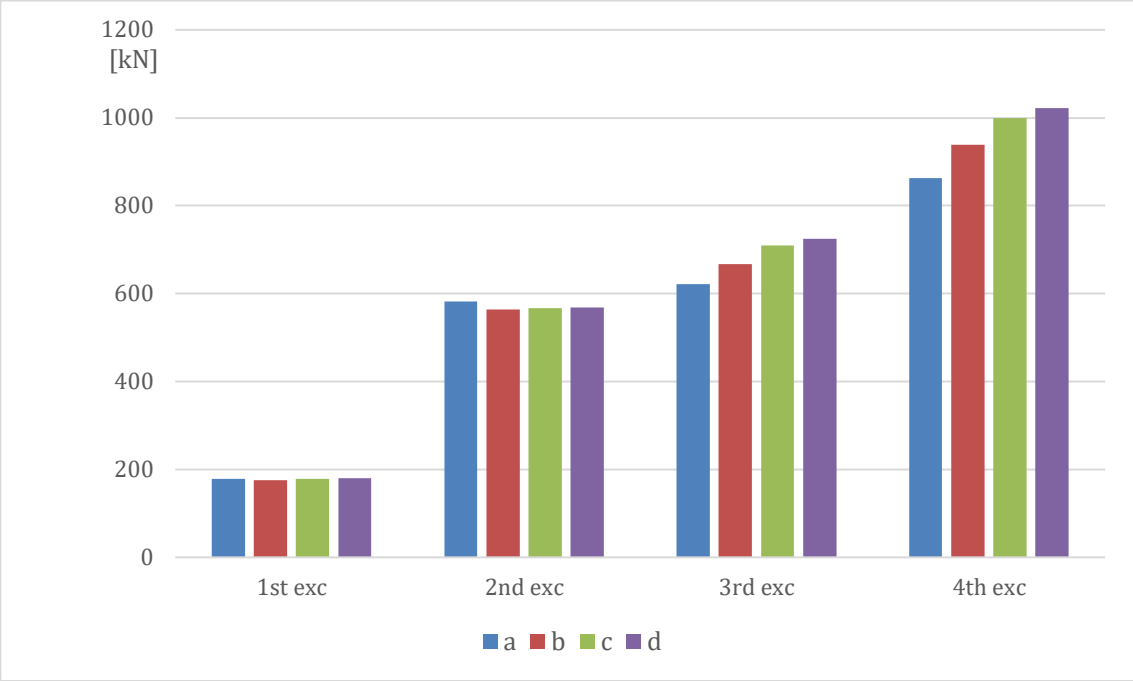

Figure 31. NGI-ADP Model. Axial forces in the micropiles embedded in the jet grout for different excavation stages and for different piles.

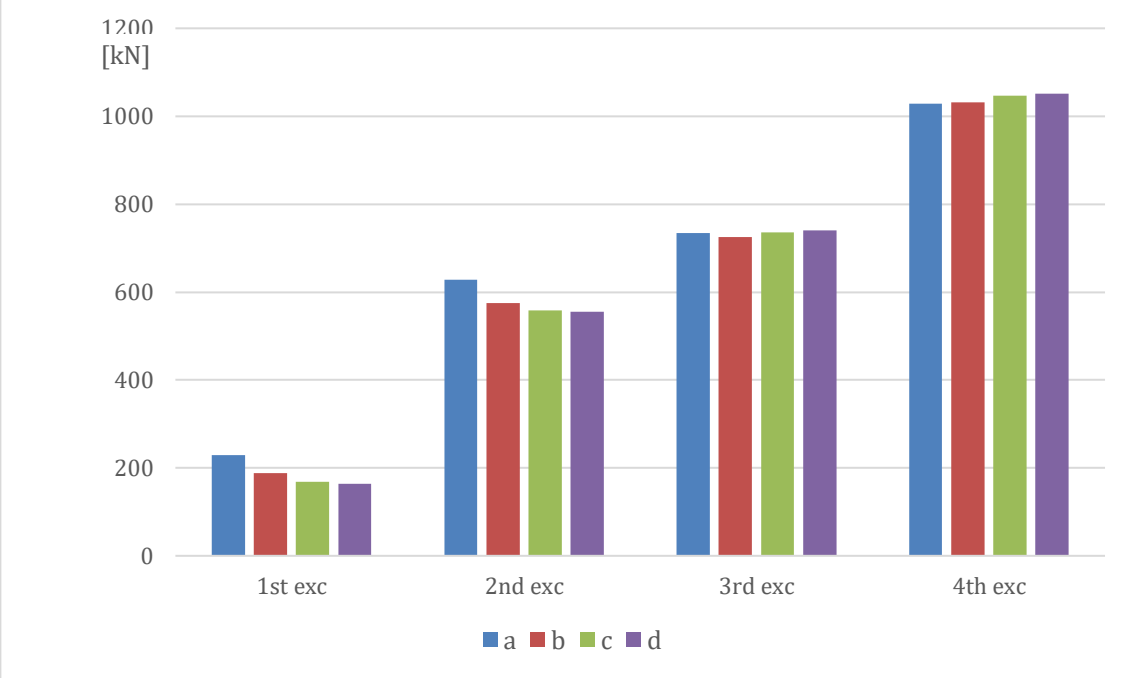

Figure 32. SS Model. Axial force in the micropiles embedded in the jet grout for different excavation stages and for different piles.

6.2.4 Failure by Uplift Check

The failure by uplift check was only done for the SS model as the pore water pressure needed to be considered. To check whether there will be a problem with failure by uplift the pore water pressure was compared with the vertical stress. If the pore water pressure was higher than the vertical pressure from the soil, there is a high risk of failure by uplift. In the stage where the installation of the top slab happens, the pore water pressure is higher than the vertical soil stress, as can be seen in Figure 33 between level −18 and −20, and there is a failure. This is located on top of the jet grout plug and to make this more visible it is possible to look at the tension cut-off points that can be seen in Figure 34. In the next stage, the third excavation stage, the water conditions were altered to have the head at level −18, i.e. an open flow to the excavation bottom. This was to symbolize relief wells being installed and then there are no overlapping of the water pressure curve and no tension cut-off points in the results.

This result is valid even for the model variation that used the recommended value of *k* but one can see somewhat fewer tension cut-off points.

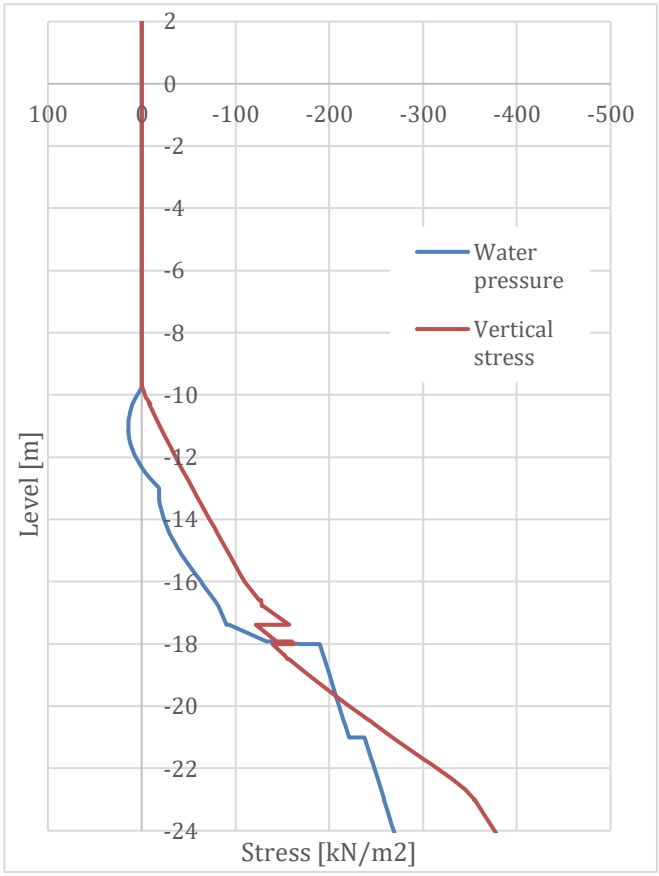

Figure 33. Installation of top slab stage where the pore water pressure is higher than the vertical stress.

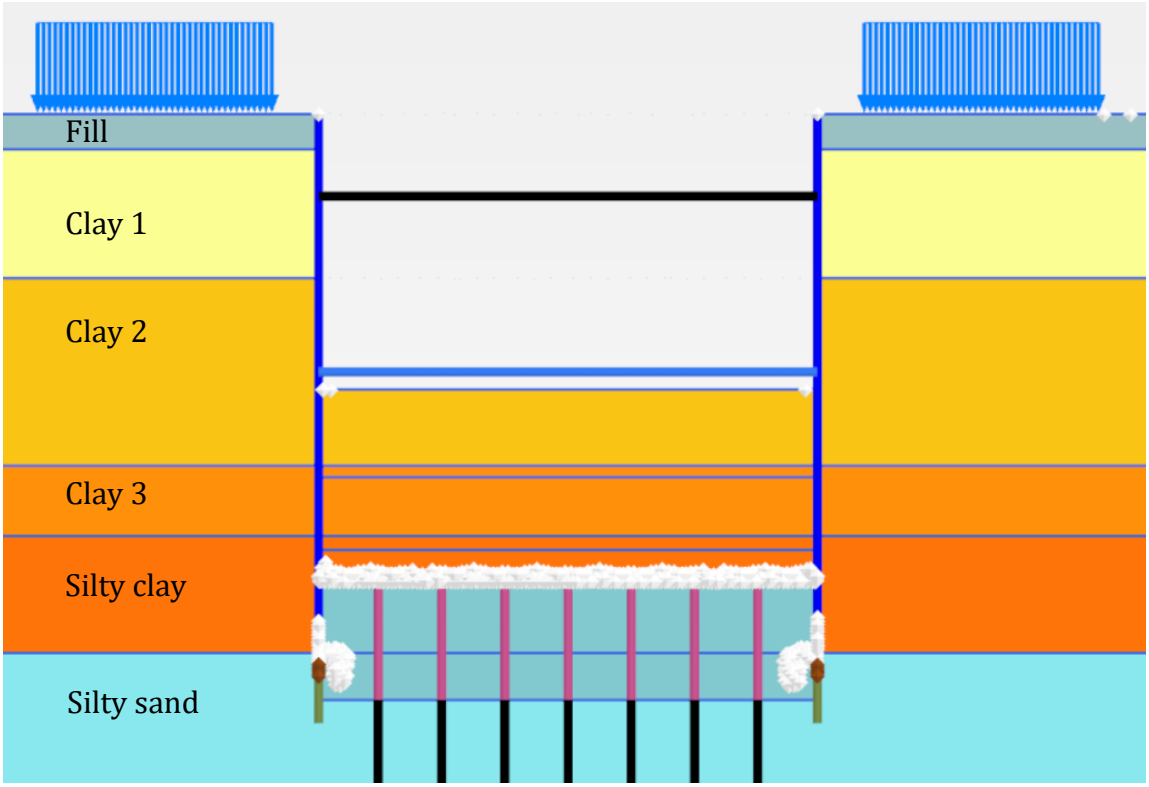

Figure 34. Tension cut-off points at the installation of top slab stage. The points indicate a failure by uplift.

7 Discussion

In this section the results are discussed and the choice of calculations methods and PLAXIS models are discussed and explained.

7.1 Analytical Calculations

The analytical calculations were performed in line with the checks that Modoni et al. (2016) gives in their article "Design of Jet Grouted Excavation Bottom Plugs" since those coincided well with the research questions asked. The calculations could also be performed in line with Eurocode standards.

The calculations gave a SF for the plug´s structural failure of 0.78, much below the limit of 1.65. However, the calculation did not take the micropiles interaction into consideration. In the PLAXIS simulation this interaction had a large impact and therefore the result for the analytical calculation is in this case not taken too much into account. It does however show the importance of the micropiles working sufficiently.

The calculation of the SF for the overall uplift failure also resulted in a result below the limit, 1.1 instead of 1.65. In this case the construction could be made more secure with for example an installation of anchors.

The SF for the plug uplift failure is 1.75 and above the limit. That is not too large of a safety margin, which is good, as that can make a construction unnecessary expensive.

7.2 Hydraulic Conductivity

The value of a jet grout plug's hydraulic conductivity is difficult to calculate as the literature study shows, because of the diameter and alignment often deviate from the intended design. The permeability of the jet grout plug in this study is instead considered using a probabilistic method and a MATLAB model proposed by Brinck and Stigenius (2019). The model has not been entirely validated, as is stressed by the authors themselves, but is used as an estimation tool.

The calculation of the model shows that there will be a leakage through the jet grout plug with 100 % certainty with the intended design of a column diameter of 1.8 m and a centre-to-centre distance of 1.4 m. The calculated amount of leakage through the plug will not even be able to handle with pumping and infiltration according to the code of practice's allowed value. However, with a smaller c/c-distance of 1.2 m, the permeability can be within manageable limits and controlled with relief wells and a pumping and infiltration system.

For a jet grout plug to be a completely watertight construction it requires perfection and that would make it very expensive. This thesis additionally shows that the difficulty with water tightness increases with depth, and the jet grout plug studied in this thesis is to be performed at a depth of more than 20 m from ground level, which is considered a large depth. Hence, a watertight construction in the case studied here is to perceive as impossible and the requirements of 100 % overlap of the jet grout columns cannot be fulfilled.

One of the research questions was how watertight the jet grout plug needed to be for it to work properly. The results show that with enough relief wells there will not be any failure by uplift in the excavation pit. Failure by hydraulic uplift is shown in the PLAXIS model as the water pressure is higher than the vertical stress in excavation stage of the installation of the top slab (Figure 34). This is then managed in PLAXIS modelling relief wells with setting the water conditions to open flow down to the bottom of the pit.

However, despite the failure due to uplift in the PLAXIS model, the simulation can continue because the plug is modelled with some tension strength and in addition the plug is fastened with micropiles to the bedrock. The soil in the pit will nonetheless be unstable and during the real construction work a failure by hydraulic uplift is dangerous and important to investigate.

7.3 Calculations in PLAXIS

The model in PLAXIS showed that it is important with the jet grout material's strength and stiffness parameters for the micropiles to be securely embedded in the grout. The model variations with the removal of some or all micropiles showed that the model with all micropiles removed failed. These results together with the conclusions about the ground not being entirely grouted show that it is important to test the capacity and check that the micropiles are securely fastened with in-site pull out tests.

The only sign of k in the jet grout plug having significance in the PLAXIS model was in the displacement of the excavation bottom in the third excavation stage. It was in this stage that the flow to the excavation bottom was set to open simulating relief wells, but even so there are too large displacements for all model variations, except the one with the lower value of k. That is the k reached with a different design of the c/c-distance of 1.2 m. However, equilibrium was not even fully reached even for this model variation.

The displacement in the jet grout plug were shown to be very similar (around 45 mm) in the different models in PLAXIS. This increases the reliability in the results.

7.4 Models in PLAXIS

The numerical calculations made with PLAXIS 2D were performed with several model variations to check the construction as well as the model's sensitivity. Furthermore, the different models also fulfil different purposes. In this section it is explained why some models have been used and others not.

The different models in PLAXIS have been tested with different properties and values set to different soil and jet grout parameters. This is because the soil and jet grout are not homogeneous materials and which parameters to use can never be certain as is already explained in the literature study chapter. For the parameters of structures such as steel struts and the sheet pile walls reasonable values were taken from different product data sheets when values needed were missing in the project's construction documents.

The NGI-ADP model is good for checking if the overall construction will work and to test the method of building in the short term and against failure by uplift. Safety factor for displacements was checked and, in the NGI-ADP model, weak links were also tested such as removing some or all of the micropiles and, also, changing the properties of the jet grout to have half of its shear strength.

The SS model is good for modelling change in the pore pressure as the soil can be set to drained in this model. Time effects are possible in the SS model which makes it possible for the clay to be able to consolidate and in that way see some movements in the surroundings. However, when it comes to clay the test to set the excavation pit as open for one year is not a lot of time either as consolidation can take a much longer time. One year was though considered enough as the construction will be finished and closed within that time limit.

The results found with the different models coincide well with each other and they do not deviate from the results made in project *Korsvägen*, increasing the reliability of all models. The two models used in this thesis, the NGI-ADP and the SS model are also to some extent chosen because of the parameter values found in the beginning from the project *Korsvägen*.

One of the shortcomings of the models is that Mohr-Coulomb is not the best model to capture bending failure and take the significance of cracks into consideration. For this purpose, a plasticity damage model like a concrete model could have been better and coming closer to capture the failure mechanism (Waichita et al. 2020).

7.5 The Models vs Reality

To be able to get values closer to the reality in the PLAXIS model one should do in-situ tests of the jet grouted material before construction starts as is described in the literature study. This should also be done for the friction soils as the values in this thesis were taken from literature studies. It would be better to take samples from the site and make laboratory tests of them to hopefully get values truer to the actual site.

For this thesis work no consideration was taken to how the area has been used before, for example, its stress history and the effect this has on ongoing settlements in the area. Prior usage highly affects the consolidation of clay soil so this would have been good to have taken into consideration.

In the SS model, the one taking permeability and consolidation into consideration, the lower aquifer was set to have a constant flow and constant *k*. Even if there will be a change in pressure it will only be temporarily and not lead to a permeable lowering of the ground water. To some extent this is true, but it is also stated in one of the construction documents (RKFM 2019-05-24) that the storativity of the lower aquifer is low making the levels sensitive to extraction. The effects of lowering the water pressure could then have large effects to the surroundings with settlements and possible damage to surrounding buildings. It is not explicitly stated how low the storativity is and maybe the pumping and infiltration systems can manage a return of water. This was assumed in this thesis to use the type of model in PLAXIS that has been done.

If there is too much water coming through the relief wells maybe an additional jet grout round is needed. But it will be very difficult to know where in the plug the leakage is. However, as soon as the excavation reaches the top of the jet grout plug and one can see the leakages they will most likely be prioritized and fixed fast with injections.

7.6 Design Validation

To study a design in the geotechnical field the procedure can be outlined as it is done in this thesis work. Analytical calculations are made for the ULS and then the SLS is checked with numerical simulations that also works as a confirmation of the analytical calculations. High enough safety factors should be reached and expected values of the movements and forces should be found. These values are then later used to validate the design, comparing the calculated values to measured deformations and forces in the actual construction to see that these correlates. If larger deviations are observed measures can be taken to prevent the construction from failure. To follow this method and additionally have back-up plans, such as adding more retaining structures, more jet grouting etc., is called the observational method (Spross & Johansson 2017).

7.7 Further Work

There are many models and different material settings to be used in PLAXIS and to investigate this design with other models would be interesting further work. Current research is now looking at the use of concrete models for jet grout constructions and this would be interesting to look more into. A concrete model which is described above is one possible example and also to set the friction soil parameters according to Hardening Soil with Mohr-Coulomb failure criterium.

Further work that also would be relevant is to do simulations in the add-on module for ground water flow (PlaxFlow 2D) that exist for PLAXIS, which was not available to use in this thesis work. This application would be useful in checking how the water moves in the model and to check change in the pore water pressure in the lower aquifer. This would make it easier to answer the question about the importance of sealing of the jet grout plug. This model would however require more information of the flow in the lower aquifer.

Furthermore, calculations and simulations in PLAXIS could be more accurate if pre-production tests on site of the jet grout had been made and one could use the actual data of the different jet grout parameters. So, to run the models again after such pre-production tests have been performed would be an idea.

8 Conclusion

The research questions that were to be answered in this thesis are listed below with short and conclusive answers:

- *How should a jet grout plug be designed to make a sufficiently secure construction in a deep excavation under the ground water table?*

The results of the design presented in this thesis show a design of a jet grout plug that together with the additional structures works sufficiently enough to make a secure construction for a deep excavation below the ground water table.

- *How should a jet grout plug be designed for it to work properly against failure by uplift?*

To work properly against failure by uplift the design of the jet grout plug does not have a large influence since it is not realistic to make it completely watertight. Instead, the use of relief wells makes sure that the pore water pressure is not larger than the vertical stress from the soil, otherwise failure by uplift is a real danger.

- *What properties does a jet grout plug need to function as a sealing component?*

To work as a sealing component the jet grout column pattern and the centre-to-centre distance between the columns are important factors together with the alignment and diameter of the jet grout columns. It is the absence of untreated ground that can make a jet grout plug a completely watertight construction. The soil has a higher permeability compared to the soilcrete and the piping effect makes untreated parts even more a threat against the plug being watertight.

- *How watertight does the jet grout plug need to be for it to work properly?*

This thesis results show that the jet grout plug does not need to be completely watertight to work properly in the excavation construction. However, to work properly against settlements it is not the water tightness of the jet grout plug that decides whether it will work properly. Instead, it is the pumping and infiltration system together with the, in this case, sensitivity of the lower aquifer that decides the risk of settlements.

- *What properties does a jet grout plug need to function as a support level at excavation bottom?*

For the jet grout plug to function as a support level the jet grout material needs to be a good enough soilcrete mixture with a sufficient UCS but the whole ground does not need to be treated. In other words, the jet grout columns do not need to form a complete plug.

9 References

Akin, M.K. (2019) "Experimental studies on the physico-mechanical properties of jet-grout columns in sandy and silty soils" *Journal of African Earth Sciences 116: 190-197.* DOI: 10.1016/j.jafrearsci.2016.01.011

Arroyo, M., Gens, A., Alonso, E., Modoni, G., Croce, P., (2007) *Informes Sobre Tratamientos de Jet Grouting*. ADIF LAV Madrid-Barcelona-Francia, Tramo Torrasa-Sants. Report of the Universidad Politecnicha de Catalunya, p. 110 ([in Spanish]).

Burke, G. K. (2012) "The State of the Practice of Jet grouting" *Proceedings of the Fourth International Conference on Grouting and Deep Mixing*, New Orleans. Louisiana. United States

Brinck, M., Stigenius, K. (2019) *Jet grouting as a method for sealing sheet pile excavations in Swedish conditions. A probabilistic approach*. Degree project in Soil and Rock Mechanics. KTH Royal Institute of Technology. Stockholm

Cheng, S.-H., Liao, H.-J., Yamazaki, J., Wong, R. K. N. and Iwakubo, T. (2019) "Alignment of Vertical and Inclined Jet Grout Columns for Waterproofing," *Geotechnical Testing Journal* 43(2): 325-338.
DOI: 10.1520/GTJ20180324

Croce, P., Flora, A., Modoni, G. (2014) *Jet grouting – Technology, Design and Control*. CRC Press. Taylor & Francis Group. ISBN: 978-1-4822-4718-3

Das, B.M., Sobhan, K. (2017) *Principles of Geotechnical Engineering. Ninth Edition, SI.* Cengage Learning. ISBN: 978-1-305-97095-3

EN 12716:2018
Execution of special geotechnical work – Jet grouting. European standard.

EN 1997-1:2005
Eurocode 7: Geotechnical design – Part 1: General rules

Eramo, N., Modoni, G., Arroyo, M. (2011) "Design control and monitoring of a jet grouted excavation bottom plug" *7th International Symposium on Geotechnical Aspects of Underground Construction in Soft Ground*.
DOI: 10.13140/2.1.1665.7282

Essler, R., Yoshida, H. (2004) *Jet grouting. Ground improvement, 2nd edn*. Taylor and Francis, New York, pp 160-196

Flora, A., Modoni, G., Croce, P., Siepi, M., Kummerer, C. (2017) "What Future for Jet Grouting? A European Perspective" *Grouting 2017* GSP 287: 358-382
DOI: 10.1061/9780784480786.035

Hsieh, H-S., Wang, C-C., Ou, C-Y. (2003) "Use of Jet Grouting to Limit Diaphragm Wall Displacement of a Deep Excavation" *Journal of Geotechnical and Geoenvironmental Engineering* 129(2): 146-157.
DOI: 10.1061/ASCE1090-0241(2003)129:2(146)

Larsson, R., Sällfors, G., Bengtsson, P-E., Alén, C., Bergdahl, U., Eriksson, L. (2007) *Skjuvhållfasthet – utvärdering i kohesionsjord.* Statens geotekniska institut (SGI). Information 3. Linköping.

Larsson, R. (2008) *Jords egenskaper*. Statens geotekniska institut (SGI). Information 1. Linköping.

L'Heureux, J-S., Ozkul, Z., Lacasse, S., D'Ignazio, M., Lunne, T. (2017) "Bestemmelse av hviletrykk (K0) i norske leirer – anbefalinger basert på en sammenstilling av lab-, felt-og erfaringsdata. A revised look at the coefficient of earth pressure at rest for Norwegian Clays." *Fjellsprengningsteknikk - bergmekanikk - geoteknikk*. Oslo 2017. Foredrag 35.
URI: http://hdl.handle.net/11250/2491814

Lindgård, A., Ofstad, C.S. (2016) *An evaluation of methods to determine K'_0 in Clays*. Literature study and pilot experiments conducted at Tiller in connection with NGTS. Project Thesis. Department of Civil and Transport Engineering. Norwegian University of Science and Technology (NTNU). Trondheim.

Lunne, T., Berre, T., Strandvik, S. (1997) "Sample Disturbance Effects in Soft Low Plastic Norwegian Clay" *Symposium on Recent Developments in Soil and Pavement Mechanics*. pp. 81-102. Rio de Janeiro, Brazil.

Modoni, G., Flora, A., Lirer, S., Ochmanski, M., Croce, P. (2016) "Design of Jet Grouted Excavation Bottom Plugs" *Journal of Geotechnical and Geoenvironmental Engineering*. 142(7): 04016018.
DOI: 10.1061/(ASCE)GT.1943-5606.0001436.

Niederleithinger, E., Guerreros, J.C.G. (2015) "Quality Assurance of Jet Grouting Columns Using Seismic Methods" *Near Surface Geoscience 2015 - 21st European Meeting of Environmental and Engineering Geophysics*. pp.1-5. Turin, Italy.
DOI: 10.3997/2214-4609.201413679

Olsson, M. (2010) *Calculating long-term settlement in soft clays – with special focus on the Gothenburg region.* Report 74. SGI - Swedish Geotechnical Institute. Linköping

Olsson, M. (2013) "On Rate-Dependency of Gothenburg Clay" Department of Civil and Environmental Engineering, Division of GeoEngineering, Chalmers University of Technology. ISBN 978-91-7385-911-0

Pan, Y., Liu, Y., Hu, J., Sun, M., Wang, W. (2017) "Probabilistic investigations on the watertightness of jet-grouted ground considering geometric imperfections in diameter and position" *Canadian Geotechnical Journal* 54(10): 1447-1459.
DOI: 10.1139/cgj-2016-0671

Spross, J., Johansson, F. (2017) "When is the observational method in geotechnical engineering favourable?" *Structural Safety,* 66: 17-26
DOI: 10.1016/j.strusafe.2017.01.006

Ticono, A.J., Correia, G., Cortez, P. (2018) "Jet grouting column diameter prediction based on a data-driven approach" *European Journal of Environmental and Civil Engineering*, 22(3): 338-358.
DOI: 10.1080/19648189.2016.1194329

Toraldo, C., Modoni, G., Ochmański, M., Croce, P. (2017) "The characteristic strength of jet-grouted material" *Géotechnique* 68(3): 262-279.
DOI: 10.1680/jgeot.16.P.320.

TRVFS 2011:12
Trafikverkets författningssamling
Trafikverkets föreskrifter om ändring i Vägverkets föreskrifter (VVFS 2004:43) om tillämpningen av europeiska beräkningsstandarder

Trafikverket (2014) *Trafikverkets tekniska krav för geokonstruktioner TK Geo 13*.
Dokument-ID TDOK 2013:0667

Waichita S., Jongpradist P., Schweiger H.F. (2020) "Numerical and experimental investigation of failure of a DCM-wall considering softening behaviour" *Computers and Geotechnics* 119 (2020) 103380
DOI: 10.1016/j.compgeo.2019.103380

Wanik L., Mascolo M.C., Bzówka J., Modoni G., Shen J.S.L. (2017) "Experimental Evidence on the Strength of Soil Treated with Single and Double Fluid Jet Grouting" *Proc. of the grouting 2017: grouting, deep mixing, and diaphragm walls*, Honolulu, July 9-12, 2017

Wen, D. (2015) *Use of Jet Grouting in Deep Excavations*. (Chapter 4) *Ground Improvement Case Histories - Chemical, Electrokinetic, Thermal, and Bioengineering Methods*. pp. 109-122. Elsevier Ltd.
DOI: 10.1016/B978-0-08-100191-2.00004-6

Construction Documents from the West Link Tunnel Project

Project section *Korsvägen*

Bygghandling 2019-11-05a – Bygghandling, Stödkonstruktioner och geoteknik. Delområde 5310, Liseberg Väst II.
Projektnamn: Västlänken och Olskroken planskildhet.
Filnamn: E05-16-025-5310_0-1210

Bygghandling 2019-11-05b – Bygghandling, Jetinjektering och grundvatten. Delområde 5310, Liseberg Väst II.
Projektnamn: Västlänken och Olskroken planskildhet.
Filnamn: E05-16-025-5310-0_0-1211

MUR – Markteknisk undersökningsrapport, Geoteknik. Delområde 5310, Liseberg Väst 1 och Liseberg Väst 2.

2018-12-21
Filnamn: E05-11-004-5320-0_0-1850
Med bilagor.

RKFM 2019-04-30 – Redogörelse för konstruktionsarbetets förutsättningar och metoder (RKFM), Permanenta betongkonstruktioner. Delområde 5310, Liseberg.
Projektnamn: Västlänken och Olskroken planskildhet.
Filnamn: E05-18-582-5310-0_0-2002

RKFM 2019-05-24 – Redogörelse för konstruktionsarbetets förutsättningar och metoder (RKFM), Stödkonstruktioner, geoteknik och grundvatten. Delområde 5310, Liseberg Väst II.
Projektnamn: Västlänken och Olskroken planskildhet.
Filnamn: E05-16-025-5310-0_0-1110

RKFM 2019-10-23 – Redogörelse för konstruktionsarbetets förutsättningar och metoder (RKFM), Stödkonstruktioner, geoteknik och grundvatten. Delområde 5320, Liseberg Öst I.
Projektnamn: Västlänken och Olskroken planskildhet.
Filnamn: E05-16-025-5320-0_0-1100

SU 2019-08-26 – Särskild utredning, Jet Grouting. Delområde 5310, Liseberg Väst II.
Projektnamn: Västlänken och Olskroken planskildhet.
Filnamn: E05-16-025-5310_0-1212

Project section *Centralen*

Design-PM 2019-02-12 – Design-PM, soil parameters and FEA constitutive models.
Projektnamn: Västlänken
Centralen
Granskningshandling
Filnamn: E02-50GT-013-2000-0_0-2501

Yannie J. (2020) Internal communication about the E02 Centralstationen design methods and assumptions in PLAXIS 2D.

Jet Grout Contractor Information

Keller “The Soilcrete – Jet Grouting Process”. Brochure 67-03E

10 Appendices

Appendix A – Calculation of Friction Angles in Clay

Appendix B – Soil Tests for NGI-ADP Constitutive Soil Model

Appendix C –Soft Soil (SS) Parameters

Appendix D – Analytical Calculations: Safety Factors

Appendix E – MATLAB Code

Appendix F – Analytical Calculations: Hydraulic Conductivity

Appendix A – Calculation of Friction Angles in Clay

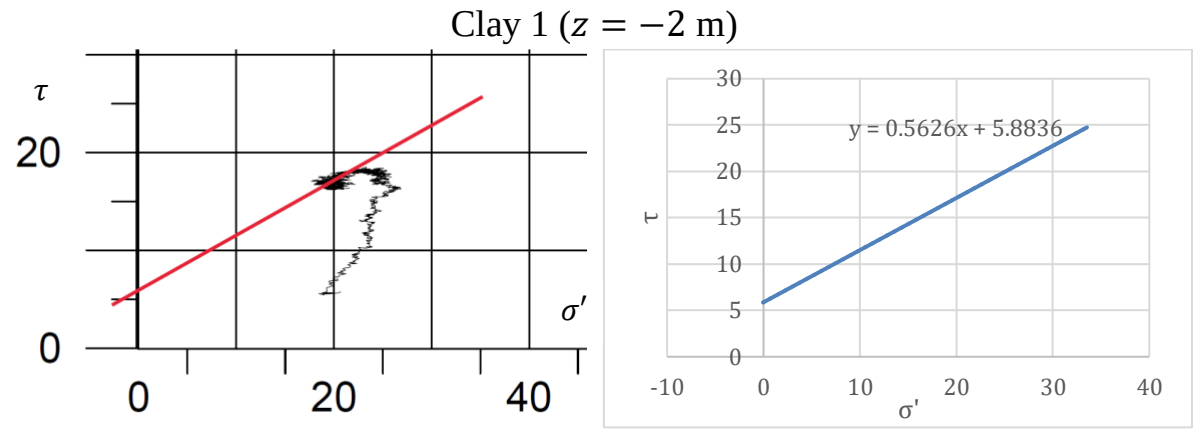

Figure 35. Clay 1.

The friction angle is calculated using "sin" of the inclination since the Triaxial test results are shown not as the tangent to the Mohr-circle but as the highest shear strength.
Clay 1: $\sin\phi = 0.5626 \Rightarrow \phi = \arcsin(0.5626) \approx 34°$
The value of the cohesion is where the curve meets the y-axis $\approx$ 6 kPa.

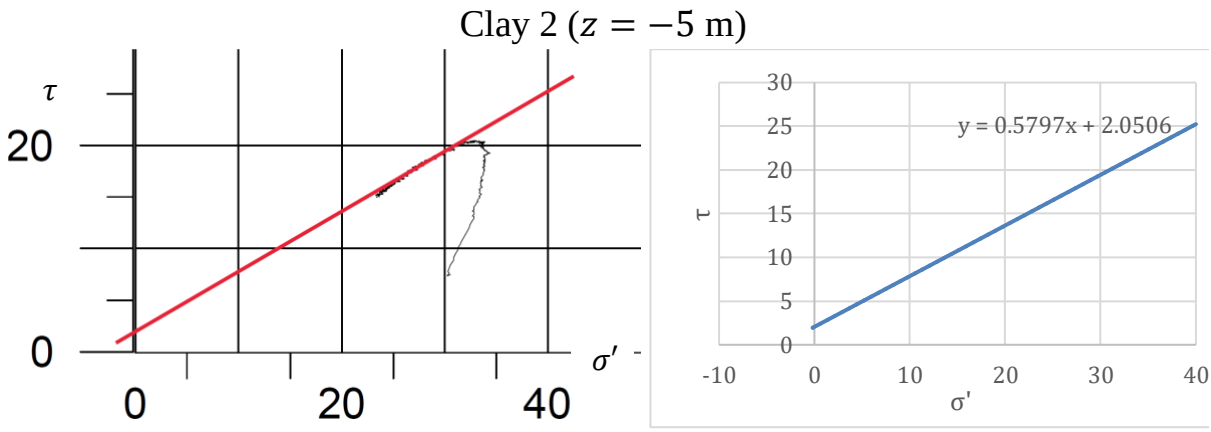

Figure 36. Clay 2.

Clay 2: $\phi \approx 35°$
$c \approx 2$ kPa

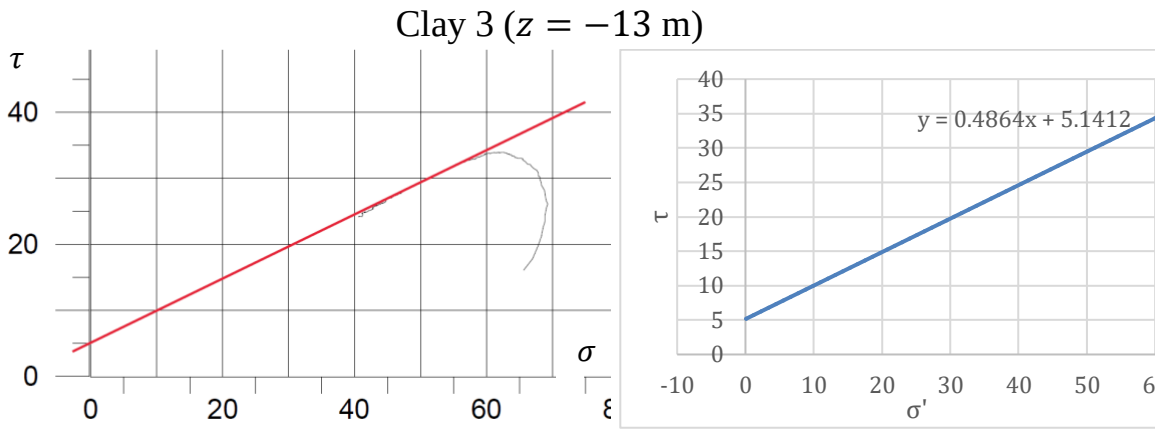

Figure 37. Clay 3.

Clay 3: $\phi \approx 29°$
$c \approx 5$ kPa

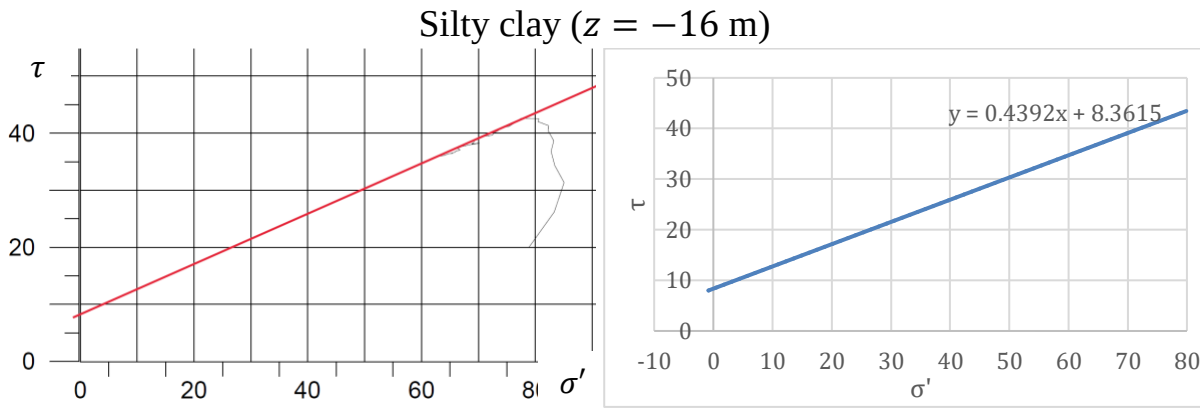

Figure 38.

Silty clay: $\phi \approx 26°$
$c \approx 8$ kPa

Layer	Friction angle, ϕ [°]	Cohesion, c [kPa]
Clay 1	34	6.0
Clay 2	35	2.0
Clay 3	29	5.0
Silty clay	26	8.0

Appendix B – Soil Tests for NGI-ADP Constitutive Soil Model

The triaxial tests as well as the direct simple shear (DSS) tests from geotechnical investigation (MUR) made in the project were used to check and calibrate the parameters for the conctitutive soil models PLAXIS to be as similar to the real soil behaviour as possible.

The $\frac{G}{s_u^A}$ and γ_f^C parameters – Triaxial tests

The MUR data was digitized using the WebPlotDigitizer tool (https://automeris.io/WebPlotDigitizer/) and the pertaining parameters calculated using the data in Excel. Below is one example of how the parameters were obtained.

The strain, ε, in the graph is transformed to shear strain, γ:

$$\gamma = \frac{3}{2}\varepsilon$$

to get the shear modulus of the graph as G:

$$G = \frac{\tau}{\gamma}$$

where τ = shear stress.

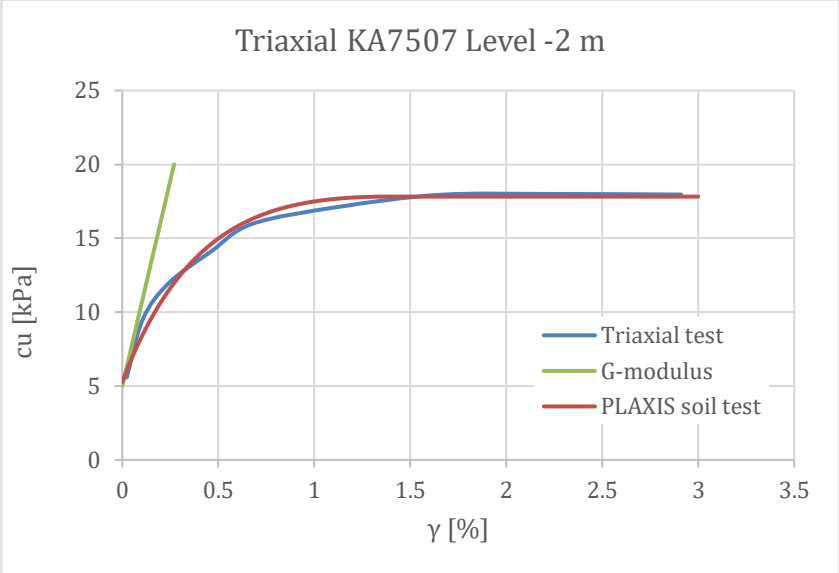

Figure 39. Graph from Excel to get the shear modulus to insert in PLAXIS.

One of the parameters to set in PLAXIS is $\frac{G}{s_u^A}$ and to get this, the G-modulus is divided with the maximum shear stress obtained from the triaxial compression test (in this case approximately 18 kPa for the test in Figure 39), so:

$$\frac{G}{s_u^A} \approx 300$$

This value is used in the PLAXIS soil test and together with the compressive shear strain parameter, γ_f^C , these are changed to match the corresponding test. The same procedure is then conducted with the other borehole levels and the result graphs are shown in Figure 40.

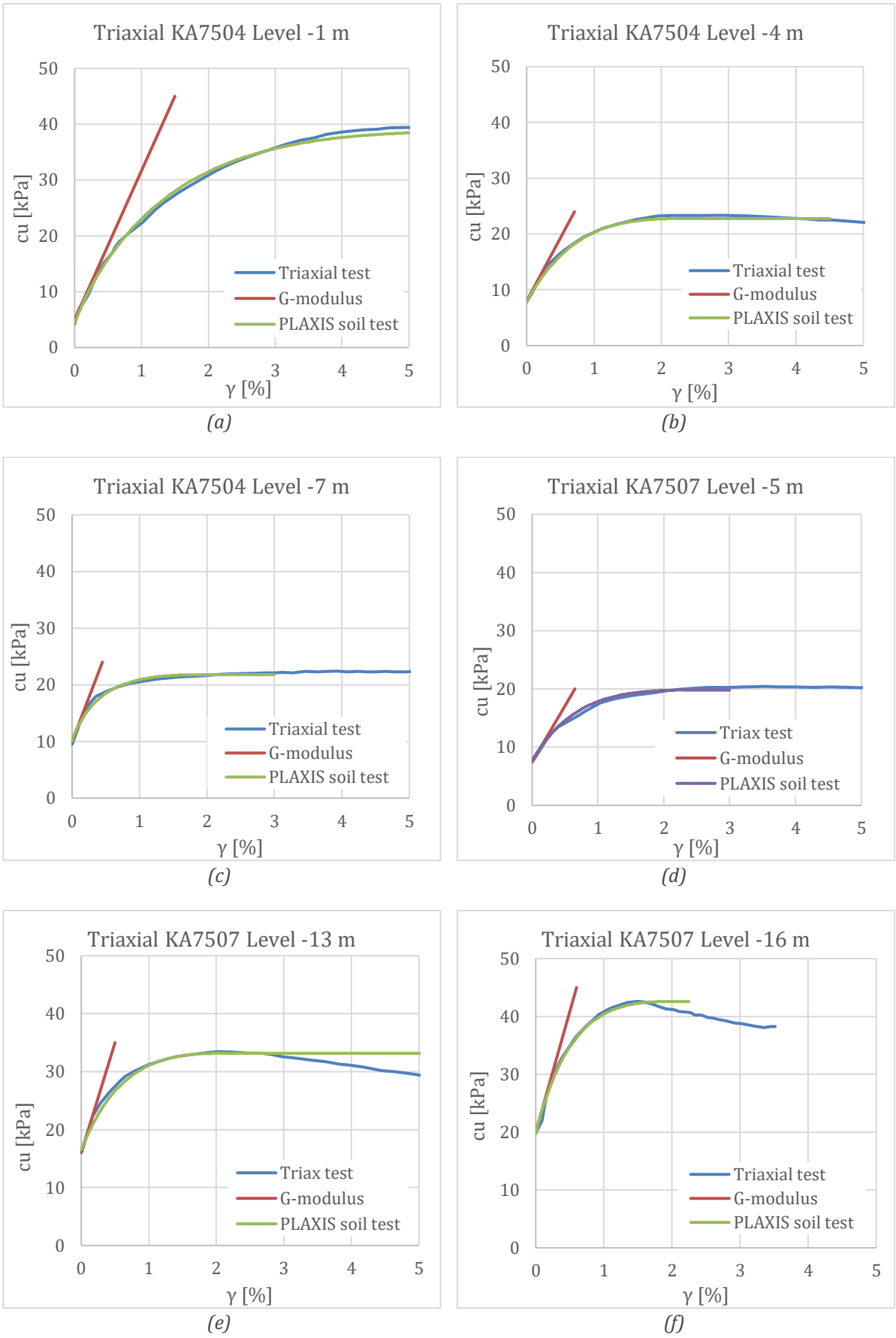

Figure 40. PLAXIS triaxial soil tests compared to laboratory triaxial tests.

All triaxial tests were performed as undrained compression tests and the settings made for each test are shown in Table 30. The consolidation strain is also presented as this value indicates the quality of the laboratory test, where 0-2 % is excellent/very good, 2-5 % is good/fair and values larger than that are considered poor (Lunne et al. 1997).

Table 30. Triaxial soil test settings.

Borehole and Level	K_0	Initial cell pressure, σ'_{xx} [kPa]	$s^A_{u,ref}$ [kPa]	τ_0/s^A_u	Consolidation strain [%]
KA7504 -1 m	0.6	13.4	39	0.021	1.24
KA7504 -4 m	0.6	23.2	23	0.036	1.42
KA7504 -7 m	0.6	30.2	22	0.175	4.26
KA7507 -2 m	0.6	15.8	18	0.030	1.05
KA7507 -5 m	0.6	23.1	20.5	0.156	1.42
KA7507 -13 m	0.6	49.6	33.5	0.211	2.17
KA7507 -16 m	0.6	59.1	43	0.344	2.27

The results obtained from the different triaxial soil tests are shown in Figure 41 and Figure 42. From these the value of G/s^A_u is selected to be 150 and γ^C_f is set to 3 %.

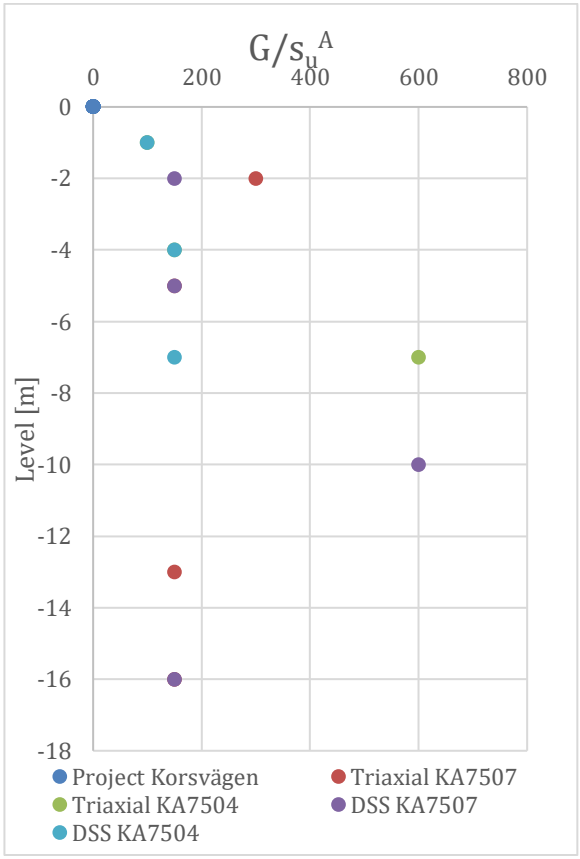

Figure 41. The $\frac{G}{s_u^A}$ parameter gotten from PLAXIS soil tests compared to the ones used in the project section Korsvägen.

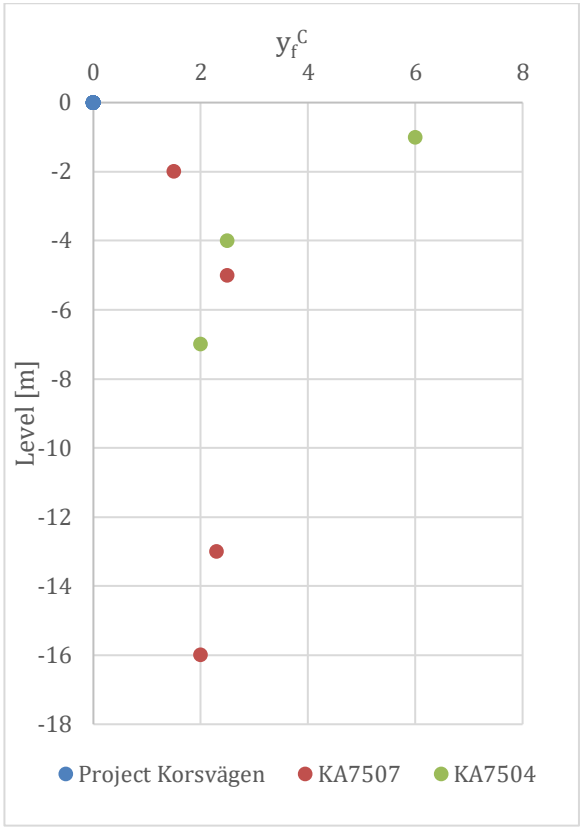

Figure 42. The γ_f^C parameter gotten from PLAXIS triaxial soil test compared to the ones used in the project section Korsvägen.

The γ_f^{DSS} parameter – DSS tests

A similar procedure as for the Triaxial tests was done to get the DSS-parameter for the PLAXIS model. PLAXIS DSS tests were compared, the value of $\frac{G}{s_u^A}$ and γ_f^{DSS} was altered until the shape of the curves coincided (Figure 43).

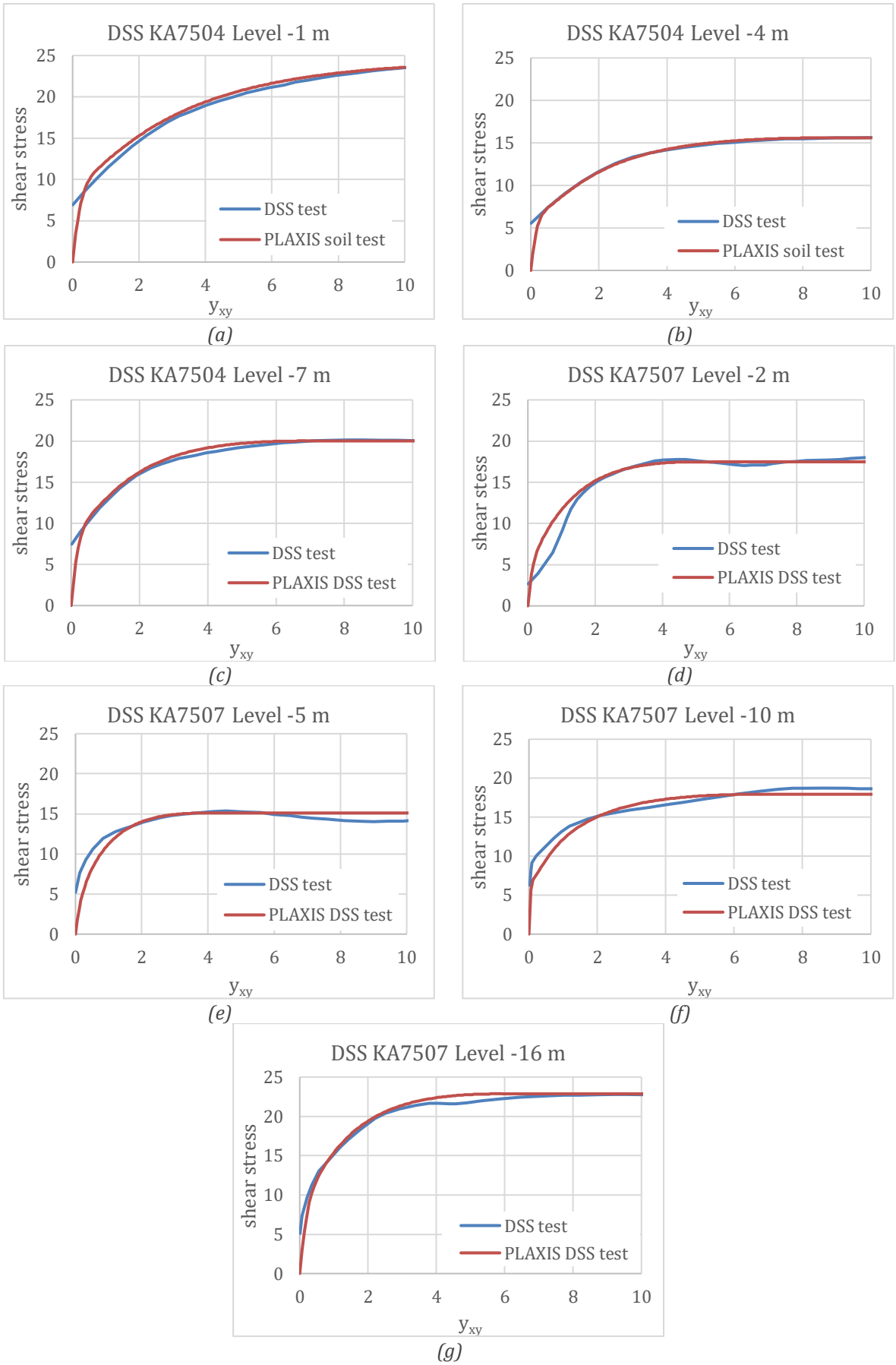

Figure 43. DSS test from PLAXIS soil tests compared to laboratory tests.

The DSS soil tests were all performed as undrained tests and the settings for each test can be seen in Table 31 as well as the consolidation strain. The calibration led to the selection of the γ_f^{DSS} parameter to be 5%.

Table 31. DSS soil test settings.

Borehole and Level	K_0	Initial stress, σ_{yy} [kPa]	$s_{u,ref}^A$ [kPa]	τ_0/s_u^A	Consolidation strain [%]
KA7504 -1 m	0.6	74.8	37	0.021	2.79
KA7504 -4 m	0.6	42.5	24	0.036	2.89
KA7504 -7 m	0.6	68.0	29	0.175	10.3
KA7507 -2 m	0.6	26.3	26.9	0.030	7.7
KA7507 -5 m	0.6	38.5	21.9	0.156	3.96
KA7507 -10 m	0.6	69.7	26	0.196	3.88
KA7507 -16 m	0.6	82.5	29.5	0.344	4.21

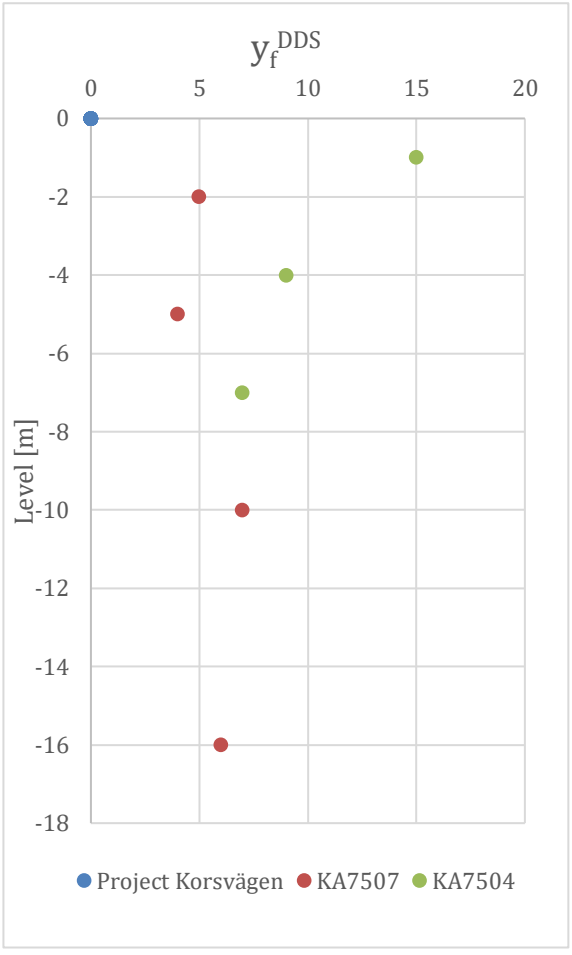

Figure 44. γ_f^{DSS} parameters gotten from the DSS soil test in PLAXIS compared to the ones used in the project section Korsvägen.

The γ_f^E parameter

The parameter for the passive loading, the γ_f^E (E=extension), could not be evaluated with laboratory tests as no passive triaxial tests could be found in the geotechnical investigation report (MUR). There will, however, be no clay on the passive side of the secant pile walls, which could be a reason as why no passive triaxial tests have been performed. The structure of the secant pile walls is instead entirely supported by struts and the jet grout plug.

The value of the γ_f^E parameter is however something that must be used in the PLAXIS model, and as it must be a value larger than γ_f^{DSS}. In this case it is set to 6 % based on values obtained for the design of *Centralen* (one other section of the *Västlänken* in Gothenburg) (Design-PM 2019-02-12).

Appendix C –Soft Soil (SS) Parameters

Soil Tests for PLAXIS

The parameters to be calibrated using the soil test in PLAXIS are the modified swelling index, κ^* and the modified compression index, λ^*. These parameters can be calibrated using the CRS test mode in the software. However, they were adjusted using the triaxial test mode as this test is more relevant for excavation problems. Initially, these parameters can be estimated with the following empirical equations (Olsson 2010):

$$\lambda^* \approx \frac{1.1 \cdot \sigma'_{vc}}{M_L} \quad (5)$$

$$\kappa^* \approx \frac{2 \cdot \sigma'_{v}}{M} \quad (6)$$

where,
σ'_v = vertical effective stress, (the average between the blue lines in Figure 45)
σ'_{vc} = vertical preconsolidation stress (the average between the blue lines in Figure 45)
M = critical state line (upper red horizontal line in Figure 45)
M_L = constant constrained modulus between stresses σ'_c and σ'_L, Swedish method. (lower red horizontal line in Figure 45)

The CRS-tests give the following graph, shown in Figure 45. From that figure the necessary parameters for equation (5) and (6) can be estimated. The λ^*-value can be calculated close to its true practical value, whereas κ^* often is overestimated (Olsson 2010). Therefore, λ^* is calculated with the equation to be used in the soil test and the κ^*-value is altered until the PLAXIS soil test gets as closely as possible match with the real triaxial test. An example is shown in Figure 46.

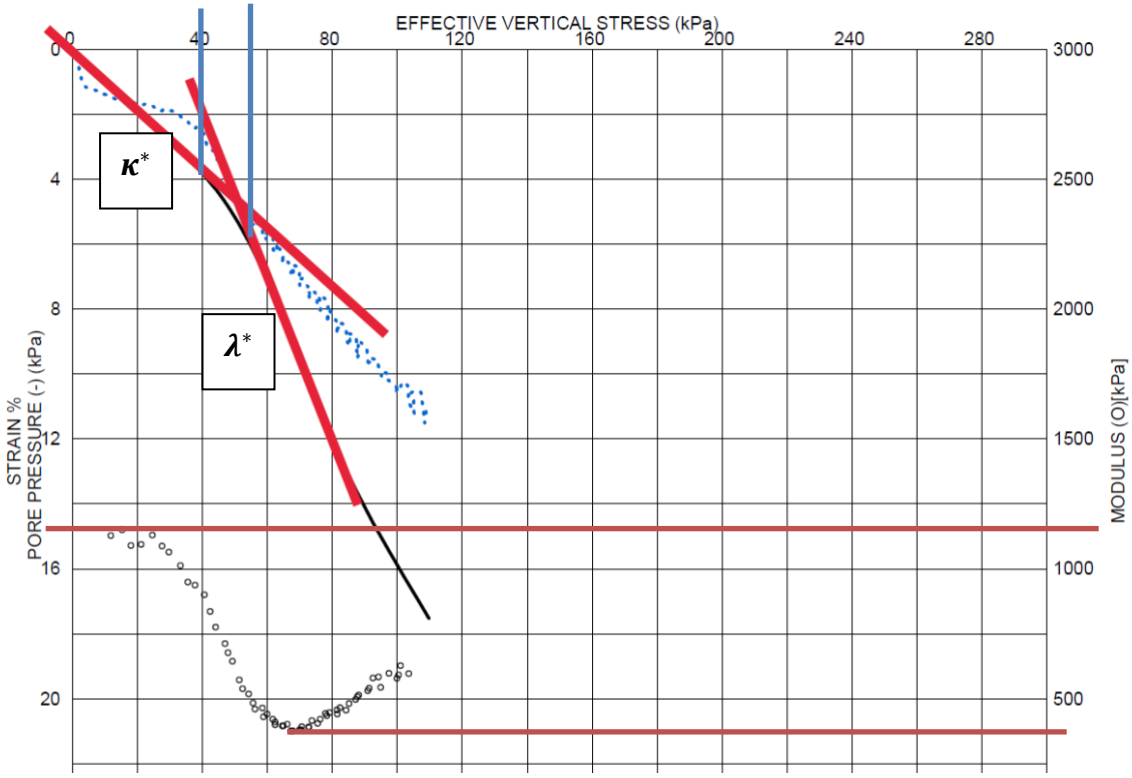

Figure 45. CRS-test. (E05-11-013-5310-0_0-1852)

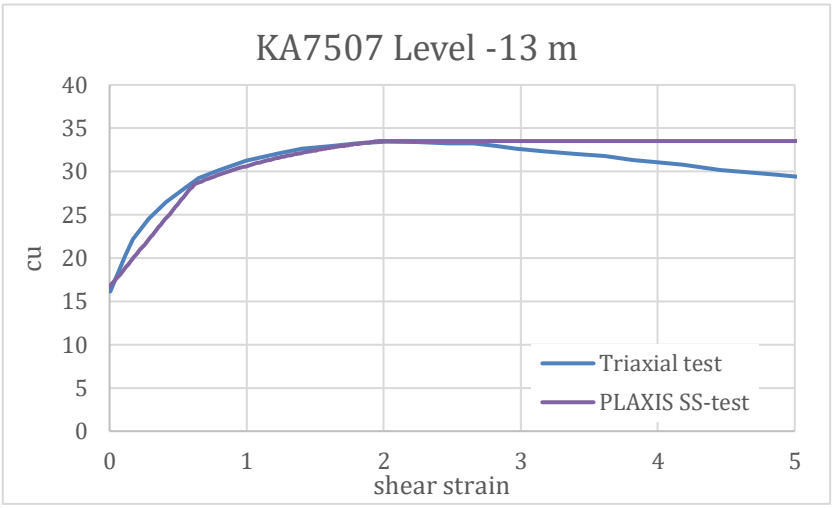

Figure 46. PLAXIS soft soil test compared to triaxial test from project section Korsvägen.

The triaxial soil test in PLAXIS was set up as an undrained compression test, with K_0 = 0.6. The Initial horizontal soil pressure, σ'_{xx}, was obtained from the projects triaxial tests and the vertical pre-consolidation stress was calculated with OCR· σ'_v.

The estimated values of κ^* and λ^* for each clay layer are presented in Table 32.

Table 32. The parameters κ^* and λ^* for each clay layer.

PLAXIS parameters	Clay 1	Clay 2	Clay 3	Silty Clay
$\boldsymbol{\lambda^*}$	0.15	0.16	0.3	0.3
$\boldsymbol{\kappa^*}$	0.01	0.022	0.03	0.025

Hydraulic conductivity, *k*

From CRS-tests (MUR bilaga 2):

Sektion/borrhål Djup/nivå (m)	Jordart	Densitet t/m³	Vatten-kvot w %	σ'_c kPa	σ'_L kPa	M_0 kPa	M_L kPa	C_V m²/s	k_i m/s	Kommentar
KA7504										
3,0	Le	1,57	68	87	177	2460	1250	9,0E-08	5,5E-10	Korrigerat värde
6,0	Le	1,54	78	50	122	1350	690	2,5E-08	1,8E-10	
9,0	Le	1,53	76	82	154	1990	1020	9,0E-08	5,9E-10	Korrigerat värde
13,0	(si)Le	1,70	45							Gick ej att utvärdera
15,0	siLe	1,89	38							Gick ej att utvärdera

Sektion/borrhål Djup/nivå (m)	Jordart	Densitet t/m³	Vatten-kvot w %	σ'_c kPa	σ'_L kPa	M_0 kPa	M_L kPa	C_V m²/s	k_i m/s	Kommentar
KA7507										
4,0	gyLe (sk)	1,43	100	30	82	810	520	4,0E-08	4,4E-10	
7,0	gyLe	1,45	96	40	70	1100	370	9,0E-08	6,9E-10	
12,0	(gy)(si)Le (sk)	1,51	82	82	108	2270	340	1,1E-07	1,1E-09	
18,0	Le	1,46	97	111	140	3800	310	2,0E-07	1,0E-09	

To get an estimated value of the hydraulic conductivity, *k*, an average of the tests was taken:

Clay 1

$\frac{5.5\cdot10^{-10}+1.8\cdot10^{-10}+4.4\cdot10^{-10}}{3} = 3.9\cdot10^{-10}$ m/s

To get m/day → $3.9\cdot10^{-10}\cdot 86\,400$ s $= 3.4\cdot10^{-5}$ m/day (input in PLAXIS)

Clay 2

$\frac{5.9\cdot10^{-10}+1.1\cdot10^{-9}}{2} = 8.45\cdot10^{-10}$ m/s → $=7.3\cdot10^{-5}$ m/day

Clay 3

$1.0\cdot10^{-9}$ m/s → $= 8.6\cdot10^{-5}$ m/day

Silty clay
$1.0 \cdot 10^{-9}$ m/s → = $8.6 \cdot 10^{-5}$ m/day

The results are compiled in Table 33.

Table 33. The hydraulic conductivity, k, for each clay layer (input for PLAXIS).

	Clay 1	**Clay 2**	**Clay 3**	**Silty clay**
Hydraulic conductivity, *k* [m/day]	3.4E-5	7.3E-5	8.6E-5	8.6E-5

Appendix D – Analytical Calculations: Safety Factors

The analytical calculations are based on the steps described in Modoni et al. (2016) in Section 4.1 and are calculated for the ultimate limit state, ULS, according to Eurocode 7 with the use of partial factors.

Uplift equilibrium - of the Whole Structure

Uplift forces: U = Water pressure

Downward forces: W_{jet} = Jet grout plug self-weight

W_w = Secant pile walls self-weight

T_{mp} = Micro-piles, tension force

R_{sw} = Bond resistance between secant pile wall and soil

U

Unit weight water: $\gamma_w := 10\frac{kN}{m^3}$

Height ground water pressure (under jet grout plug): $h_w := 23m + 3.54m = 26.54m$

Width of jet grout plug: $B := 21.3m$

Thickness of secant pile wall: $t_w := 1.2m$

$$U := \gamma_w \cdot h_w \cdot (B + 2 \cdot t_w) \cdot 1m = 6.29 \times 10^3 \cdot kN$$

W_{jet}

Unit weight jet grout material: $\gamma_{jet} := 16.5\frac{kN}{m^3}$

Thickness/height of jet grout plug: $h_{jet} := 5m$

$$W_{jet} := \gamma_{jet} \cdot h_{jet} \cdot B \cdot 1m = 1.757 \times 10^3 \cdot kN$$

W_w

Unit weight concrete: $\gamma_c := 24.5\frac{kN}{m^3}$

Length secant pile walls: $l_w := 23.5m$

$$W_w := \gamma_c \cdot l_w \cdot t_w \cdot 1m = 690.9 \cdot kN$$

T_{mp}

Characteristic bond strength, micropile and jetgrout, $q_{sk.jet} := 400kPa$ (Demand from project)

Partial factor, (shaft resistance, tension): $\gamma_a := 1.4$ (Eurocode 7 p.123 Table A.16)

Design bond strength, micropile and jetgrout: $q_{sd.jet} := \frac{q_{sk.jet}}{\gamma_a} = 285.7 \cdot kPa$

Diameter of drillhole: $D := 0.300m$

Resistance interface jet grout/micropile annulus grout: $T_{mp} := \pi \cdot D \cdot h_{jet} \cdot q_{sd.jet} = 1.346 \times 10^3 \cdot kN$

In one meter of the construction a number of approx. $n := 2.7$ micropiles is going to be used.

(n from E05-16-025-5310-0_0-1210)

$\frac{T_{mp}}{5} = 269.279 \cdot kN$ per m

Check that resistance interface bedrock/micropile is not smaller.

$q_{sk.bedrock} := 1000kPa$

$q_{sd.bedrock} := \frac{q_{sk.bedrock}}{\gamma_a} = 7.143 \times 10^5 Pa$

$D_{bedrock} := 0.150m$ $h_{bedrock} := 4m$

$T_{bedrock} := \pi \cdot D_{bedrock} \cdot h_{bedrock} \cdot q_{sd.bedrock} = 1.346 \times 10^3 \cdot kN$ OK!

R_{sw}

Undrained shear strength of the clay: $s_u := 15\text{kPa}$

Interface bond between secant pile wall and soil: $R_{inter} := 0.7$

Bond strength: $R_d := R_{inter} \cdot s_u = 1.05 \times 10^4\ \text{Pa}$

$R_{sw} := R_d \cdot l_w \cdot 1\text{m} = 246.75\text{kN}$

Safety factor, $SF > 1.65$ (TK Geo 13 chapter 2.4 table2.4-1, for consequence class 3 (CC3)
(quick clay, TRVFS 2011:12)

(Forces from weight take x0.9 according to TK Geo 13, chapter: 2.3.2.2 Upplyftning)

$$SF := \frac{\left(W_{jet} \cdot 0.9 + 2 \cdot W_w \cdot 0.9 + n \cdot T_{mp} + 2 \cdot R_{sw}\right)}{U} = 1.106 \quad < 1.65 \text{ NOT OK!}$$

Uplift equilibrium - of the Jet Grout Plug

Uplift forces: U_{jet} = Water pressure under jet grout plug

Downward forces: W_{jet} = Jet grout plug self-weight

T_{mp} = Micro-piles, tension force

$R_{w.jet}$ = Bond resistance: secant pile wall and jet grout plug

U_{jet}

$U_{jet} := \gamma_w \cdot h_w \cdot B \cdot 1m = 5.653 \times 10^6 N$

$R_{w.jet}$

Shear strength of jet grout material, 1000-5000 kPa, $s_{u.jet} := 1000kPa$

Partial factor: $\gamma_s := 1.5$

$$s_{u.d.jet} := \frac{s_{u.jet}}{\gamma_s} = 6.667 \times 10^5 Pa$$

Bond length secant wall and jet grout: $h_{w.jet} := 3.5m$

$R_{w.jet} := s_{u.d.jet} \cdot h_{w.jet} \cdot 1m = 2.333 \times 10^6 N$

Safety factor, SF

$$SF := \frac{(R_{w.jet} \cdot 2 + W_{jet} \cdot 0.9 + n \cdot T_{mp})}{U_{jet}} = 1.748 > 1.65 \quad OK!$$

Structural Performance of the Jet Grout Plug

Moment equilibrium around point O

Clockwise forces: U_{jet} = Water pressure on jet grout plug

Counterclockwise forces: W_{jet} = Weight of jet grout plug

F_c = Compression force

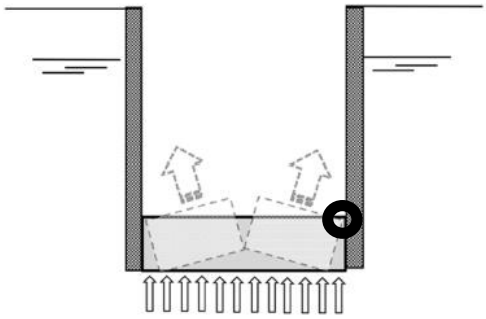

Calculations are done on one half of the plug.

F_c

Compressive strength of the jet grout material, between 2-10 MPa: $f_{mk} := 2MPa$

Partial factor: $\gamma_m := 1.5$ DIN 4093 according to RKFM_Geo_LisebergVästll

$$f_{md} := \frac{0.85 \cdot f_{mk}}{\gamma_m} = 1.133 \times 10^6 \, Pa$$

Height of compressive zone: $h_c := \frac{h_{jet}}{2} = 2.5m$

$$F_c := f_{md} \cdot h_c \cdot 1m = 2.833 \times 10^3 \cdot kN$$

Lever arms:

- for U: $l_U := \frac{B}{4} = 5.325m$
- for W_{jet}: $l_{W.jet} := \frac{B}{4} = 5.325m$
- for F_c: $l_{F.c} := \frac{h_{jet}}{4} = 1.25m$

Clockwise moments:

$$M_U := \frac{U_{jet}}{2} \cdot l_U = 1.505 \times 10^4 \, kN \cdot m$$

Counterclockwise moments:

$$M_{W.jet} := \frac{W_{jet}}{2} \cdot l_{W.jet} = 4.679 \times 10^{3}\ kN \cdot m$$

$$M_{F.c} := F_c \cdot l_{F.c} = 3.542 \times 10^{3}\ kN \cdot m$$

$$SF := \frac{M_{W.jet} + 2 \cdot M_{F.c}}{M_U} = 0.781 \quad < \quad 1.65 \quad \text{NOT OK!}$$

Appendix E – MATLAB Code

```
%-------------------------------------------------------------------------
% Probabilistic simulation of holes between three jet grout columns
% Part of the master thesis: Jet grouting as a method for sealing sheet
% pile excavations in Swedish conditions
% AF 262X Degree Project in Soil and Rock Mechanics
% 2019-01-28, Changed 2019-04-02.
% Mårten Brinck and Karl Stigenius
%-------------------------------------------------------------------------
% Modified 2020-09-07 by Ida Lundin.
% Part of master thesis: Jet Grout Plug in Deep Excavations
% AF 262X Degree Project in Soil and Rock Mechanics
%-------------------------------------------------------------------------
clc, close all, clear all
%=========================================================================
% Input:
%=========================================================================
% General input and needed variables
%-------------------------------------------------------------------------
N = 5000; % Number of grid iterations
pf = zeros(N,1); % Empty vector for failure
% indication
x = 1:N; % Plot v for failure prob.
fp = zeros(N,1); % Empty vector for logging
% failure probability
% Input and variables needed for the grid:
%-------------------------------------------------------------------------
ht = 20; % Column depth (top)
hb = ht+5; % Column depth (bottom)
inp.cx = 1.4; cx = inp.cx; % Centre-dist. in x-dir.
inp.cy = 1.4; cy = inp.cy; % Centre-dist. in y-dir.
m = 15; inp.m = m; % Number of columns in x-dir.
n = 72; inp.n = n; % Number of columns in y-dir.
h_pos = (m+(m-2))*(n-1); % Number of possible holes
p_mu = 0.038; % Mean value position
p_sig = 0.02; % Std. div. position
d_mu = 1.8; inp.r = d_mu/2; % Mean value column diameter
d_sig = 0.18; % Std. div. column diameter
a_mu = 0.005; % Mean value inclination
a_sig = 0.0025; % Std. div. inclination
Gri = figure('Name','Grid');
out = Grid(inp); % Creates and plots the
% idealized grid
g_x = out.gx; % X-coordinates for the grid
g_y = out.gy; % Y-coordinates for the grid
no = out.n; % Number of columns
P_Area = out.A; % Coverage area of the grid
sc_x = zeros(no,1); % Empty v for x-cor. at surface
sc_y = zeros(no,1); % Empty v for y-cor. at surface
tc_x = zeros(no,1); % Empty v for x-cor. at top
tc_y = zeros(no,1); % Empty v for y-cor. at top
bc_x = zeros(no,1); % Empty v for x-cor. at bottom
bc_y = zeros(no,1); % Empty v for y-cor. at bottom
A = []; % Empty v for collecting the
% individual hole areas
AP = zeros(N,1); % Empty v for collecting the
% total hole area of a grid
%=========================================================================
% Calculations
```

```
%=========================================================================
% For loop generating grids based on the input data for the grid and the
% probabilistic input for the column properties. The grids are checked for
% holes between all possible combinations of three adjacent columns and
% hole area is calculated if a hole appears.
%-------------------------------------------------------------------------
for count = 1:N
% Simulation of stochastic variables
%-------------------------------------------------------------------------
alpha_p = rand(1,no)*2*pi; % Azimuth for pos.
pos = normrnd(p_mu,p_sig,no,1); % Horizontal pos. of column
dia = normrnd(d_mu,d_sig,no,1); % Diameter of column
alpha_inc = rand(1,no)*2*pi; % Azimuth for inc.
beta = normrnd(a_mu,a_sig,no,1); % Vertical inclination
% Calculation of the centre-points on the surface
%-------------------------------------------------------------------------
for i = 1:no
sc_x(i) = g_x(i) + pos(i) * cos(alpha_p(i));
sc_y(i) = g_y(i) + pos(i) * sin(alpha_p(i));
end
% Calculating the centre-position at column top
%-------------------------------------------------------------------------
for j = 1:no
tc_x(j) = sc_x(j) + ht*sin(beta(j)) * cos(alpha_inc(j));
tc_y(j) = sc_y(j) + ht*sin(beta(j)) * sin(alpha_inc(j));
end
% Calculating the centre-position at column bottom
%-------------------------------------------------------------------------
for j = 1:no
bc_x(j) = sc_x(j) + hb*sin(beta(j)) * cos(alpha_inc(j));
bc_y(j) = sc_y(j) + hb*sin(beta(j)) * sin(alpha_inc(j));
end
% Failure control
%-------------------------------------------------------------------------
pfg = zeros(h_pos,1); % Vector for storing if a hole
% appears
pfgi = 1; % Variable for hole index
AG = 0; % Variable for summing the hole
% area of the grid
% Double for loop, the outer going through each row and the inner, all
% combinations in that row.
for iii=0:n-2
% Logical check if the current row is odd or even, changing variables
% used to combine the three adjacent columns correctly.
if logical(mod(iii,2))==true
oe = 1;
eo = 0;
else
oe = 0;
eo = 1;
end
% Inner for loop
for ii=1:m-1
% Reseting inp struct
inp = [];
% Picking out three adjacent columns forming a triangle pointing
% uppwards
inp.dia = [dia(ii+m*iii) dia(ii+1+m*iii) dia(m+ii+m*iii+oe)];
inp.tc_x= [tc_x(ii+m*iii) tc_x(ii+1+m*iii) tc_x(m+ii+m*iii+oe)];
inp.tc_y= [tc_y(ii+m*iii) tc_y(ii+1+m*iii) tc_y(m+ii+m*iii+oe)];
inp.bc_x= [bc_x(ii+m*iii) bc_x(ii+1+m*iii) bc_x(m+ii+m*iii+oe)];
```

```
inp.bc_y= [bc_y(ii+m*iii) bc_y(ii+1+m*iii) bc_y(m+ii+m*iii+oe)];
% Checking for hole and if so, calculating the hole area
out = circ(inp);
% Storing the hole indication
pfg(pfgi)= out.pf;
% Adding one to the hole index
pfgi = pfgi+1;
% If hole was found storing the area in the A vector and adding it
% the total hole area of the grid
if out.pf == -1
A(length(A)+1) = out.A;
AG = AG+out.A;
end
%--------------------------------------------------------------------------
% Reseting inp struct
inp = [];
% Picking out three adjacent columns forming a triangle pointing
% downwards
inp.dia = [dia(m+ii+m*iii) dia(m+ii+m*iii+1) dia(ii+m*iii+eo)];
inp.tc_x= [tc_x(m+ii+m*iii) tc_x(m+ii+m*iii+1) tc_x(ii+m*iii+eo)];
inp.tc_y= [tc_y(m+ii+m*iii) tc_y(m+ii+m*iii+1) tc_y(ii+m*iii+eo)];
inp.bc_x= [bc_x(m+ii+m*iii) bc_x(m+ii+m*iii+1) bc_x(ii+m*iii+eo)];
inp.bc_y= [bc_y(m+ii+m*iii) bc_y(m+ii+m*iii+1) bc_y(ii+m*iii+eo)];
% Checking for hole and if so, calculating the hole area
out = circ(inp);
% Storing the hole indication
pfg(pfgi)= out.pf;
% Adding one to the hole index
pfgi = pfgi+1;
% If hole was found storing the area in the A vector and adding it
% the total hole area of the grid
if out.pf == -1
A(length(A)+1) = out.A;
AG = AG+out.A;
end
end
end
% Stores the total hole area of the checked grid
AP(count) = AG;
% Checking if the analyzed grid contains one or more holes
if sum(pfg<0)/h_pos > 0
pf(count) = -1;
else
pf(count) = 1;
end
% Calculating the failure probability after the n'th iteration
fp(count) = sum(pf<0)/count;
end
%==========================================================================
% Results
%==========================================================================
% Plotting the failure probability as a func. of checked grids
figure, plot(x,fp)
xlabel({'Number of grids checked'})
ylabel({'Probability for one or more holes'})
% Displaying the result
disp(['The probability that there is one or more holes in the grid is: '...
,num2str(fp(end)*100),'%,'])
disp(['using ',num2str(N),' iterations.'])
% Preperation of the results
%--------------------------------------------------------------------------
```

```
y_int = 0.8; % The degree of confidence
AP = sort(AP); % Sorting the hole areas
HA = AP(round(length(AP)*y_int)); % Picking the hole area defined by
% the confidence
AP = (AP/P_Area)*100; % Normalizing the hole areas
HA_N = (HA/P_Area)*100; % Normalizing the picked area
% Plotting a histogram of the hole size probability and displaying results
%--------------------------------------------------------------------------
fig = figure('Position',[40 80 900 400]);
subplot(1,3,[2 3]);
h = histogram(AP,'BinWidth',0.002,'Normalization','pdf'); hold on
plot([HA_N;HA_N],[0;3*max(h.Values)/4],'r','LineWidth',2);
title('Results');
str1 = ['\leftarrow The hole area is ',num2str(HA_N,3),'% of the'];
str2 = [' total plug area with ',num2str(y_int*100),'% certainty'];
str3 = ['The probability for at least one hole is ',...
num2str(fp(end)*100),'%'];
str4 = ['and the total hole area in the plug is smaller'];
str5 = ['then ',num2str(HA,3),'m^2 with ',num2str(y_int*100),...
'% certainty.'];
strr = {{str1,str2},{str3,str4,str5}};
text([HA_N HA_N],[(2*max(h.Values)/3) (max(h.Values)*0.9)],strr)
xlim([-0.01 (h.BinLimits(2))])
xlabel('$Normalized\ total\ hole\ area,\ \frac{Hole\ area}{Plug\ area}, \
[\%]$','Interpreter','latex')
ylabel('$Probability\ density$','Interpreter','latex')
mu='<HTML>&mu;<sub>';
sig='<HTML>&sigma;<sub>';
cc='<HTML>cc<sub>';
sqm='<HTML>m<sup>2';
subplot(1,3,1);
title ('Input parameters');
namess = {'Parameter','Unit','Value'};
param = {[mu 'd'],[sig 'd'],[mu 'p'],[sig 'p'],[mu 'i'],[sig 'i'],...
'm',[cc 'x'],'n',[cc 'y'],'Top depth','Bottom depth',...
'Column length','Plug area','Number of columns'};
units = {'m';'m';'m';'m';'rad';'rad';'no.';'m';'no.';'m';'m';'m';...
'm';sqm;'no.'};
t = {d_mu;d_sig;p_mu;p_sig;a_mu;a_sig;m;cx;n;cy;ht;hb;...
hb-ht;P_Area;no};
tab = [param' units t];
uit=uitable(fig,'RowName',[],'ColumnName',namess,'ColumnWidth',...
{130 50 84},'Data',tab,'Position',[50 20 265 355]);
fprintf('The hole area in the examined plug will be smaller than %.3f m^2
which \nis %.4f%% of the total plug area, with %.0f%% certainty.\n',
(HA),(HA_N),(y_int*100))
function out = Grid(inp)
%--------------------------------------------------------------------------
% Sub routine for Main_Bottom_Plug.m
% Function for creation of grid
% Part of the master thesis: Jet grouting as a method for sealing sheet
% pile excavations in Swedish conditions
% AF 262X Degree Project in Soil and Rock Mechanics
% 2019-01-28, Changed 2019-04-01
% Mårten Brinck and Karl Stigenius
%--------------------------------------------------------------------------
% Creates and returns a triangular grid of columns
%--------------------------------------------------------------------------
% Input:
m = inp.m; % Number of columns in the x-dir.
n = inp.n; % Number of columns in the y-dir.
```

```
cx = inp.cx; % Centre-dist. in x-dir.
cy = inp.cy; % Centre-dist. in y-dir.
gx = zeros(m*n,1); % Creates empty vector for x-cor.
gy = zeros(m*n,1); % Creates empty vector for y-cor.
y = 0; % Start-value for y(first row)
% Double for loop for creation of grid. The outer for each "y-value"(row)
% the inner for each "x-value"
for i = 1:n
y = y+cy;
% If func. for setting the first x-value in i each row(odd or even row)
if logical(mod(i,2))==true
x=0;
else
x=cx/2;
end
for j = 1:m
x = x+cx;
gx(j+(i-1)*m) = x-cx;
gy(j+(i-1)*m) = y-cy;
end
end
% Coverage area of the grid
out.A = ((m-1)*cx+inp.r)*((n-1)*cy+inp.r);
% Plotting the grid and compiling the output
%--------------------------------------------------------------------------
plot(gx,gy,'*'), axis equal, title({'Idealized grid'}), hold on
viscircles([gx gy],ones(n*m,1)*inp.r);
out.gx = gx;
out.gy = gy;
out.n = m*n;
end
function out = circ(inp)
%--------------------------------------------------------------------------
% Sub routine for Main_Bottom_Plug.m
% Function for calculating if three circles overlap
% Part of the master thesis: Jet grouting as a method for sealing sheet
% pile excavations in Swedish conditions
% AF 262X Degree Project in Soil and Rock Mechanics
% 2019-01-29, Changed 2019-03-12
% Mårten Brinck and Karl Stigenius
%--------------------------------------------------------------------------
% Calculating the radius from the input diameter
r(1) = inp.dia(1)/2;
r(2) = inp.dia(2)/2;
r(3) = inp.dia(3)/2;
[r,I] = sort(r,'descend'); % Sorting the the colums, descending
% Picking out the coordinates from the input and sorting them in the same
% order as the radious
for i=1:3
tc_x(i) = inp.tc_x(I(i));
tc_y(i) = inp.tc_y(I(i));
bc_x(i) = inp.bc_x(I(i));
bc_y(i) = inp.bc_y(I(i));
end
% Arranging the coordinates in two matrixes to be able to run them through
% the for loop
c_x = [tc_x' bc_x'];
c_y = [tc_y' bc_y'];
% A for loop that runs first the top of the columns through a hole check
% then the bottom
for tb = 1:2
```

```
% Calculating the actual centre-distances between the columns
d(1) = sqrt((c_x(1,tb)-c_x(2,tb))^2 + (c_y(1,tb)-c_y(2,tb))^2);
d(2) = sqrt((c_x(1,tb)-c_x(3,tb))^2 + (c_y(1,tb)-c_y(3,tb))^2);
d(3) = sqrt((c_x(2,tb)-c_x(3,tb))^2 + (c_y(2,tb)-c_y(3,tb))^2);
% Calculating the cos and sin values of the angle between the lines
% connecting the centre-point 1-2 and 1-3
ctp = (d(1)^2+d(2)^2-d(3)^2)/(2*d(1)*d(2));
stp = sqrt(1-ctp^2);
% Calculating the cos and sin values of the angle between the lines
% connecting the centre-point 2-1 and 2-3
ctb = -(d(1)^2+d(3)^2-d(2)^2)/(2*d(1)*d(3));
stb = sqrt(1-ctb^2);
% The acctual hole checking, devided into 9 cases dependent where case 1 is
% no hole at all
if (r(1)+r(2)) > d(1) && (r(1)+r(3)) > d(2) && (r(2)+r(3)) < d(3)
% Hole case 3
x12 = (r(1)^2 - r(2)^2 + d(1)^2)/(2 * d(1));
y12 = 1/(2*d(1))*...
sqrt(2*d(1)^2*(r(1)^2+r(2)^2)-(r(1)^2-r(2)^2)^2-d(1)^4);
x13p = (r(1)^2-r(3)^2+d(2)^2)/(2*d(2));
y13p = -1/(2*d(2))*...
sqrt(2*d(2)^2*(r(1)^2+r(3)^2)-(r(1)^2-r(3)^2)^2-d(2)^4);
x13 = x13p*ctp-y13p*stp;
y13 = x13p*stp+y13p*ctp;
x232 = d(1) + ctb * r(2);
y232 = stb * r(2);
x233 = ctp*d(2) - ctb * r(3);
y233 = stp*d(2) - stb * r(3);
X = [x12;x13;x233;x232];
Y = [y12;y13;y233;y232];
pf(tb) = -1;
A(tb) = polyarea(X,Y);
hole_case(tb) = 3;
elseif (r(1)+r(2)) > d(1) && (r(2)+r(3)) > d(3) && (r(1)+r(3)) < d(2)
% Hole case 4
x12 = (r(1)^2 - r(2)^2 + d(1)^2)/(2 * d(1));
y12 = 1/(2*d(1))*...
sqrt(2*d(1)^2*(r(1)^2+r(2)^2)-(r(1)^2-r(2)^2)^2-d(1)^4);
x23b = (r(2)^2-r(3)^2+d(3)^2)/(2*d(3));
y23b = 1/(2*d(3))*...
sqrt(2*d(3)^2*(r(2)^2+r(3)^2)-(r(2)^2-r(3)^2)^2-d(3)^4);
x23 = x23b*ctb-y23b*stb+d(1);
y23 = x23b*stb+y23b*ctb;
x131 = ctp * r(1);
y131 = stp * r(1);
x133 = ctp * (d(2) - r(3));
y133 = stp * (d(2) - r(3));
X = [x12;x23;x133;x131];
Y = [y12;y23;y133;y131];
pf(tb) = -1;
A(tb) = polyarea(X,Y);
hole_case(tb) = 4;
elseif (r(1)+r(3)) > d(2) && (r(2)+r(3)) > d(3) && (r(1)+r(2)) < d(1)
% Hole case 5
x13p = (r(1)^2-r(3)^2+d(2)^2)/(2*d(2));
y13p = -1/(2*d(2))*...
sqrt(2*d(2)^2*(r(1)^2+r(3)^2)-(r(1)^2-r(3)^2)^2-d(2)^4);
x13 = x13p*ctp-y13p*stp;
y13 = x13p*stp+y13p*ctp;
x23b = (r(2)^2-r(3)^2+d(3)^2)/(2*d(3));
y23b = 1/(2*d(3))*...
```

```
sqrt(2*d(3)^2*(r(2)^2+r(3)^2)-(r(2)^2-r(3)^2)^2-d(3)^4);
x23 = x23b*ctb-y23b*stb+d(1);
y23 = x23b*stb+y23b*ctb;
x121 = r(1);
y121 = 0;
x122 = d(1) - r(2);
y122 = 0;
X = [x13;x23;x122;x121];
Y = [y13;y23;y122;y121];
pf(tb) = -1;
A(tb) = polyarea(X,Y);
hole_case(tb) = 5;
elseif (r(1)+r(2)) > d(1) && (r(1)+r(3)) < d(2) && (r(2)+r(3)) < d(3)
% Hole case 6
x12 = (r(1)^2 - r(2)^2 + d(1)^2)/(2 * d(1));
y12 = 1/(2*d(1))*...
sqrt(2*d(1)^2*(r(1)^2+r(2)^2)-(r(1)^2-r(2)^2)^2-d(1)^4);
x131 = ctp * r(1);
y131 = stp * r(1);
x133 = ctp * (d(2) - r(3));
y133 = stp * (d(2) - r(3));
x232 = d(1) + ctb * r(2);
y232 = stb * r(2);
x233 = ctp*d(2) - ctb * r(3);
y233 = stp*d(2) - stb * r(3);
X = [x12;x131;x133;x233;x232];
Y = [y12;y131;y133;y233;y232];
pf(tb) = -1;
A(tb) = polyarea(X,Y);
hole_case(tb) = 6;
elseif (r(1)+r(3)) > d(2) && (r(2)+r(3)) < d(3) && (r(1)+r(2)) < d(1)
% Hole case 7
x13p = (r(1)^2-r(3)^2+d(2)^2)/(2*d(2));
y13p = -1/(2*d(2))*...
sqrt(2*d(2)^2*(r(1)^2+r(3)^2)-(r(1)^2-r(3)^2)^2-d(2)^4);
x13 = x13p*ctp-y13p*stp;
y13 = x13p*stp+y13p*ctp;
x232 = d(1) + ctb * r(2);
y232 = stb * r(2);
x233 = ctp*d(2) - ctb * r(3);
y233 = stp*d(2) - stb * r(3);
x121 = r(1);
y121 = 0;
x122 = d(1) - r(2);
y122 = 0;
X = [x13;x233;x232;x122;x121];
Y = [y13;y233;y232;y122;y121];
pf(tb) = -1;
A(tb) = polyarea(X,Y);
hole_case(tb) = 7;
elseif (r(2)+r(3)) > d(3) && (r(1)+r(2)) < d(1) && (r(1)+r(3)) < d(2)
% Hole case 8
x23b = (r(2)^2-r(3)^2+d(3)^2)/(2*d(3));
y23b = 1/(2*d(3))*...
sqrt(2*d(3)^2*(r(2)^2+r(3)^2)-(r(2)^2-r(3)^2)^2-d(3)^4);
x23 = x23b*ctb-y23b*stb+d(1);
y23 = x23b*stb+y23b*ctb;
x121 = r(1);
y121 = 0;
x122 = d(1) - r(2);
y122 = 0;
```

```
x131 = ctp * r(1);
y131 = stp * r(1);
x133 = ctp * (d(2) - r(3));
y133 = stp * (d(2) - r(3));
X = [x23;x122;x121;x131;x133];
Y = [y23;y122;y121;y131;y133];
pf(tb) = -1;
A(tb) = polyarea(X,Y);
hole_case(tb) = 8;
elseif (r(1)+r(2)) < d(1) && (r(1)+r(3)) < d(2) && (r(2)+r(3)) < d(3)
% Hole case 9
x124 = d(1) - r(2) - (d(1)-r(1)-r(2))/2;
y124 = 0;
x134 = (r(1) + (d(2)-r(1)-r(3))/2) * ctp;
y134 = (r(1) + (d(2)-r(1)-r(3))/2) * stp;
x234 = d(1) + (r(2) + (d(3)-r(2)-r(3))/2) * ctb;
y234 = (r(2) + (d(3)-r(2)-r(3))/2) * stb;
X = [x124;x134;x234];
Y = [y124;y134;y234];
pf(tb) = -1;
A(tb) = polyarea(X,Y);
hole_case(tb) = 9;
else
x12 = (r(1)^2 - r(2)^2 + d(1)^2)/(2 * d(1));
y12 = 1/(2*d(1))*...
sqrt(2*d(1)^2*(r(1)^2+r(2)^2)-(r(1)^2-r(2)^2)^2-d(1)^4);
if ((r(3)^2 > ((x12-d(2)*ctp)^2+(y12-d(2)*stp)^2)) &&...
(r(3)^2 < ((x12-d(2)*ctp)^2+(y12+d(2)*stp)^2)))
% Hole case 1, no hole
X = 0;
Y = 0;
pf(tb) = 1;
A(tb) = 0;
hole_case(tb) = 1;
else
% Hole case 2
x13p = (r(1)^2-r(3)^2+d(2)^2)/(2*d(2));
y13p = -1/(2*d(2))*...
sqrt(2*d(2)^2*(r(1)^2+r(3)^2)-(r(1)^2-r(3)^2)^2-d(2)^4);
x13 = x13p*ctp-y13p*stp;
y13 = x13p*stp+y13p*ctp;
x23b = (r(2)^2-r(3)^2+d(3)^2)/(2*d(3));
y23b = 1/(2*d(3))*...
sqrt(2*d(3)^2*(r(2)^2+r(3)^2)-(r(2)^2-r(3)^2)^2-d(3)^4);
x23 = x23b*ctb-y23b*stb+d(1);
y23 = x23b*stb+y23b*ctb;
X = [x12;x13;x23];
Y = [y12;y13;y23];
pf(tb) = -1;
A(tb) = polyarea(X,Y);
hole_case(tb) = 2;
end
end
end
% Checking if there is a hole in both the top and bottom layer
if sum(pf<0) == 2
% Choosing the smallest area
A = min([A]);
% Checking that the area is att least one square centimeter other wise
% neglected
if A*10000>1
```

```
out.pf = -1;
out.A = A;
else
out.pf = 1;
out.A = 0;
end
% If there is'nt a hole in both top and bottom the constallation is
% regarded as water tight
else
out.pf = 1;
out.A = 0;
end
end
```

Appendix F – Analytical Calculations: Hydraulic Conductivity

Total plug area:
$A_{\text{total}} = 100 \cdot 21 = 2100\ \text{m}^2$

Jet grout columns 1.4 m c/c – results from MATLAB code:
Probability for at least one hole: 100%
Total hole area in the plug is smaller than 35.1 m^2 with 80% certainty.
The hole area is 1.71% of the total plug area with 80% certainty.

Darcy's law:
$Q = k \cdot A \cdot \frac{dh}{dL}$

Water is assumed to only flow in the untreated parts of the jet grout plug.
$A = 35.1\ \text{m}^2$
$k = 2 \cdot 10^{-4}$ m/s (the higher value in the lower aquifer)
$Q_{\text{untreated parts}} = 2 \cdot 10^{-4} \cdot 35.1 \cdot 1 = 0.00702\ \text{m}^3/\text{s}$
$k_{\text{plug}} = \frac{Q_{\text{untreated parts}}}{A_{\text{total}}} = \frac{0.00702}{2100} = 3.34 \cdot 10^{-6}\ \text{m/s} = 0.2886\ \text{m/day}$

Result to be compared with:

- limit given in different codes of practice is 0.5 l/s over 1000 m^2 (Modoni et al. 2016). (0.5 l = $5 \cdot 10^{-4}$ m^3/s over 1000 m^2 → $k_{\text{plug}} = 5 \cdot 10^{-7}$ m/s)

- required hydraulic conductivity from the project = 10^{-8} m/s

→ Results: the permeability is too large in the plug.

Jet grout columns 1.3 m c/c:
Number of columns in x-direction: 16
Number of columns in y-direction: 77

Results from MATLAB code:
Probability for at least one hole: 100%
Total hole area in the plug is smaller than 7.49 m^2 with 80% certainty.
The hole area is 0.368% of the total plug area with 80% certainty.

$k_{\text{plug}} = 7.36 \cdot 10^{-7}\text{m/s} = 0.0636\ \text{m/day}$

→ Results: still too large permeability.

Jet Grout columns 1.2 m c/c:
Number of columns in x-direction: 18
Number of columns in y-direction: 84

Results from MATLAB code:
Probability for at least one hole: 100%
Total hole area in the plug is smaller than 1.08 m^2 with 80% certainty.

The hole area is 0.0505% of the total plug area with 80% certainty.

$k_{\text{plug}} = 1.01 \cdot 10^{-7}\ \text{m/s}$

→ Results: satisfactory with code of practice, but not with the limit for the project.

Jet grout columns 1.1 m c/c:
Number of columns in x-direction: 19
Number of columns in y-direction: 91

Results from MATLAB code:
Probability for at least one hole: 99.84%
Total hole area in the plug is smaller than 0.1 m^2 with 80% certainty.
The hole area is 0.00484% of the total plug area with 80% certainty.

$k_{\text{plug}} = 9.52 \cdot 10^{-9}\ \text{m/s}$

→ Results: satisfactory hydraulic conductivity according to project requirement.